SPC 974053-1

Contract F61708-97-W0197

between

UNITED STATES AIR FORCE EUROPEAN OFFICE OF
AEROSPACE RESEARCH AND DEVELOPMENT
223/231 Old Marylebone Road, London NW1 5TH, United Kingdom

and

INSTITUTE OF CHEMICAL KINETICS AND COMBUSTION
Condensed Systems Combustion Laboratory
Russian Academy of Sciences, Novosibirsk, 630090, Russia

STUDYING THE FORMULATION EFFECTS ON STEADY-STATE AND TRANSIENT COMBUSTION BEHAVIOR OF ALUMINIZED PROPELLANTS

Final Technical Report

by

Prof. Vladimir E. Zarko, principal investigator

Novosibirsk, 1998

SPC 97-4053-1

REPORT DOCUMENTATION PAGE

form Approved
OMB No. 0704-0188

1. AGENCY USE ONLY	2. REPORT DATE	3. REPORT TYPE AND DATES COVERED
	16 JULY 1998	**FINAL, 6 JULY 97 - 6 JUNE 98**

4. TITLE AND SUBTITLE
STUDYING THE FORMULATION EFFECTS ON STEADY-STATE AND TRANSIENT COMBUSTION BEHAVIOR OF ALUMINIZED PROPELLANTS

5. FUNDING NUMBERS

6. AUTHORS
V. E. Zarko, O. G. Glotov, V. V. Karasev, V. N. Simonenko, A. B. Kiskin, A. G. Svit, L. K. Gusachenko

7. PERFORMING ORGANIZATION NAME(S) AND ADDRESS(ES)
Institute of Chemical Kinetics and Combustion Russian Academy of Sciences, Novosibirsk, 630090, Russia

8. PERFORMING ORGANIZATION REPORT NUMBER
N/A

9. SPONSORING/ MONITORING AGENCY NAME(S) AND ADDRESS(ES)
United States Air Force European Office of Aerospace Research and Development 223/231 Old Marylebone Road, London NW1 5TH, United Kingdom

10. SPONSORING / MONITORING AGENCY REPORT NUMBER
F61708-97-W0197

11. SUPPLEMENTARY NOTES

12a. DISTRIBUTION/AVAILABILITY STATEMENT

12b. DISTRIBUTION CODE

13. ABSTRACT. The objective of work was to get experimental information about combustion behavior of metalized propellant, namely on evolution of condensed combustion products (CCP) and non-steady combustion characteristics. The study has been performed on model propellant (35% HMX, 25% AP, 20% Al, 20% nitryl/DEGDN based energetic binder) using two original methods – collection of CCP particles quenched at varied distance from burning surface and use of micro-force transducer for the recoil measurements of propellant sample burning in self sustaining regime or under perturbing conditions. The propellant follows to the classical agglomeration scenario with sizable growing of agglomerates containing practically entire amount of unburnt aluminum. There are following specific peculiarities in the agglomeration behavior: (1) The main mass and size characteristics more strongly depend on pressure than on residence time for agglomerates in flame. (2) The content of unburnt aluminum in sieved fractions in the range 130-600 μm is approximately constant for each pressure levels in the range 1-64 atm. The density of agglomerates does not depend on size in the range 130-600 μm, but slightly increases with oxide content while pressure increases. (3) At pressure ~65 atm no change in aluminum content is observed for resident time of agglomerates in flame in interval 30-95 ms, and amount of free aluminum in agglomerates has lowest value as compared with that for another pressures. At atmospheric pressure there is a noticeable change in aluminum content during time interval 20-25 ms, and then it is approximately constant while residence time is 25-70 ms. At pressure ~22 atm the intermediate behavior is observed. No significant evolution of size distribution of agglomerates was observed even in the cases of 1 atm and 22 atm when burning out of aluminum took place. Regarding the fine oxide particles, we may conclude that: (4) In most cases the fine CCP particles size distribution has three modes in the size ranges 0.5-1.5 μm, 2.4-3.9 μm and 6.4-8.5 μm, with the main peak being in interval 2.4-3.9 μm. Agglomerate combustion increases the total mass of fine particles but does not make effect on their size distribution. (5) For the first time some unusual form of size distribution function (narrowing to the interval 1.5-10.5 μm) was observed in the case of pressure 24 atm and the longest residence time. There are conclusions about burning rate behavior at atmospheric conditions: (6) Self-sustaining combustion of propellant under investigation under atmospheric pressure is characterized by noticeable pulsations of the recoil force having auto-spectrum similar to isotropic turbulence where 80% of oscillations energy is released in the frequency range 0.5-10 Hz. (7) Excluding of aluminum from propellant formulation leads to significant (by order of magnitude) decrease in amplitude of chaotic recoil signal oscillations.

14. SUBJECT TERMS: Combustion, solid propellant, condensed combustion products sampling, aluminum, agglomeration, aluminum oxide, particle size distribution, particle density, aluminum combustion efficiency, burning rate, transient behavior, micro force transducer, recoil response, radiant flux.

15. NUMBER OF PAGES
74

16. PRICE CODE

17. SECURITY CLASSIFICATION OF REPORT	18. SECURITY CLASSIFICATION OF THIS PAGE	19. SECURITY CLASSIFICATION OF ABSTRACT	20. LIMITATION OF ABSTRACT

NSN 7540-01-280-5500

Standard Form 298

ABSTRACT

The objective of work was to get experimental information about combustion behavior of metalized propellant, namely on evolution of condensed combustion products (CCP) and non-steady combustion characteristics. The study has been performed on model propellant (35% HMX, 25% AP, 20% Al, 20% nitryl/DEGDN based energetic binder) using two original methods – collection of CCP particles quenched at varied distance from burning surface and use of micro-force transducer for the recoil measurements of propellant sample burning in self sustaining regime or under perturbing conditions. The propellant follows to the classical agglomeration scenario with sizable growing of agglomerates containing practically entire amount of unburnt aluminum. There are following specific peculiarities in the agglomeration behavior: (1) The main mass and size characteristics more strongly depend on pressure than on residence time for agglomerates in flame. (2) The content of unburnt aluminum in sieved fractions in the range 130-600 μm is approximately constant for each pressure levels in the range 1-64 atm. The density of agglomerates does not depend on size in the range 130-600 μm, but slightly increases with oxide content while pressure increases. (3) At pressure ~65 atm no change in aluminum content is observed for resident time of agglomerates in flame in interval 30-95 ms, and amount of free aluminum in agglomerates has lowest value as compared with that for another pressures. At atmospheric pressure there is a noticeable change in aluminum content during time interval 20-25 ms, and then it is approximately constant while residence time is 25-70 ms. At pressure ~22 atm the intermediate behavior is observed. No significant evolution of size distribution of agglomerates was observed even in the cases of 1 atm and 22 atm when burning out of aluminum took place. Regarding the fine oxide particles, we may conclude that: (4) In most cases the fine CCP particles size distribution has three modes in the size ranges 0.5-1.5 μm, 2.4-3.9 μm and 6.4-8.5 μm, with the main peak being in interval 2.4-3.9 μm. Agglomerate combustion increases the total mass of fine particles but does not make effect on their size distribution. (5) For the first time some unusual form of size distribution function (narrowing to the interval 1.5-10.5 μm) was observed in the case of pressure 24 atm and the longest residence time. There are some conclusions about burning rate behavior at atmospheric conditions: (6) Self-sustaining combustion of propellant under investigation under atmospheric pressure is characterized by noticeable pulsations of the recoil force having auto-spectrum similar to isotropic turbulence where 80% of oscillations energy is released in the frequency range 0.5-10 Hz. (7) Excluding of aluminum from propellant formulation leads to significant (by order of magnitude) decrease in amplitude of chaotic recoil signal oscillations.

Keywords

Combustion, solid propellant, condensed combustion products, sampling, aluminum, agglomeration, aluminum oxide, particle size distribution, particle density, aluminum combustion efficiency, burning rate, transient behavior, micro force transducer, recoil response, radiant flux.

ACKNOWLEDGEMENTS

The authors are grateful to O. N. Zhitnitskaya (particle size analyses), T. D. Fedotova and A. G. Kir'yanova (chemical analyses), V. L. Bizyaev (particle size analyses by «Malvern»).

TABLE OF CONTENT

1. INTRODUCTION

1.1. Background

The efficiency of aluminized propellants combustion in solid rocket motors is determined not only by conversion of chemical energy in the heat of combustion but also by the formation of condensed combustion products (CCP) from aluminum. These cause two-phase losses of specific impulse, slag formation in the combustion chamber, and erosion of the nozzles. It is well known [1] that aluminum particles may react and coagulate in a subsurface layer forming agglomerates. The agglomerates then burn in the two-phase flow generating various sized oxide particles. Condensed combustion products can consist of agglomerate residues containing non-consumed metal, oxide (smoke particles and oxide caps after burn out of agglomerate), and carbonaceous material. The metal agglomeration depends both on propellant formulation and combustion conditions. To simulate the agglomerate behavior one needs information about size distribution and structure of initially formed agglomerates and the rate of conversion of metal into oxide on the burning surface and during the motion of agglomerates in the gas flow. The smoke particles play important role in suppression of pressure oscillations in a rocket motor.

Despite the long history of studying aluminized propellant combustion, there is a strong need of valid experimental data regarding the whole history of metal behavior in the combustion wave. There should be noted difficulties in assessment and comparison between available in literature data on agglomeration process due to the lack of reliable information about size distribution of initial and final condensed particles. In fact, theoretical approaches reported in the literature do not allow to predict a priori characteristics of burning rate and condensed combustion products of metalized propellant, especially their evolution in time.

The present work is performed in continuation of studies made under contracts with EOARD and BYU. Some preliminary results have already been published [2, 3, 4, 5, 6, 7]. The objective of the previous studies was to obtain experimental information about stationary and transient combustion behavior of the aluminized solid propellants based on AP and HMX of fixed size distribution and varied types of binders. It was revealed that the combustion mechanism of these propellants strongly depends on the formulation effects. In particular, it was found that agglomeration intensity for propellant with energetic binder increases with partial replacement of AP by HMX. However, in case of propellant with inert binder replacement of butadiene rubber by isoprene one leads to stronger effect than replacement of AP by HMX.

1.2. Objectives

The objective of the present study was to get detailed experimental information about HMX/AP/Al/energetic binder model propellant in steady-state and transient regimes of combustion. The propellant under study had practically the same formulation as propellant investigated previously [2] but with some difference in HMX size distribution.

For steady-state combustion, the goal of the study was to characterize condensed combustion products sampled at pressure range 1-65 atm in dependence on residence time for burning particles in hot gaseous combustion products. The data were obtained on size distribution in wide range from 0.5 micron to thousands microns and on content of non-consumed aluminum in condensed combustion products.

For non-stationary combustion, the goal was to evaluate the recoil force response to sinusoidal and step-wise perturbations of radiant flux using computer controlled Nd-YAG laser and micro-force transducer. Additionally, the measurement of dependence of burning rate on constant radiant flux was performed for radiation driven combustion at normal conditions (room initial temperature and atmospheric pressure).

2. MANUFACTURING AND CHARACTERIZATION OF THE MODEL PROPELLANTS

The metalized propellant was designated in this work as E12 in accordance with the previous nomenclature [2]. The energetic binder based on nitryl rubber plasticized by diethylene glycol dinitrate (DEGDN) (98%) with additives (2%) was used. The propellant formulation is presented in Table 2.1. The results of particle size distribution analysis of aluminum (Al), cyclotetramethylene tetranitramine (HMX) and ammonium perchlorate (AP) powders are shown in Figs 2.2- 2.4. Two methods were employed for particle size analysis – optical microscope for coarse powders and Malvern 3600E sizer for fine powders. The following substances were used as carried liquid in Malvern analysis: hexane for AP powder, water for aluminum, acetone for CCP particles. The content of metal in virgin aluminum particles amounted 99.5%.

The mixing of components was performed in mortar made of teflon by summary weight of 100 g per batch. Curing of cylindrical slabs of propellant was made in air at 70°C during 170 hours. The density was determined on curred propellant samples.

The dependence of burning rate on pressure was estimated in course of the firing tests in sampling bomb. The bomb was pressurized with nitrogen, including pressure 1 atm. The burning rate equals 0.99±0.04 mm/s at 1 atm. The following correlation was obtained for r (mm/s) and P (atm) within the pressure range 23-65 atm: $r = 1.88 \cdot P^{0.45}$, see Fig. 2.1.

Table 2.1. Propellant E12 formulation (% mass.)

Energetic binder	Al D_{30}=14 μm	AP 200-315 μm	AP S=6000 cm^2/g	HMX 250-700 μm	Density, g/cm^3
20	20	18	7	35	1.82±0.02

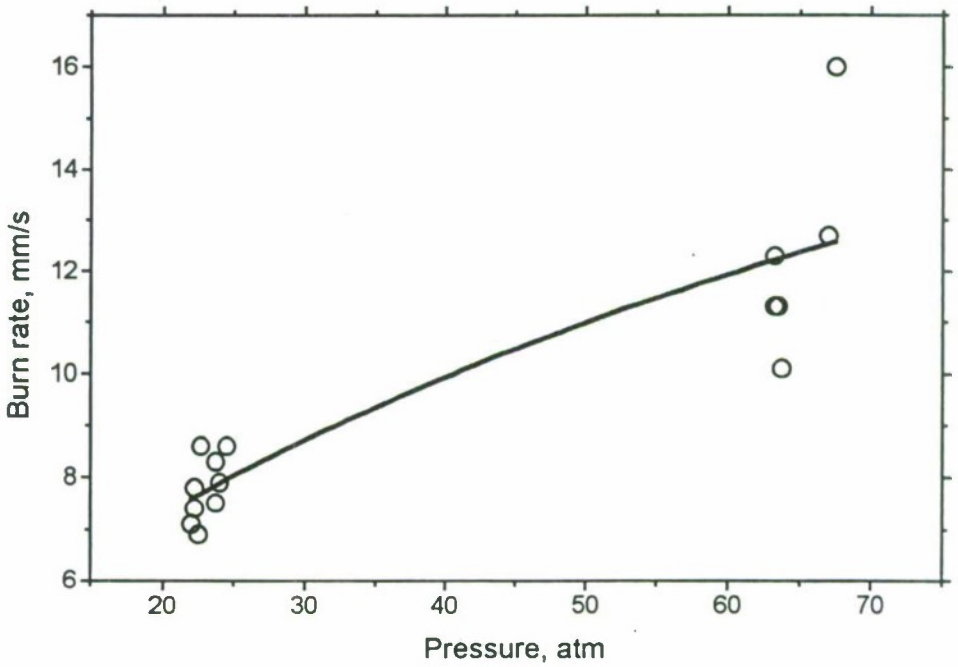

Fig. 2.1. Burning rate *vs* pressure. All experimental points are presented.

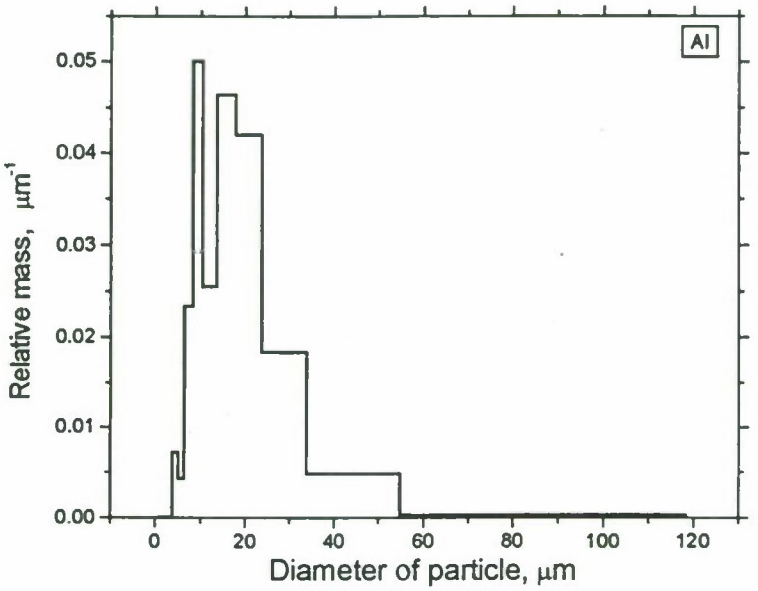

Fig. 2.2. Mass size distribution for aluminum used in manufacturing the model propellants.

Measurements were made by Malvern 3600E in water after treatment by ultrasound during 40 seconds, mixer ON, size range 0.5-118.4 μm.

D_{mn}, μm: D_{10}=9.7; D_{20}=11.0; D_{30}=12.6; D_{21}=12.5; D_{32}=16.5; D_{43}=22.3; D_{53}=26.4.

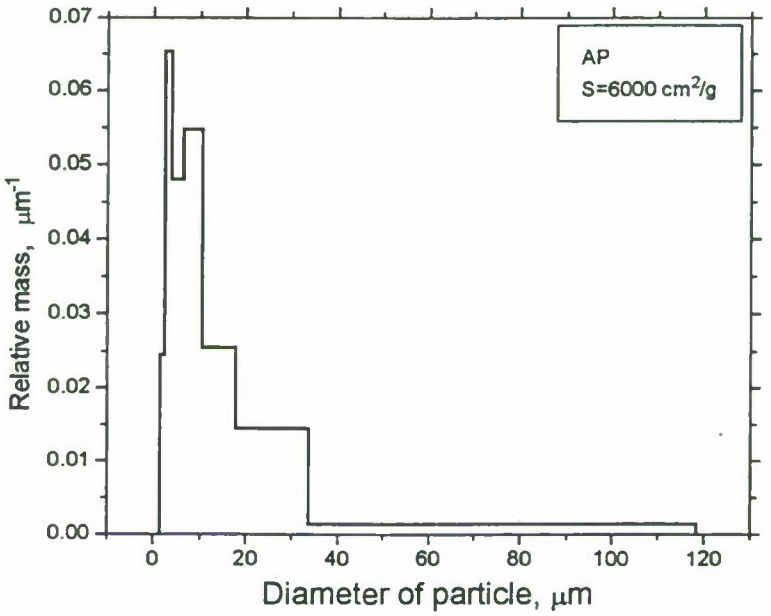

Fig. 2.3. Mass size distribution for fine AP with S = 6000 cm^2/g used to manufacture the model propellants.

Measurements were made by Malvern 3600E in hexane, mixer ON, size range 0.5-118 μm.

D_{mn}, μm: D_{10}=4.3; D_{20}=4.0; D_{30}=5.1; D_{21}=4.8; D_{32}=8.4; D_{43}=17.1; D_{53}=22.9.

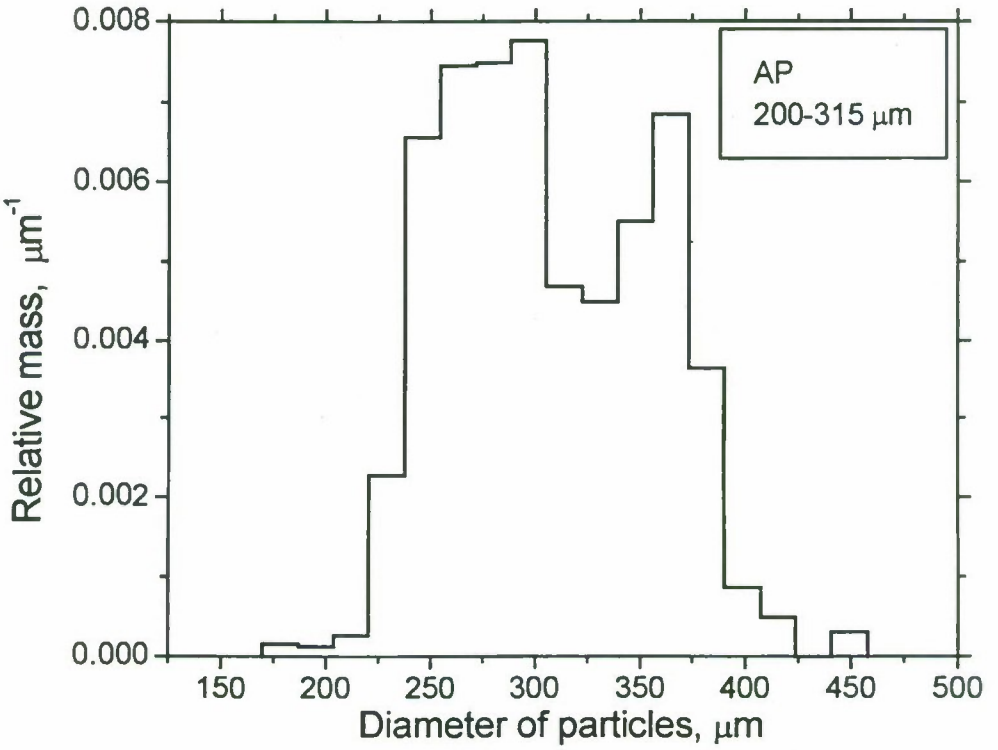

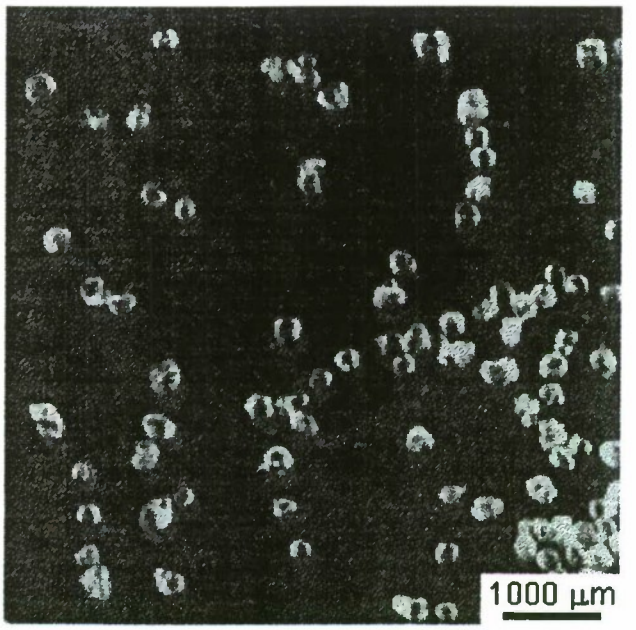

Fig. 2.4. Mass size distribution and photography image of coarse AP 200-315 μm particles used in manufacturing the model propellants.

Measurements were made by optical microscope.

D_{mn}, μm: D_{10}=284; D_{20}=288; D_{30}=292; D_{21}=292; D_{32}=299; D_{43}=306; D_{53}=310.

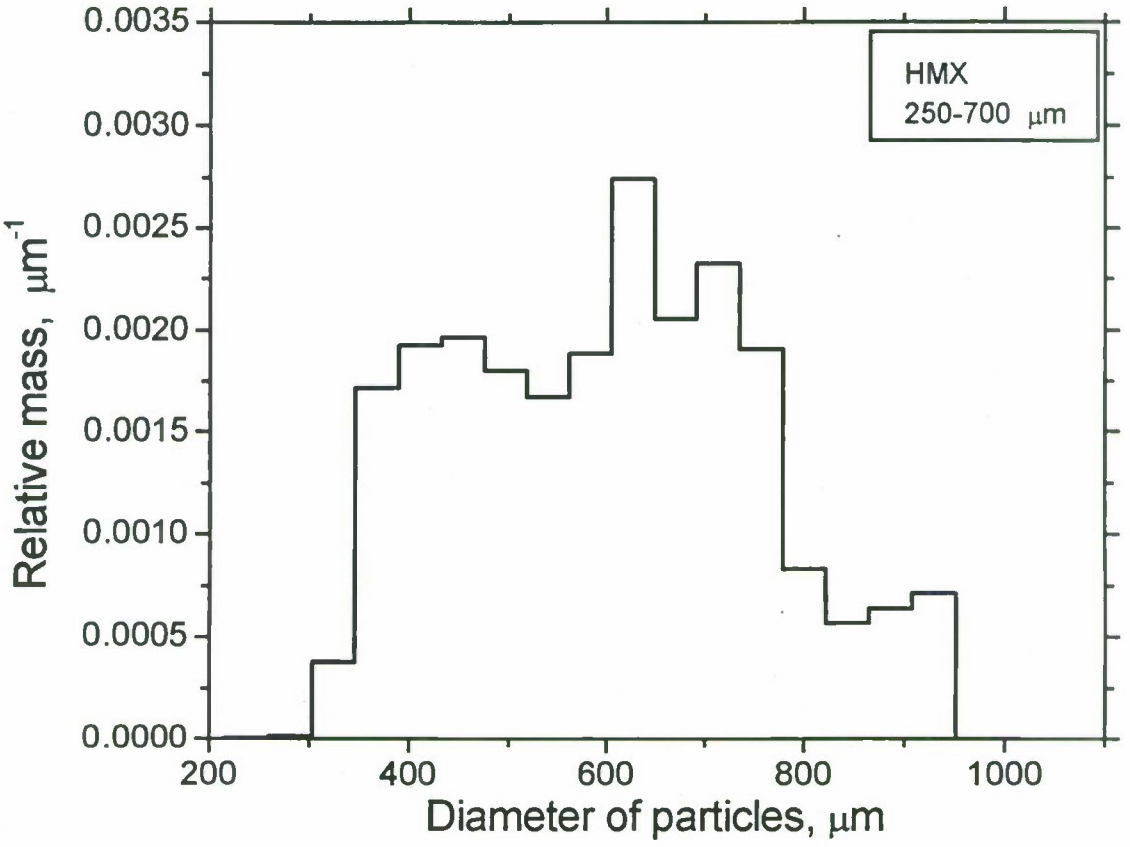

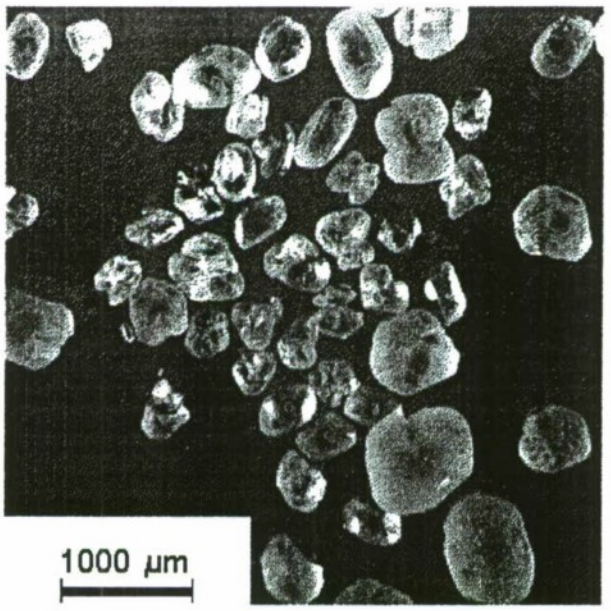

Fig. 2.5.

Mass size distribution and photography image of HMX powder with particles larger than 315 μm in size used in manufacturing the model propellants.

Measurements were made by optical microscope.

D_{mn}, μm: D_{10}=486; D_{20}=503; D_{30}=522; D_{21}=522; D_{32}=561; D_{43}=601; D_{53}=621.

3. METHOD OF SAMPLING THE CONDENSED COMBUSTION PRODUCTS

3.1. The set up and experimental procedure

The original technique designed for simultaneous sampling of agglomerates and oxide particles in one run followed by size distribution and chemical analyses has been described previously [8, 9, 10]. Below we observe briefly the particular features of the technique option used in this study.

The blow through bomb (Fig. 3.1) consists of massive case *1* supplied with gas inlet *11* and outlet *6* valves which allow to maintain an appropriate gas flow rate in the bomb. Inside the bomb there is a steel cylinder *3* of 50 mm in diameter with propellant specimen *9* mounted in the top cover *2* (inner part) of cylinder. The bottom of a cylinder is supplied with a set *4* of wire mesh screens and aerosol analytical filter AFA *5*. The propellant specimen is ignited by nichrome wire *8* and the flame torch is directed downward. The protective tube *7* is slipped over a specimen providing protection of combustion products against mixing with environmental gas. After leaving the tube the combustion products mix with cold nitrogen filling the bomb and cylinder interior through the top ring slot *10* (∅40 - ∅30 mm).

Specific features of approach used in the present work are described as follows.

- Samples for the firing tests were cut from the cured material in the form of cylinder with diameter 7 mm or 11.5 mm and height 9-11 mm in all cases. Using two different propellant sample diameters and protecting tube of 10-cm length (only with the samples having diameter 11.5 mm) allows to vary the residence time of CCP particles in flame. Thus, we used three types (*A*, *B*, *C*) of firing geometry to provide different length of initial mixing area for co-current flows of gaseous combustion products and cooling nitrogen and varied residence time for particles in flame. The sample geometry types are pictured in the Fig. 3.2.
- Mass flow rate of nitrogen through the bomb was about 1.8-2 g/s in runs at 64-67 atm, 1.1-2 g/s at pressures 22-24 atm and zero at 1 atm.
- The burning rate was calculated as specimen height divided by the burn out time. The last one was determined from pressure-*vs*-time record in the case of pressure levels 22 and 64 atm and from temporal record of light emission of burning specimen in the case of pressure 1 atm. In this case a photo diode was mounted inside the bomb in cylinder *3*, see Fig. 3.1. The difference in burning rate of samples with diameter 11.5 mm and 7 mm was not observed.
- The maximum rise of pressure during the combustion run was 12 atm in the experiments with samples 11.5 mm in diameter at initial pressure 60 atm. The characteristic pressure in the individual run was taken as a half of sum of initial and final pressures. The characteristic pressure and burning rate for given series were chosen as arithmetical mean values of characteristic pressure and burning rate for individual runs.
- Under identical conditions (pressure and diluting gas flow) several propellant samples (2-3 in the case of 11.5 mm in diameter or 5-6 in the case of 7 mm in diameter) were consecutively combusted that provided total propellant mass burnt 3-6 g and generated 1-2 g of CCP used for further analysis.
- In the previous works [2, 3] it was found that using of epoxy glue for inhibition of the lateral surface of burning sample made considerable contamination contribution into total mass of the condensed combustion products. In the present work we used for lateral surface inhibiting the hollow cylinders made of plexiglas supplied with teflon bottom. The propellant samples were

tightly inserted into cylinders through special cone director. The cylinders made of teflon were used in special tests. It was found that in this case the mass loss of the cylinder material during combustion is approximately twice larger than in the case of plexiglas cylinder. Thus the plexiglas is most proper inhibiting material for using in such experiments.

- The nominal mesh sizes of wire screens in the stack installed inside the bomb were 130, 150, 300, 450, 600, 900 and 970 μm;
- The CCP particles captured by wire screens in the bomb were divided in fractions via dry and wet sieving in acetone by using sieves with the same mesh sizes. The particles caught by the filter were extracted by way of dissolving the filter matter in acetone and then they were added to sieve fraction <130 μm. In present work the diluting followed by depositing particles via sedimentation in order to diminishing the concentration of the filter matter in solution was not executed. This allows avoiding the fine particle loss in course of pumping out the suspension and following analyzing the whole mass of collected particles (except inescapable losses during probe preparation). It was established in special tests that presence of the filter matter does not affect the results of chemical analysis and particle size analysis. All sieved fractions of CCP particles were weighed after drying with accuracy of no less than 0.00015 g and then were subjected to particle size and chemical analysis. The latter was made by permanganatometric method [10] that allows to determine the unburnt aluminum content. The mass of particles trapped by filter was calculated as difference of filter mass before and after the experiment.
- The fine (< 130 μm) particles were analyzed with commercial sizer Malvern 3600E using acetone as carrier liquid after 40 seconds treatment by ultrasound and with continuous mechanical mixing of suspension. 16 channels were employed with exponential incrementing width in size range 0.5-118.4 μm.
- Particle size analysis for particles 130-600 μm was performed using optical microscope. The particles with size exceeding 600 μm were photographed by scanner Uniscan (Russia) with following measurement of their sizes. In both cases the accuracy of size measurement has been estimated as a half of histogram sub-range. It was equal 9 μm for fractions in the size range 130-300 μm, 22 μm for fractions 300-600 μm and 27-70 μm for fractions with size exceeding 600 μm.
- The density of fine (< 130 μm) particles was assumed to be equal 3.71 g/cm^3 while the mean density of coarse (> 130 μm) particles was determined individually in each sieved fraction via procedure described below in Chapter 4.5.

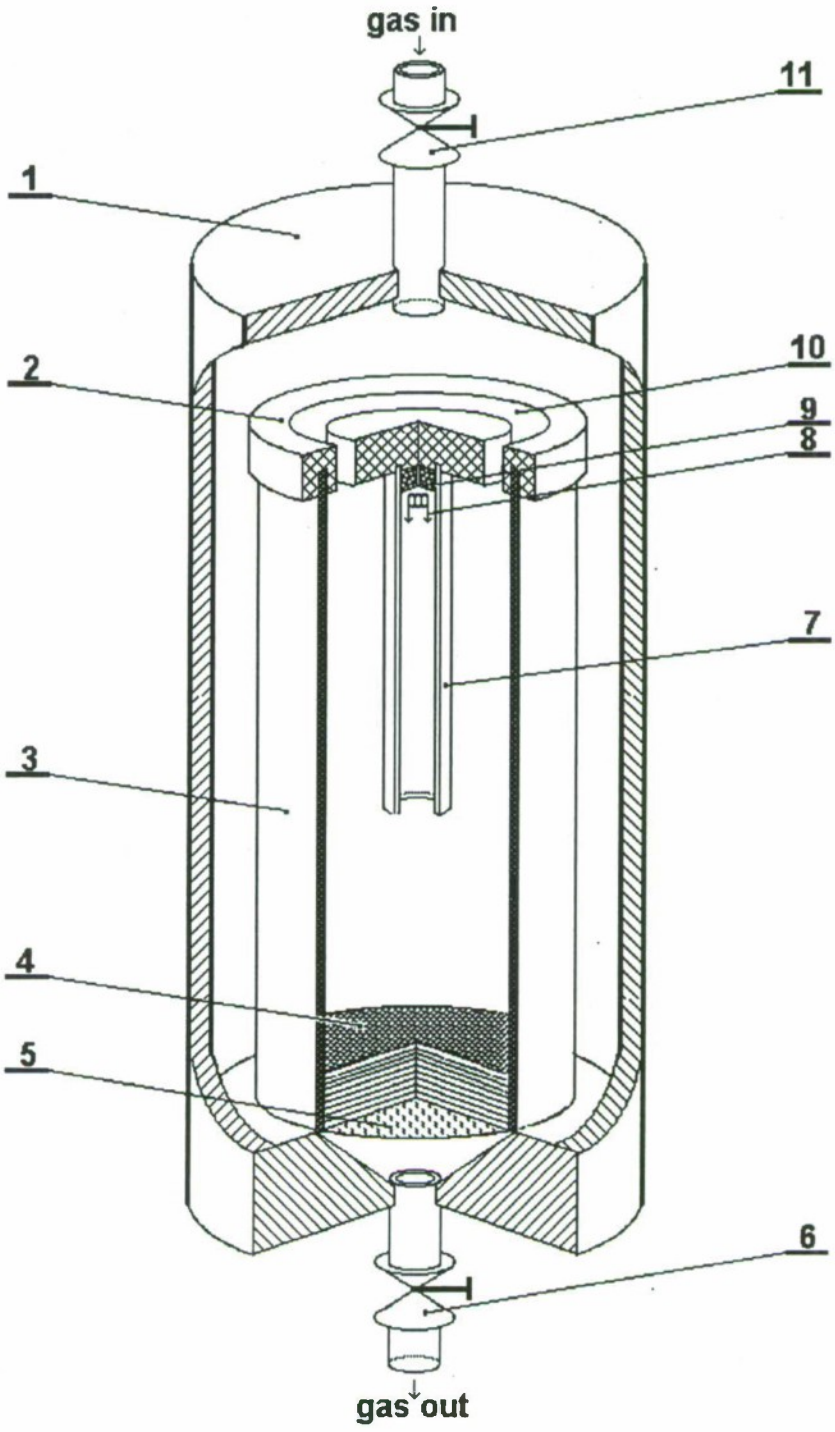

Fig. 3.1. Chart of the flow bomb for CCP sampling:

1 - bomb body,
2 - top cover of the cylinder 3,
3 - thin wall cylinder,
4 - stack of wire mesh screens,
5 - filter,
6 - gas outlet valve,
7 - protective tube,
8 - ignition wire,
9 - propellant specimen,
10 - ring slot for blowing the cylinder 3,
11 - gas inlet valve.

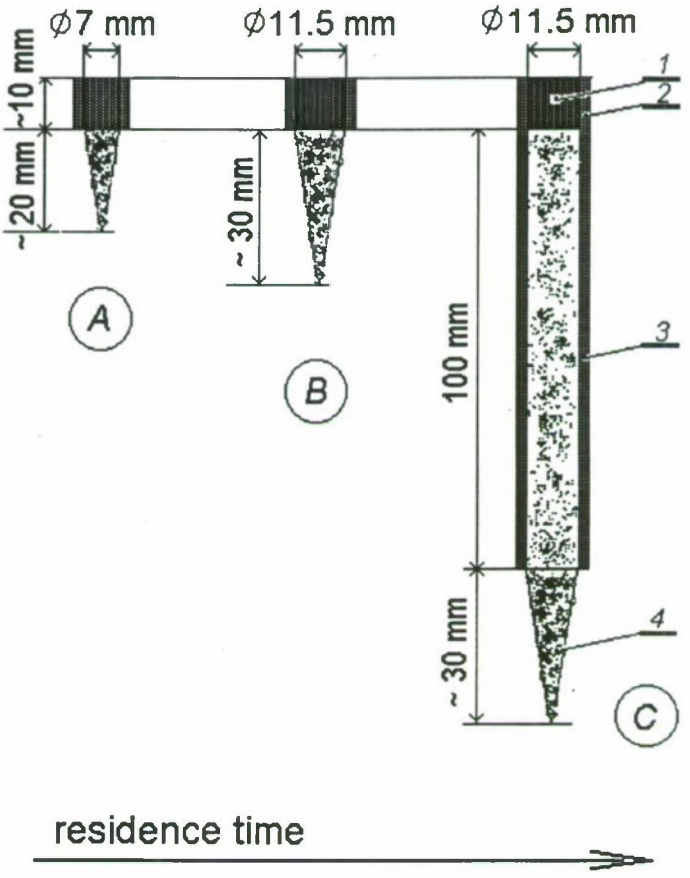

Fig. 3.2.

Three types of firing geometry (*A*, *B*, *C*) that provided variation of the residence time for agglomerate particles in flame.

1 - propellant specimen,
2 - mounting hollow cylinder,
3 - protective tube,
4 - initial mixing area.

3.2. Definition of the parameters used to characterize CCP particles.

Based on the results of above mentioned particle size analysis and chemical analysis of sieved fractions of CCP, the two mass size distribution functions were calculated using original computer code and taking into account:

- mass contribution of individual fractions and their size distribution;
- mean density of particles in particular sieve fraction of the CCP;
- overlapping the histograms corresponding to different sieve fractions.

Mass size distribution function for CCP particles, $f(D)$, in the form of distribution of relative mass of CCP, is defined as $f_i(D) = m_i /(M_{prop} \cdot \Delta D_i)$, where m_i is the mass of CCP in the i-th histogram sub-range (size interval), ΔD_i is the width of i-th size interval.

Mass size distribution function for unburnt aluminum in CCP, $f_i^{Al}(D)$, is defined as $f_i^{Al}(D) = f_i(D) \cdot \varepsilon_j^{Al}$, where $f_i(D)$ is the histogram of relative mass of CCP, ε_j^{Al} is the mass content of aluminum in the j-th sieve fraction. Index i is omitted below.

In accordance with chemical analysis results and commonly used notion the whole population of CCP particles was treated as consisting of *coarse* and *fine condensed combustion products.*

The CCP particles with size exceeding D_L are called here the *coarse* particles or ***agglomerates***. The particles with size $D<D_L$ are called *fine* or ***oxide*** particles.

For classical "readily agglomerating" propellants it is easy to establish bound size D_L as local minimum in mass size distribution function, $f(D)$, for CCP particles, as seen in Fig. 3.3a. For "weakly agglomerating" propellants it can be difficult to find such a minimum, see Fig.3.3b, because the portion of aluminum particles leaving without ignition the burning surface in the form of slightly sintered aggregates and that of individual particles with initial size can be noticeable [11]. At present time we used an universal method for determining bound size D_L, which divides coarse and fine particles. The bound size D_L corresponds to the minimum of experimental function f^{Al} (see Fig.3.3b). For propellant E12, belonging to classical "readily agglomerating" propellants, the minimum of $f^{Al}(D)$ function coincides with minimum of $f(D)$ function and is localized in the range 33-127 μm.

Dimensionless mass characteristics of CCP

The following mass characteristics were calculated for fine (smoke aluminum oxide) and coarse (agglomerate) particles on the basis of experimental mass size distribution functions for CCP particles $f(D)$ and for aluminum in CCP particles $f^{Al}(D)$. These parameters are scaled by M_{prop}, where M_{prop} is the total mass of propellant burnt. For example, $m_f = M_f / M_{prop}$ where M_f is the mass of fine particles.

m_f - mass of fine particles,

m^{Al}_f - mass of free aluminum in fine particles,

m_{ag} - mass of agglomerates,

m^{Al}_{ag} - mass of free aluminum in agglomerates,

$m_{ccp} = m_f + m_{ag}$ - total mass of CCP,

$m^{Al}_{ccp} = m^{Al}_{f} + m^{Al}_{ag}$ - total mass of aluminum in CCP,

m^{Al}_{prop} - initial mass of aluminum in propellant,

m_{ag}/m_{ccp} - mass fraction of agglomerates in CCP,

m_f/m_{ccp} - mass fraction of fine particles in CCP,

$[Al]_f = (m^{Al}_f/m_f)\cdot 100\%$ - percentage of free aluminum in fine particles,

$[Al]_{ag} = (m^{Al}_{ag}/m_{ag})\cdot 100\%$ - percentage of free aluminum in agglomerates,

$[Al] = (m^{Al}_{ccp}/m_{ccp})\cdot 100\%$ - percentage of free aluminum in CCP,

m^{Al}_f/m^{Al}_{prop} - relative quantity of free aluminum in fine particles,

$m^{Al}_{ag}/m^{Al}_{prop}$ - relative quantity of free aluminum in agglomerates*,

$m^{Al}_{ccp}/m^{Al}_{prop}$ - total relative quantity of unburnt aluminum in CCP,

$m_f : m_{ag}$ - mass ratio of fine particles and agglomerates in CCP,

$m^{Al}_f : m^{Al}_{ag}$ - mass ratio of free aluminum in fine particles and in CCP.

The ***mean diameter*** (size) of CCP particles, D_{mn}, is calculated by

$$D_{mn} = \sqrt[m-n]{\left(\sum_{i=1}^{k} D_i^m \cdot N_i\right) \Big/ \left(\sum_{i=1}^{k} D_i^n \cdot N_i\right)},$$

where D_i is the midrange and N_i is the number of particles in i-th size range. To calculate mean size D_{mn} on the basis of experimentally determined mass size distribution we used following formula to obtain effective number of particles N_i in a given i-th size interval:

$$N_i = \frac{m_i}{\frac{\pi}{6} D_i^3 \rho_p},$$

where density of CCP particles ρ_p was assumed to be the same in overall size range and equal 2.4 g/cm^3.

The mean diameters for fine particles were calculated in the size range from 0.5 μm to D_L. The mean diameters for agglomerates were calculated in the size range from D_L to D_R, where D_R is an effective maximum size of agglomerates. The procedure for determining D_R will be discussed in the next section.

*) This parameter (incompleteness of aluminum combustion) was used in our previous works [2, 3] being designated as "η".

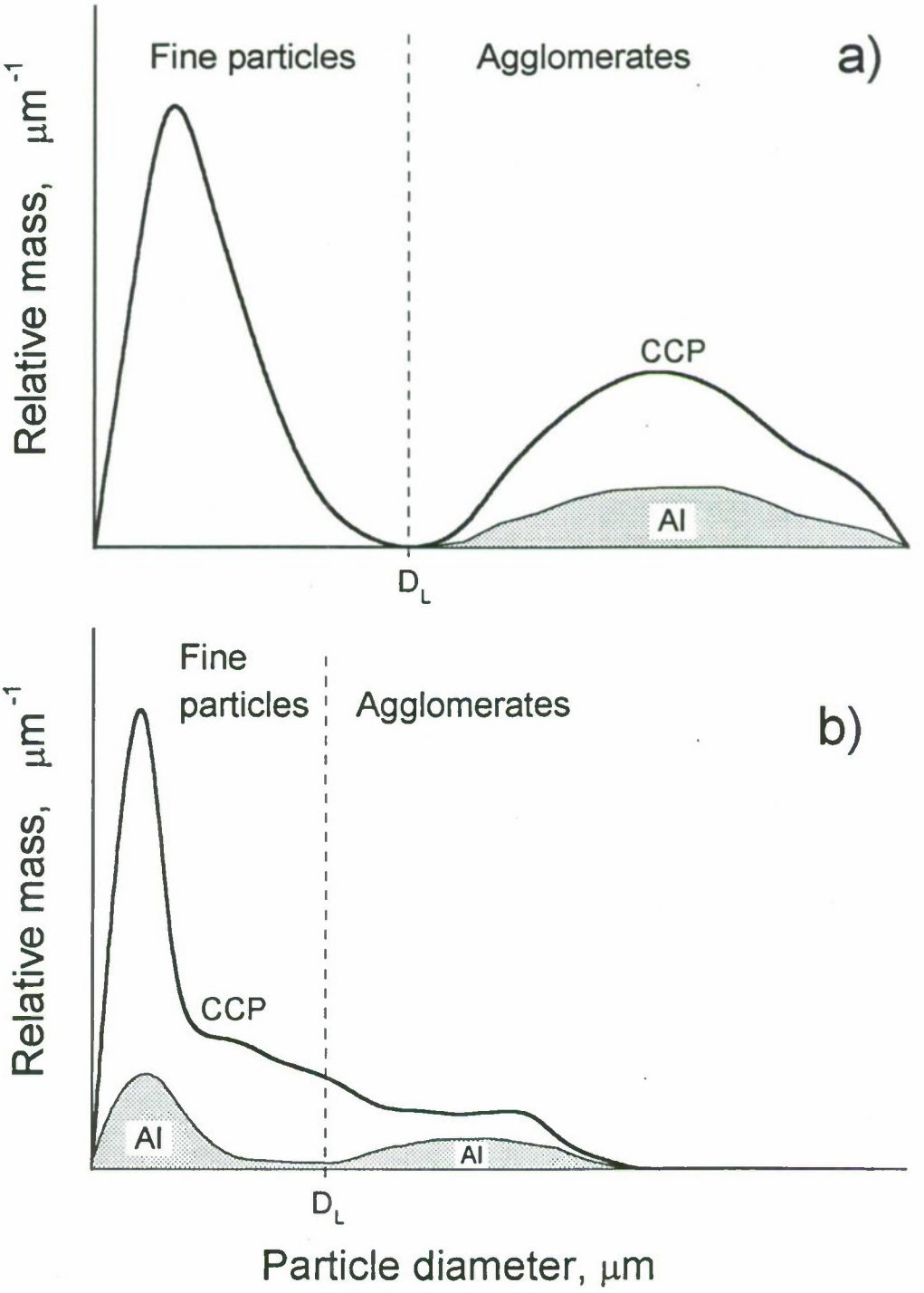

Fig. 3.3.

The scheme of determining the bound size D_L dividing the fine particles and agglomerates in CCP for "readily agglomerating" (a) and "weakly agglomerating" (b) propellants.

4. EXPERIMENTAL DATA ON CONDENSED COMBUSTION PRODUCTS

4.1. Experimental program.

Main set of experimental data. The detailed mass size distribution in the size range from 0.5 μm to 3500 μm (maximum sampled particle diameter) for condensed combustion products and for unburnt aluminum in condensed products was determined at three pressure levels 1, 22, and 64 atm in dependence of residence time for particles in flame. The variation of the residence time was provided with three types of geometry of the firing tests, see Fig. 3.2:

A) Small diameter of the propellant samples (7 mm) without protective tube (shortest residence time).

B) Normal diameter of the propellant samples (11.5 mm) without protective tube (medium residence time).

C) Normal diameter of the propellant samples (11.5 mm) with 100 mm long protective tube (longest residence time).

Each type of geometry was used at all pressure levels to determine evolution of condensed combustion products in a wide range of the experimental conditions.

Addition 1. Special "pure" experiment with propellant sample without any contaminating inhibitors covering the lateral surface was performed to verify fine particle size distribution and to check one of the assumptions about the origin of the extra large agglomerates. In this test the propellant sample was fixed by its butt-end on glass plate with glue and burnt at pressure 11.8 atm.

Addition 2. The experimental estimation of reproducibility of particles sampling and of the quality of the propellant samples manufacturing was performed via testing six small size propellant samples (weight about 0.7 g each) followed by independent treatment like as separate experimental series. These tests were made in firing geometry *A* at pressure 1 atm.

Addition 3. To check the effect of the mounting cylinder, the special tests were performed using the teflon cylinders instead of the plexiglas ones. The tests were made in firing geometry *A* at pressure 1 atm.

4.2. General characteristics of sampled CCP.

The example of mass size distribution function for sampled CCP particles is presented in Fig. 4.1 in linear (*a*) and logarithmic scale (*b*). The plots show the results obtained in one particular case at pressure 66 atm in test geometry *B*. However, it demonstrates all common features of the results obtained in this study. Examining Fig. 4.1, one may conclude that:

- The tested propellant produces classical large size agglomerates of aluminum that consist of hundreds of virgin metal particles. The contribution of agglomerates into total mass of CCP (in this particular case) amounts 0.23. The total range of CCP particle sizes is extremely wide with maximum size of agglomerates about 2200 μm, but main contribution into agglomerates mass is provided by particles with size up to approximately 600 μm. The main portion of non-consumed aluminum is localized in agglomerates that contain 0.16/(0.01+0.16)=0.94 of total mass of free aluminum in sampled CCP.

• The range of variation of relative mass (vertical axis) is also broad and amounts about 6 orders of magnitude.

• There is well pronounced boundary D_L between coarse and fine CCP particles in the mass size distribution function. The first are agglomerates containing (in dependence on particle size) 27-35% of free aluminum. The last are mainly oxide smoke particles containing less than 1% of free aluminum. The dividing size is characterized by the low value of the mass distribution function of CCP as well as low value of the mass distribution function of free aluminum in CCP (Fig. 4.1b). In presented case the size D_L is taken to be equal to 119 μm in accordance with above described approach. However, one can see in the Fig. 4.1 that for studied propellant this choice is not critical for calculations of mass size characteristics because the value of relative mass in some region to the left and to the right of D_L is also very low.

• For agglomerates the behavior of mass size distribution function for unburnt aluminum is similar to behavior of that for CCP. The reason for this similarity is that the aluminum content in agglomerates is approximately constant in sieve fractions 150-300, 300-450, and 450-600 micron at every firing condition, including the particular case presented in Fig. 4.1. Detailed data on content of unburnt aluminum in CCP are reported in Table 4.1. This fact can be treated as independence of agglomerates structure on their size and as the result of presumable aluminum oxidation at the early stage of forming the agglomerates rather than the oxidizing processes at the stage of motion of agglomerates away from the burning surface.

• In Fig.4.1b one can see that the mass distribution function of CCP exhibits non-monotonous behavior at the right hand side. There is gradual reduction of relative mass *f(D)* with diameter after maximum resulting in local minimum and then there are local maxima that correspond to individual extra large size CCP particles. As will be shown below, it is the result of transient burning out of the last portion of propellant sample (thin layer near the butt-end of mounting cup – sample holder). Therefore, we disregard these particles as normally formed agglomerates. The agglomerates with size exceeding D_R were excluded from calculations, when determining mean sizes D_{mn} , but they were taken into account when determining mass characteristics of CCP particles. The effective maximal size of agglomerates D_R was determined on the basis of the experimental *f(D)* function as a local minimum size after the function becomes non-monotonous (interruptive).

• In Fig. 4.1b one can see that the mass size distribution function for fine (oxide) CCP particles has the main peak located in the range 2.4-3 μm that corresponds to fifth size interval of Malvern's histogram. This fact was observed also in our previous investigations and by other authors. The mechanism of formation of oxide particles with such size is not clear yet.

In order to provide detailed description of experimental data on sampled CCP particles we will discuss separately the results corresponding to the coarse and fine size CCP. The reason for this is the natural division of total size distribution of CCP into 2 global modes that are seen from plots in Fig. 4.1.

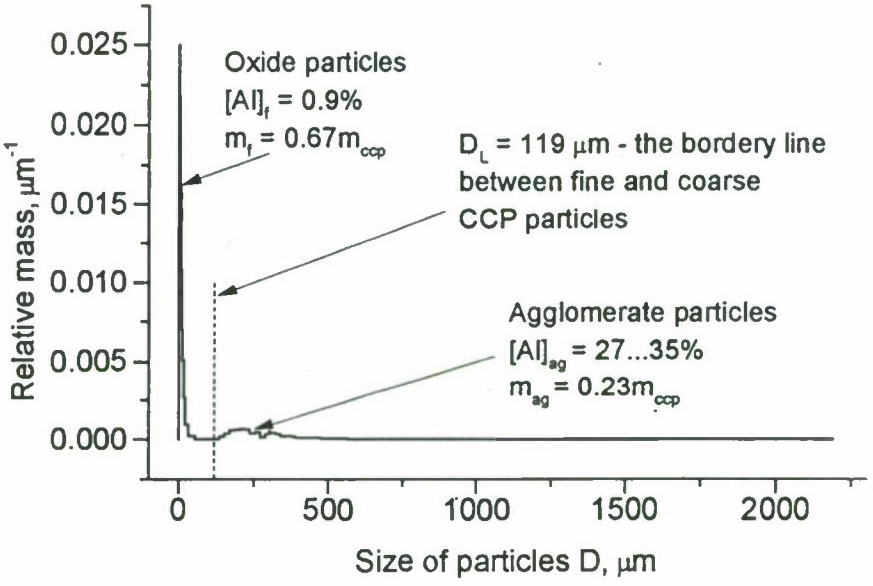

a)

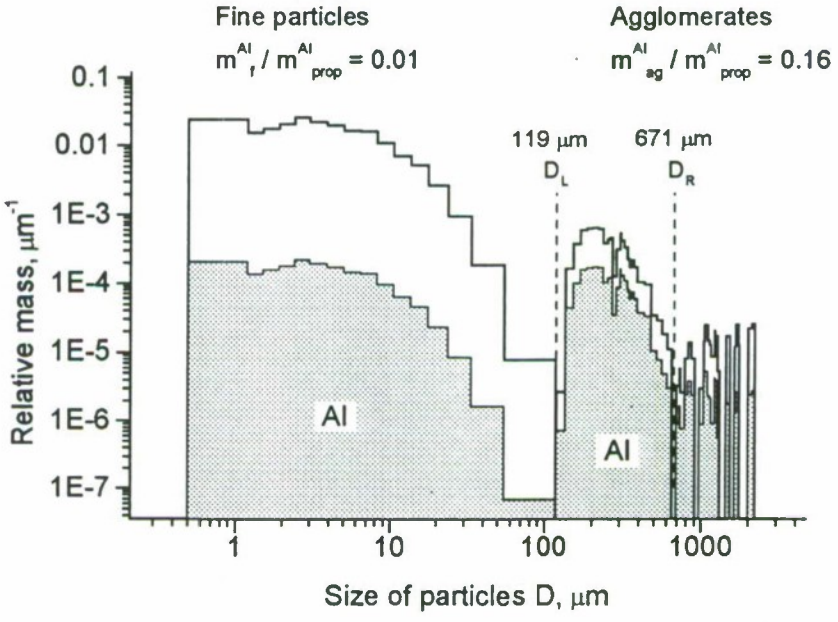

b)

Fig. 4.1.

Typical relative mass size distribution *f(D)* of CCP particles plotted in linear (a) and in logarithmic (b) scale. Additionally, in Fig. 4.1 (b) is presented the mass size distribution $f^{Al}(D)$ of free aluminum in CCP (bottom shadowed histogram). It should be noted that in the case (b) the area under histogram curves is **not** proportional to value of mass of particles.

Firing conditions: pressure 66 atm, sampling geometry *B*.

Table 4.1. Chemical analysis data on unburnt aluminum (% mass.) for individual sieve fractions of CCP particles

P, atm	Type of the test geometry	< 130 μm	130-300 μm	300-450 μm	450-600 μm	600-900 μm	900-960 μm	> 960 μm
1	A	1.76±0.14	49.2±0.15	46.8±1.0	53.1±0.9	46.9	49.3	
1	B	0.49±0.02	51.2±0.2	45.0±0.3	41.6±1.0	36.4	≅40.2	
1	C	$2.3\pm0.1_3$	45±2	44.8±0.1	45.0±1.5	39.9	24.6	
22.3	A	0.30±0.06	47.8±0.5	47.8±1.3	≅47.3	≅40	33.7	
23.8	B	$1.20\pm0.03_4$	45.7±0.5	49.9±0.3	≅44.5			
24.3	C	0.93±0.06	$38.0\pm0.2_3$	40.9±0.2	≅36.8	≅27	≅27	
63.5	A	0.46±0.04	$22.8\pm1.0_3$	37.0±0.4	≅27.0	≅26.3	≅27.5	
65.8	B	0.87±0.08	26.6±1.6	34.9±0.1	≅26.8	≅29	≅10.6	
67.3	C	0.47±0.02	23.8±0.1	30.4±0.1	≅24.4	≅23.2	27.2	

Comments:

1. The data in extended boxes correspond to the joint fraction with small absolute mass.
2. The data presented correspond to the mean result of analyses of independent probes. The figure after sign ± corresponds to standard error of determined value. This figure is not written if mass of given fraction of CCP was too small to repeat an analysis and only one determination was made. The number N of independent determinations of aluminum content in most cases was equal 2 excluding the cases when N=3 or N=4. These cases marked by numerical sub-script that corresponds to the value N.
3. The sign ≅ in some boxes corresponds to low accuracy data due to small absolute mass of the probe (fraction).

4.3. Agglomeration characteristics of propellant and evolution of coarse CCP particles.

4.3.1. Effective maximal size of agglomerates.

Most of experimental data reported below are obtained with propellant samples inserted into plexiglas tube supplied with bottom plug made of teflon. The value D_R corresponding to local minimum at right wing of *f(D)* function was taken as effective maximal size of agglomerates in calculation of the mean characteristic size of agglomerate D_{mn}. To find out the cause of appearance of extra large agglomerates the special test was carried out. The propellant sample with diameter 11.5 mm was fixed by its butt-end on glass plate with fast drying glue "Moment-2" and burnt at pressure 11.8 atm. The mean burning rate estimated by burning time was about 8.6 mm/s that close to the burning rate at pressure level 20 atm because the lateral surface of propellant sample was not inhibited. Sampled particles were thoroughly studied. The residue on glass plate was examined by optical microscope. Then the precipitated particles were subjected to particle size and chemical analyses (the last one was made with particles extracted from glass).

The overall view of residue is presented in Fig. 4.2. One can observe the white colored area on the glass plate covered with fine oxide particles (Fig. 4.2a, *1*), numerous coarse particles, adhered to plate (Fig. 4.2a and 4.2b, *2*), and the arc-shaped propellant residue (Fig. 4.2a and 4.2b, *3*). Black area is covered by soot-like material.

The agglomerate size distributions for particles on the glass plate and for all agglomerates including particles from glass plate are presented in Fig. 4.3. It is evident that the elongated right tail in mass size distribution is caused mainly by particles from the glass plate. We assume that these particles are presented in CCP in ordinary experiments with teflon bottom plug which do not retain particles after end of combustion. This assumption gives the basis for establishing the effective maximal size of agglomerates D_R as local minimum in "normal" size distribution function and for calculating the agglomerate mean size D_{mn} in the size interval from D_L to D_R.

The results on determining free aluminum content corresponding to the case of burning of non-inhibited sample are presented in Table 4.2 (shadowed lines) along with the data obtained in sampling geometry type *B* at pressures 1 atm and 23.8 atm. The abbreviation "NA" – not available – means the absence of particles in given fraction.

Table 4.2. Comparison of chemical analysis data (unburnt aluminum % mass.) obtained in geometry *B* (pressures 1 and 23.8 atm) and for non-inhibited sample (P = 11.8 atm).

P, atm	< 130 μm	130-300 μm	300-450 μm	450-600 μm	600-900 μm	900-960 μm	> 960 μm
1	0.49±0.02	51.2±0.2	45.0±0.3	41.6±1.0	36.4	≅40.2	NA
11.8	0.31±0.05	51±3	48.8		≅50		
Particles from glass plate			≅33.6				
23.8	1.20±0.03	45.7±0.5	49.9±0.3	≅44.5			

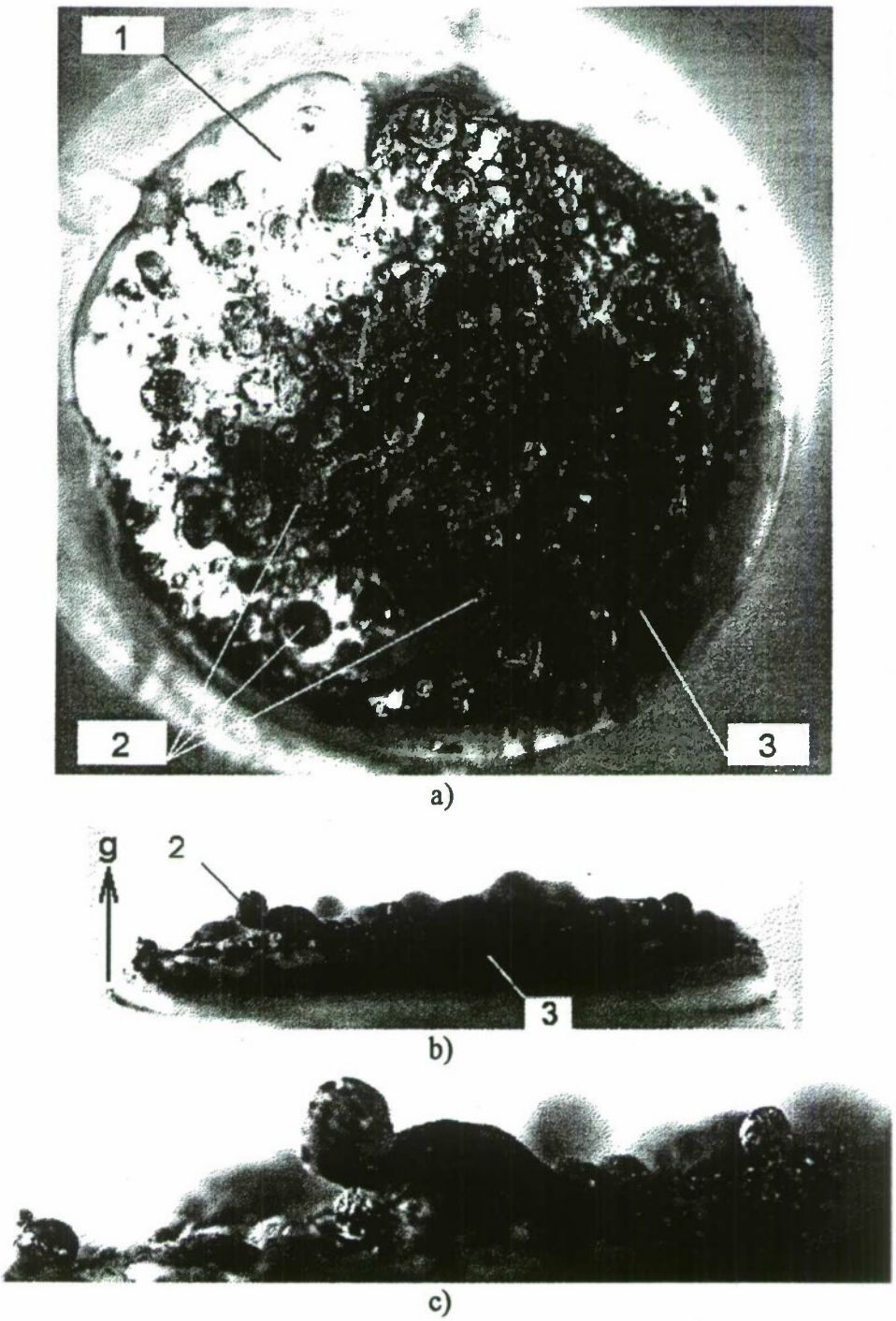

Fig. 4.2. The residue of non-inhibited propellant sample after combustion on the glass plate. Sample diameter is 11.5 mm. Vector g represents the gravity force direction during combustion.

a) front view; b) side view; c) enlarged fragment of the picture (b).

1 - area covered with fine smoke oxide particles;

2 - extinguished agglomerates;

3 - arc-shape residue of extinguished propellant material (unfocused).

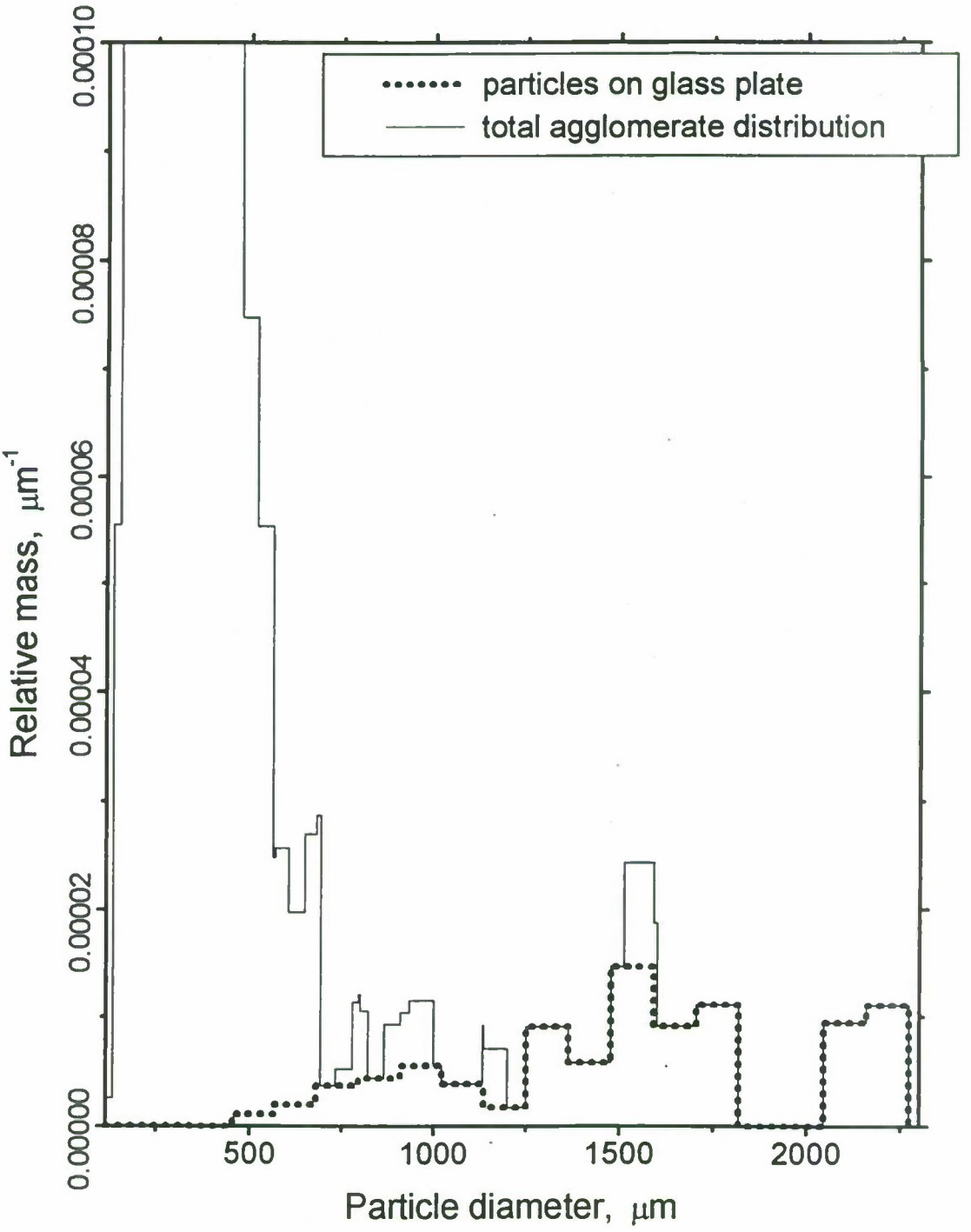

Fig. 4.3. Mass size distribution of the condensed combustion products sampled during combustion of non-inhibited propellant sample fixed on glass plate. Pressure 11.8 atm.

4.3.2. Size distribution of coarse CCP particles and unburnt aluminum content.

The mass size distribution of coarse CCP particles (or agglomerates) and the size distribution of unburnt aluminum in agglomerates calculated on the basis of chemical analysis results (Table 4.1) are presented in Figs. 4.4-4.6. The characteristic sizes of agglomerates D_{mn} calculated in size range (D_L-D_R) are presented in Table 4.3, the mass parameters are presented in Table 4.5. For comparison, the characteristic sizes D_{mn} calculated in size range (D_L-D_{max}) are presented in Table 4.4. In this case D_{max} is the true maximal size of sampled particles. It can be easily seen (Table 4.4) that the characteristic sizes D_{32}-D_{53} turn out excessively large and this is result of including abnormal large particles into size distribution.

Analyzing the data corresponding to different pressure levels, one may conclude:

- The agglomerate size decreases with pressure. The main portion of agglomerate mass is in the size range from D_L to approximately 780-810 μm at atmospheric pressure, from D_L to 660-790 μm at pressure about 22 atm, and from D_L to 670-680 μm at pressure about 64 atm. Correspondingly, the mean agglomerate size decreases with pressure. This effect is most pronounced for the highest order size (D_{30} and higher). For example, D_{43} is 380-405 μm, 290-311 μm and 272-303 μm, Table 4.3.
- Relative agglomerate mass m_{ag}, contribution of agglomerates into total CCP mass m_{ag}/m_{ccp}, and proportion between masses of agglomerate and oxide particles m_{ag}/m_f decrease with pressure.
- In all cases practically entire amount (91-99%) of free aluminum is in agglomerates. The percentage of non-burnt aluminum in agglomerates $[Al]_{ag}$ amounts 26-50% and decreases with pressure as well as the relative mass of free aluminum in agglomerates m^{Al}_{ag} and incompleteness of aluminum combustion in agglomerates $m^{Al}_{ag}/m^{Al}_{prop}$.

Examination of agglomerate structure under microscope showed that they are aggregates made of individual (close to original size) particles covered as whole with relatively thin oxide layer (like sack). The structure is similar for agglomerates in different size range. Indirect evidence for this could be the fact that the content of unburnt aluminum in sieved fractions 130-300, 300-450, 450-600 mm is approximately the same in pressure range 1-64 atm (see Table 4.1).

There are several models of agglomeration [12, 13, 14, 15, 16, 17] that may be used for evaluating the agglomerate size. Unfortunately, there is too little known about the real properties of the surface layer at elevated temperatures and pressures and it is difficult to predict quantitatively the size of agglomerate. Note one important feature of agglomerate size distribution evolution with pressure for propellant under study: the sizes of small order, e. g. D_{10}, change in less extent than the high order ones. It means that the fraction of largest particles becomes less and one may assume that at elevated pressures the formation of agglomerates due to coalescence of original particles from several neighboring "pockets" becomes less pronounced.

Let us consider now the evolution of agglomerates in dependence on residence time in flame. First we would like to give some comments on the way of calculation of the particle motion characteristics.

The real poly modal size distribution of agglomerates was replaced by mono-modal one with size corresponding to mean size D_{30}, determined for particles sampled in geometry type *A*.

The density of particles was taken from experimental data as mean density in corresponding size interval. It was assumed be equal 2.16 g/cm^3 in all calculations.

The residence time t_{res} of particles in flame (*or* in hot products of propellant combustion) in accordance with [9] was calculated by the formula

$$t_{res} = (t_{res}|_L + t_{res}|_{L+h})/2,$$

where $t_{res}|_L$ is the time which particle spends to pass a distance L which is equal to sum of protective tube length L_{tube} and characteristic length L_{mix} of initial area for mixing length of the hot combustion products with co-current flow of nitrogen, $t_{res}|_{L+h}$ is the time which particle spends to pass a distance $L+h$, here h is the propellant sample length. Thus, we take into account the difference in residence time for particles starting from front surface at the begining of combustion and starting from bottom of mounting cylinder (sample holder) at the end of combustion.

The characteristic length of mixing L_{mix} is calculated by the formula [18] for turbulent co-current coaxial streams taking into consideration the difference in temperature and density of mixing gases.

It is assumed that the initial velocity of particle equals zero and the particle is accelerated due to gravity force and drag (Stokes law) force action. The velocity of gaseous combustion products is determined by the mass continuity equation in the form

$$V_{gp} = \rho_{NM} \cdot r \cdot (1-\alpha)/\rho_{gp},$$

where ρ_{NM} is the density of non-metalized part of metalized propellant, r is the burning rate, α is the mass fraction of non-gasified part of propellant (equal in our case to aluminum content in propellant α_{Al}), ρ_{gp} is the density of gaseous combustion products and is calculated according to the equation of state for ideal gas. The value ρ_{NM} is calculated by the formula

$$\rho_{NM} = \rho_{prop} \cdot (1-\alpha_{Al})/(1-\rho_{prop} \cdot \alpha_{Al}/\rho_{Al}),$$

where ρ_{prop} ·and ρ_{Al} are the densities of propellant and aluminum, correspondingly. The temperature of gaseous combustion products T_{gp}, used for ρ_{gp} calculation, was taken equal to the flame temperature obtained in thermodynamics calculation at given pressure. The Russian code ASTRA-2 was used. The molecular mass of gaseous combustion products M_{gp}, used in Stokes law, also was taken from thermodynamics calculation. It should be underlined that M_{gp} is not mean but only gaseous product molecular mass. Dynamic viscosity of the gaseous combustion products is described by formula [19]:

$$\mu = (0.87 \cdot 10^{-7}) \cdot M_{gp}^{0.5} \cdot T_{gp}^{0.65},$$

where μ in [Pa·s], T_{gp} in [K]. The values M_{gp} and μ are used in the Stokes law.

The results of calculations are presented in Tables 4.6a and 4.6b. Parameter Z designates the mass fraction of condensed products in total mass of combustion products.

The data presented in Table 4.6a correspond to pure propellant. The data in Table 4.6b were obtained taking into account the real mass loss of sample holding cylinder and protective tube due to ablation process during propellant sample combustion. In this case the calculations were made for the effective "propellant" formulation consisting of mass of propellant itself and plexiglas mass burnt out in course of propellant combustion. The plexiglas mass lost was determined experimentally. One may see that in the experiments with protective tube the accompanying combustion of plexiglas leads to noticeable reduction in the flame temperature (and slightly changes another parameters). The lower values from Table 4.6b were used in the calculation of the residence time. It is interesting to note that thermodynamics calculations showed the presence in condensed combustion products of some amounts of alternative products – soot and aluminum nitride. In all cases of combustion without tube the calculated condensed combustion products consisted of aluminum oxide only.

The data on real experimental parameters (pressure, burning rate, nitrogen flow rate) and on calculated parameters for mixing of freezing nitrogen with combustion products (gaseous combustion products temperature and velocity, length of initial mixing area) as well as calculated

residence time are presented in Table 4.7. Particle diameter D_{part} corresponding to mean size D_{30} was calculated in the size range D_L-D_R for agglomerates sampled in geometry type *A*.

The effect of residence time on $m^{Al}_{ag}/m^{Al}_{prop}$ – relative amount of free aluminum in agglomerates – is shown in Fig. 4.7. The confidence intervals (bars) were estimated via reproducibility test [2, 3]. Briefly, this test consists of repetition of the whole experimental series at given conditions followed by data treatment that includes particle size and chemical analyses. Then final parameters (for example, $m^{Al}_{ag}/m^{Al}_{prop}$) are treated as different realizations of probabilistic value for which one may determine the confidence interval by traditional statistical approach using the Student coefficient [20, 21]. In presented cases the numerical value of confidence interval was calculated for 70%-reliability and was equal about 5-6% of evaluated value $m^{Al}_{ag}/m^{Al}_{prop}$.

Examining Fig. 4.7 one can see the specific behavior of aluminum consumption at different pressures. At pressure level ~ 65 atm no change in aluminum content is observed in time interval 30-95 ms, and amount of free aluminum in agglomerates has lowest value as compared with that for another pressures. Obviously, in this case a significant portion of aluminum was consumed and during the first stage of formation and detachment from the burning surface the rest of metal was encapsulated and could not burn entirely. At atmospheric pressure there is noticeable change of aluminum content in time interval 20-25 ms, and then it is approximately constant while residence time is 25-70 ms. If the slow oxidation of aluminum is caused by capsulation, it is necessary to note that the level of limiting consumption value depends on pressure. At pressure ~22 atm the intermediate behavior is observed.

The data in Table 4.3 and Figs. 4.4-4.6 indicate that there is no significant evolution in size distribution of agglomerates even in the cases of 1 atm and 22 atm when burning out of aluminum is observed. So it has a single meaning that some consumed portion of agglomerate aluminum is replaced by aluminum oxide (another part of oxide mass go out with gas flow in the form of smoke particles). The agglomerate mass is modified very slightly during this process, see Table 4.5.

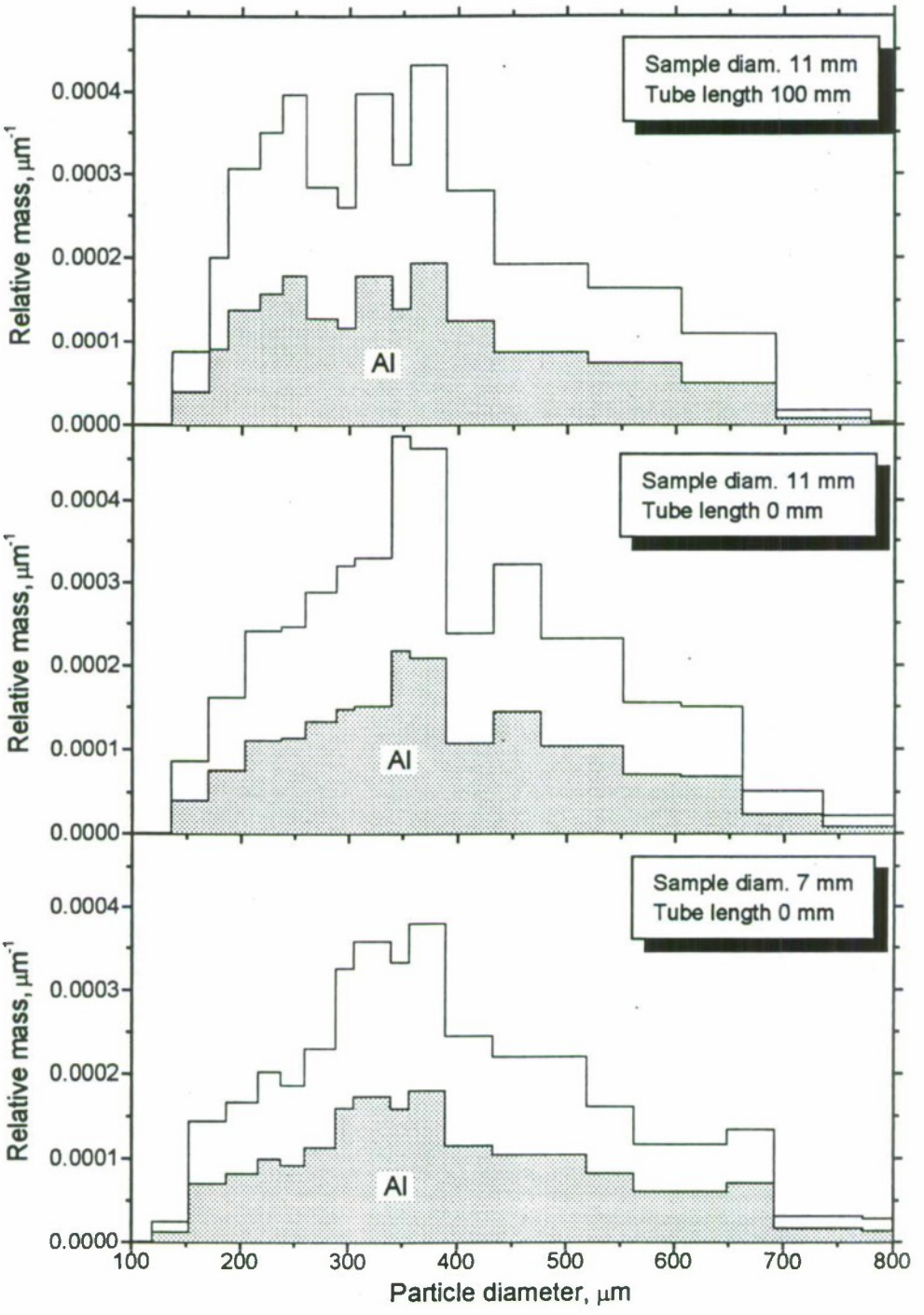

Fig. 4.4.

Mass size distribution of coarse CCP particles and unburnt aluminum (shadowed) in coarse CCP particles at varied firing geometry type (bottom – *A*, middle – *B*, top – *C*. The residence time increases from the bottom to top). Pressure 1 atm.

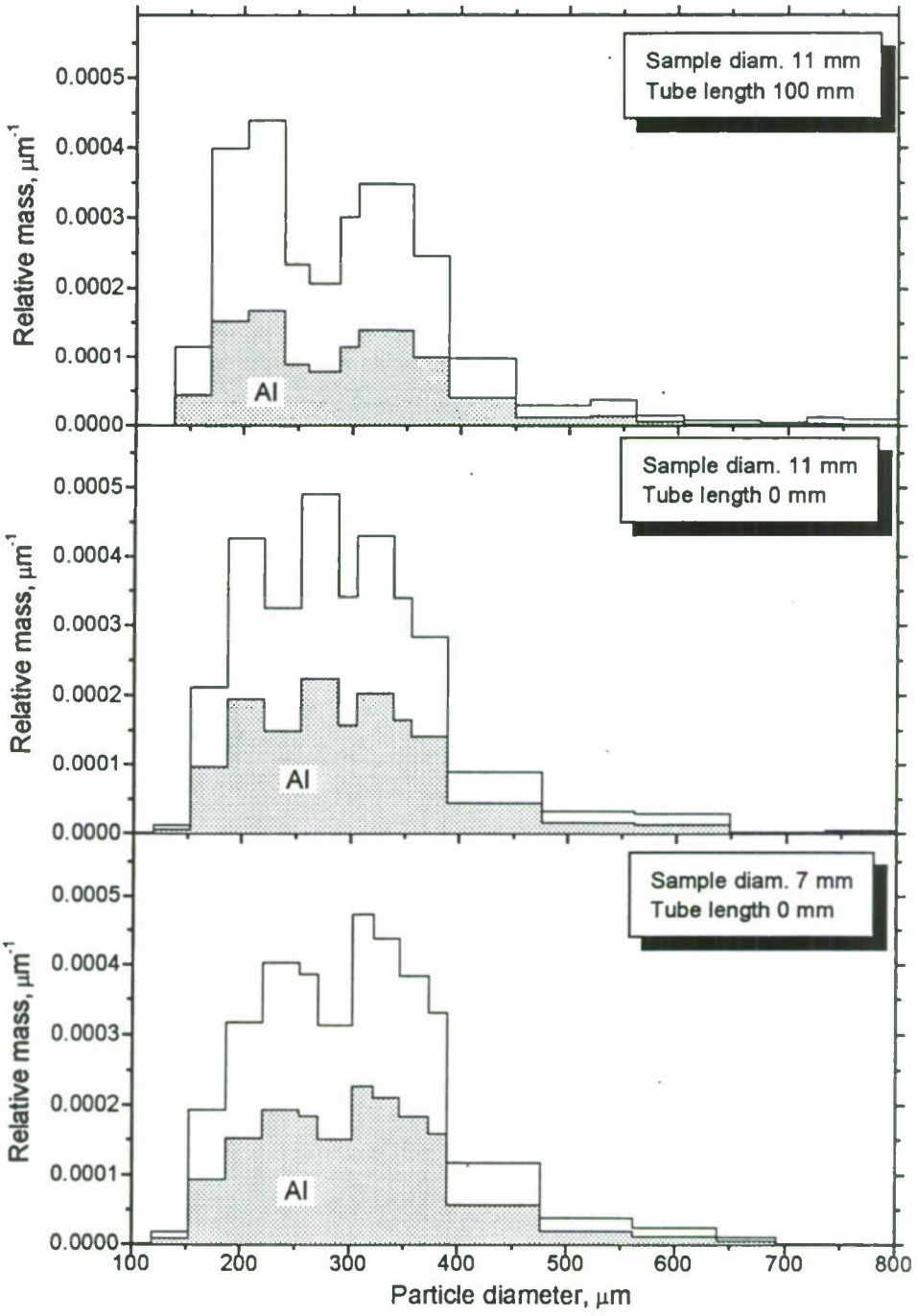

Fig. 4.5.

Mass size distribution of coarse CCP particles and unburnt aluminum (shadowed) in coarse CCP particles at varied firing geometry type (bottom – *A*, middle – *B*, top – *C*. The residence time increases from the bottom to top). Pressure level ~20 atm, more precisely 22.3, 23.8 and 24.3 atm in the cases of *A*, *B* and *C* geometry type, correspondingly.

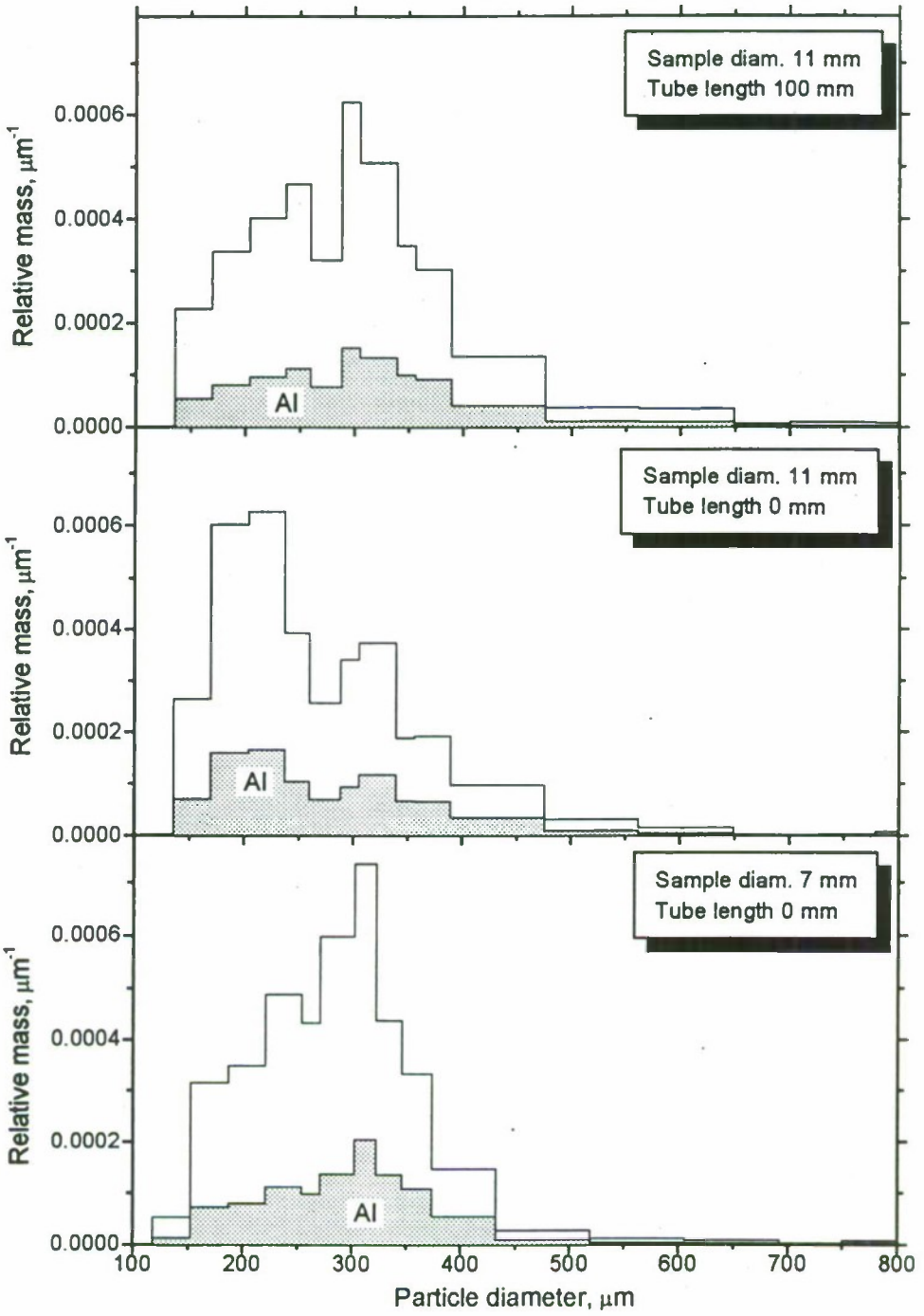

Fig. 4.6.

Mass size distribution of coarse CCP particles and unburnt aluminum (shadowed) in coarse CCP particles at varied sampling geometry type (bottom – *A*, middle – *B*, top – *C*. The residence time increases from the bottom to top). Pressure level 60 atm, more precisely 63.5, 65.8 and 67.3 atm in the cases of *A*, *B* and *C* geometry type, correspondingly.

Table 4.3. Agglomerate mean diameter D_{mn} (μm), calculated in the size range D_L-D_R, in dependence on sampling conditions.

P, atm	Geometry type	D_L-D_R, μm	D_{10}	D_{20}	D_{30}	D_{21}	D_{32}	D_{43}	D_{53}
1	A	119 - 800	260	280	302	302	351	405	430
1	B	119 - 779	275	294	314	314	358	404	426
1	C	127 - 806	252	269	288	286	330	380	405
22.3	A	87 - 790	238	249	260	259	284	311	325
23.8	B	95 - 771	234	243	253	253	275	301	316
24.3	C	87 - 662	222	231	241	240	263	290	306
63.5	A	127 - 671	225	234	244	244	265	286	297
65.8	B	119 - 671	207	215	224	223	244	272	288
67.3	C	44 - 696	223	234	246	245	272	303	320

Table 4.4. CCP particle mean diameter D_{mn} (μm), calculated in the size range D_L-D_{max}, in dependence on sampling conditions.

P, atm	Geometry type	D_L-D_{max}, μm	D_{10}	D_{20}	D_{30}	D_{21}	D_{32}	D_{43}	D_{53}
1	A	119-2537	265	295	340	327	451	714	897
1	B	119-1625	277	300	327	324	389	490	564
1	C	127-2450	253.9	274	302	295	366	515	652
22.3	A	87–3542	238.8	251	269	263	310	513	863
23.8	B	95–1818	234	244	257	255	283	337	397
24.3	C	87–2209	223	234	253	246	294	426	578
63.5	A	127–1905	226	237	251	248	283	371	482
65.8	B	119–2191	208	217	234	227	270	417	608
67.3	C	44–1900	224	237	255	250	296	411	541

Table 4.5. Mass characteristics of coarse CCP particles, calculated in the size range D_L-D_{max}, in dependence on sampling conditions.

P, atm	Geom. type	m_{ag}	m_{ag}/m_{ccp}	m_{ag}/m_f	m^{Al}_{ag}	m^{Al}_{ag}/m^{Al}_f	$[Al]_{ag}$, %	$m^{Al}_{ag}/m^{Al}_{prop}$
1	A	0.1682	0.528	53:47	0.0818	97:3	49.6%	0.409
1	B	0.1535	0.500	50:50	0.0700	99:1	45.6%	0.35
1	C	0.1518	0.483	48:52	0.0660	95:5	43.5%	0.33
22.3	A	0.1106	0.302	30:70	0.0514	99:1	46.5%	0.257
23.8	B	0.1022	0.297	30:70	0.0478	94:6	46.8%	0.239
24.3	C	0.0985	0.210	21:79	0.0366	91:9	37.2%	0.183
63.5	A	0.1233	0.320	32:68	0.0327	96:4	26.4%	0.164
65.8	B	0.1208	0.333	33:67	0.0327	94:6	27.1%	0.164
67.3	C	0.1273	0.329	33: 67	0.0327	96:4	25.7%	0.164

Table 4.6a. Thermodynamics data calculated for "pure" propellant.

P, atm	T_{gp}, K	M_{gp}	Z (Al_2O_3)
1	3234	18.7	0.329
22.3	3634	19.6	0.328
23.8	3642	19.7	0.328
24.3	3645	19.7	0.328
63.5	3765	19.9	0.331
65.8	3769	19.0	0.331
67.3	3772	19.9	0.331

Table 4.6b. Thermodynamics data calculated for real experiments when the propellant combustion is accompanied with ablation of plexiglas tube.
These data were used in residence time calculations.

P, atm	Geometry type	T_{gp}, K	M_{gp}	Z (total)	Z(AlN)	Z(soot)
1	A	2843	18.1	0.28	0	0
1	B	3030	18.2	0.30	0	0
1	C	1975	17.5	0.20	0.10	0
22.3	A	3216	18.5	0.30	0	0
23.8	B	3412	19.0	0.31	0	0
24.3	C	2248	16.4	0.29	0	0.06
63.5	A	3408	18.8	0.31	0	0
65.8	B	3430	19.0	0.31	0	0
67.3	C	2433	18.1	0.24	0.02	0.003

Table 4.7. The sampling experiment parameters and calculated data on residence time t_{res}

P, atm	Geometry type	r, mm/s	N_2 flow rate, g/s	T_{gp}, K	V_{gp}, m/s	L_{mix}, cm	D_{part}, μm	t_{res}, ms
1	A	1	0	2843	18	1.8	302	20.4
1	B	1	0	3030	21	2.7	302	22.3
1	C	1.1	0	1975	13	3.0	302	68
22.3	A	7.6	2	3216	7	1.8	260	26.4
23.8	B	7.9	1.3	3412	7	2.7	260	30.8
24.3	C	8.3	1.1	2248	5	2.9	260	85
63.5	A	11.3	2	3408	3.7	1.7	244	31.5
65.8	B	12.7	1.8	3430	4.0	2.6	244	37
67.3	C	16	2	2433	3.6	2.9	244	92

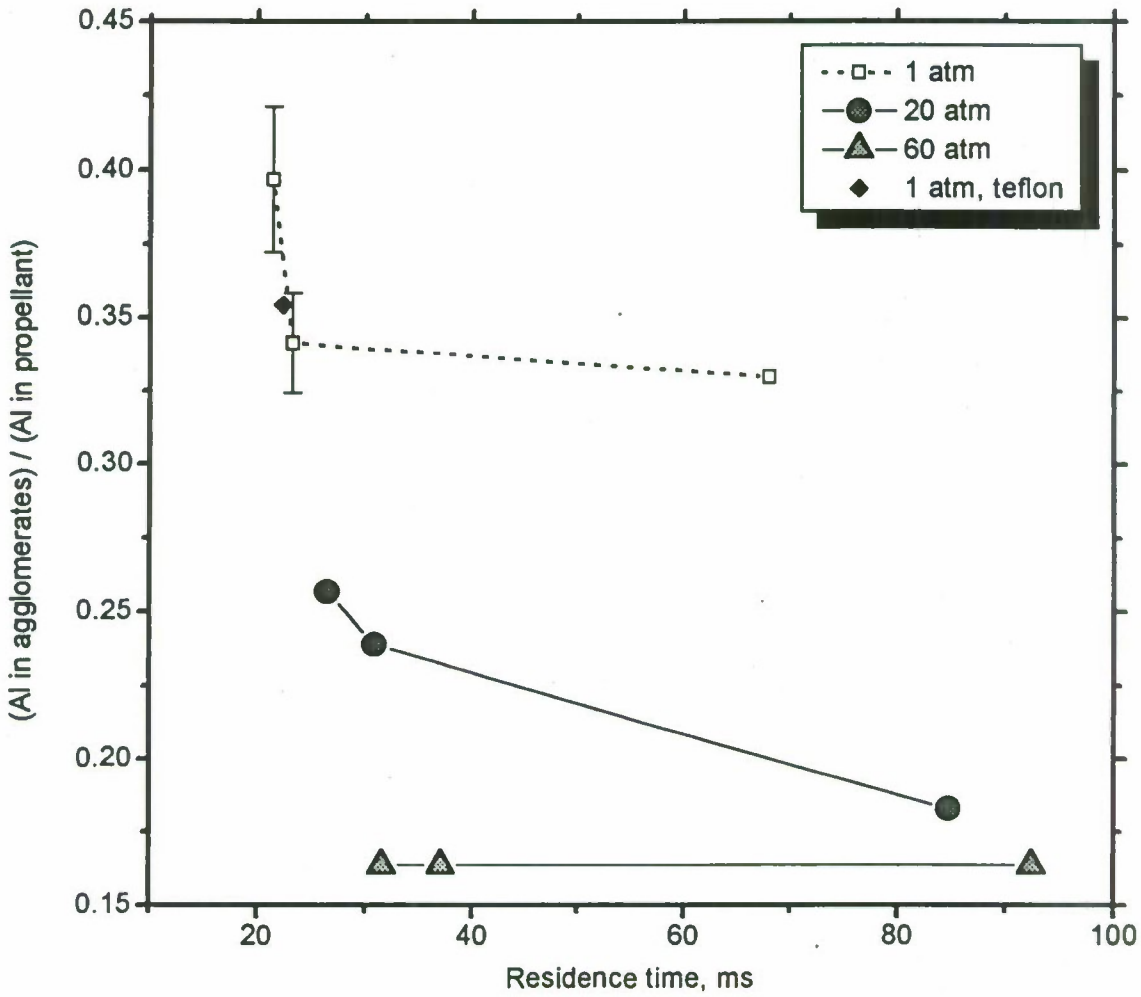

Fig. 4.7. Incompleteness of aluminum combustion *vs* agglomerate residence time.

Diamond-shape point corresponds to experimental series with teflon propellant holder instead of plexiglas one. The pictured confidence intervals were estimated via reproducibility test (see text for more details).

4.4. Density of coarse CCP particles.

The density of agglomerates is important parameter in calculation of the particles velocity field inside solid rocket motor. In present work 122 determination of the sampled agglomerates density was performed for sieved individual fractions of CCP with size exceeding 130 μm. To obtain density value a given CCP fraction was placed on the inclined copper plate to eliminate electric charge and particles of round shape were selected. After that the particles were weighed and examined by microscope. The density was calculated by the formula

$$\rho = m \Big/ (N \frac{\pi}{6} D_{30}^3),$$

where m is the mass of particles, N is their number, D_{30} is the average size.

The estimated error [21] can be calculated as

$$\Delta\rho = \rho \cdot \sqrt{\left(\frac{3\Delta D_{30}}{D_{30}}\right)^2 + \left(\frac{\Delta m}{m}\right)^2 + \left(\frac{\Delta N}{N}\right)^2}.$$

To calculate $\Delta\rho$ the instrumental errors of the method were taken as follows:

- ΔD_{30} = 9, 22, 30-70 μm - in dependence on fraction size,
- Δm = 0.00015 g (scale characteristic),
- ΔN =0.

Figure 4.8 presents complete data set on the mean density of CCP particles *vs* particle diameter, including the extra large particles that are not "normal" agglomerates. One can see a common trend to the decrease of mean density with particle size. The selected data for agglomerates in size range D_L-D_R are presented in Fig. 4.9 for different pressure levels. Taking into account the relatively high experimental error (see example in Fig. 4.10) it is hard to talk about any significant trend for data presented in Fig. 4.9. It should be noted that measurement of particle size gives main contribution into summary error $\Delta\rho$.

Figure 4.11 demonstrates correlation between agglomerate density and free aluminum content. As a result of difference in neat aluminum density (2.7 g/cm^3) and aluminum oxide density (approximately 3.9 g/cm^3), the agglomerate density increases with aluminum oxide content in agglomerates. It is interesting no note that the higher pressure, the wider variation of free aluminum content in agglomerate population. One of possible explanation for this fact is as follows. Starting from burning surface with approximately the same aluminum content, the agglomerates with different size have different acceleration and spend different time to pass the "freezing" distance. Thus, the relatively slowly moving agglomerates can reach higher combustion completeness. This effect strongly depends on pressure. The higher pressure, the smaller gas velocity and the longer residence time for gas that involves the higher "differentiation" of agglomerate population in terms of velocity, residence time and achieved combustion completeness. The correlation density-aluminum content is presented in Fig 4.12 for one selected fraction of CCP through all experimental conditions. The data correspond to sieved fraction 130-300 μm that has maximum weight among other agglomerate fraction practically at all firing conditions.

The results obtained can be summarized as follows.

- The sampled agglomerate density in most cases less than neat aluminum density that indicates that the agglomerates are not compact solid particles. Sometimes one may see the gaseous cavern inside the agglomerate, Fig. 4.13.
- The strongly pronounced correlation between "normal" agglomerate size and density has not been observed. The following approximate equation was obtained after treatment of the set of experimental data corresponding to particles with size in interval D_L-D_R:
$\rho = 2.16 + 2.13698 \cdot 10^{-6} \cdot D_{10}$, where ρ in g/cm^3, D_{10} in μm. The value $\rho = 2.16$ g/cm^3 was used in the subsequent calculations of agglomerate residence time.
- There is correlation between density and free aluminum content. The more aluminum in agglomerates is replaced with oxide, the higher their density.

It should be noted that only first statement is common, but the last two are specific for propellant under study.

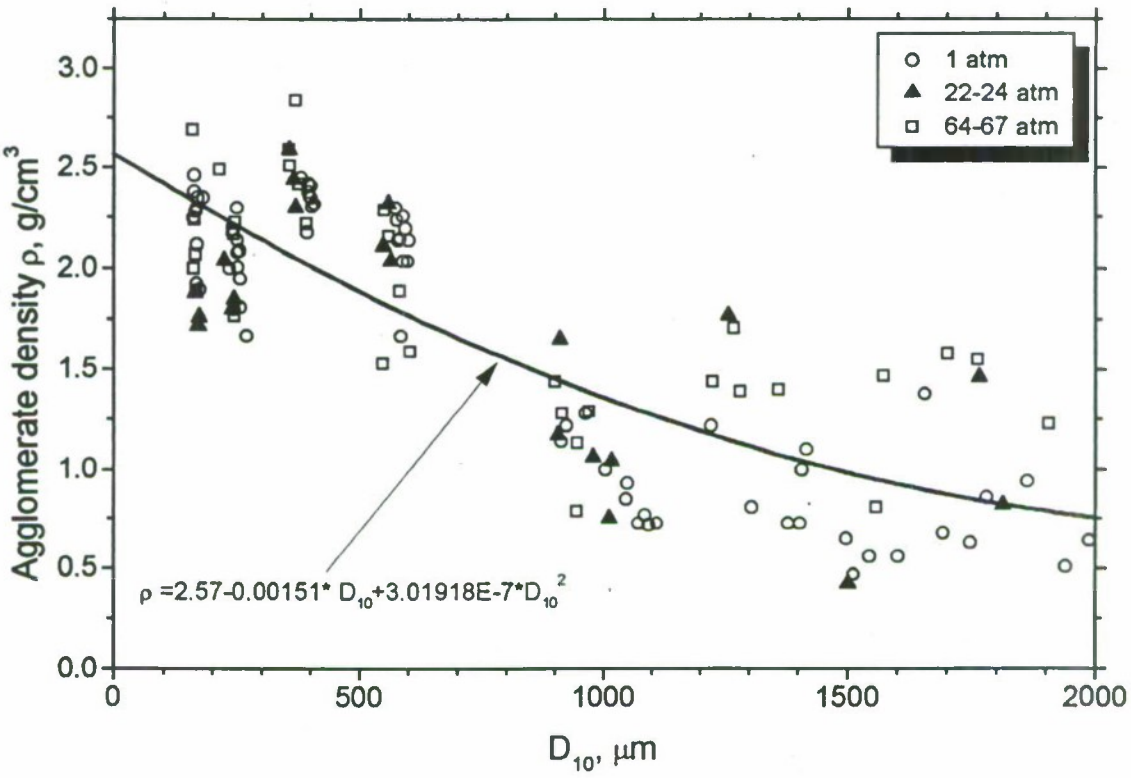

Fig. 4.8. Mean density of coarse CCP particles *vs* diameter. Whole data set is presented.

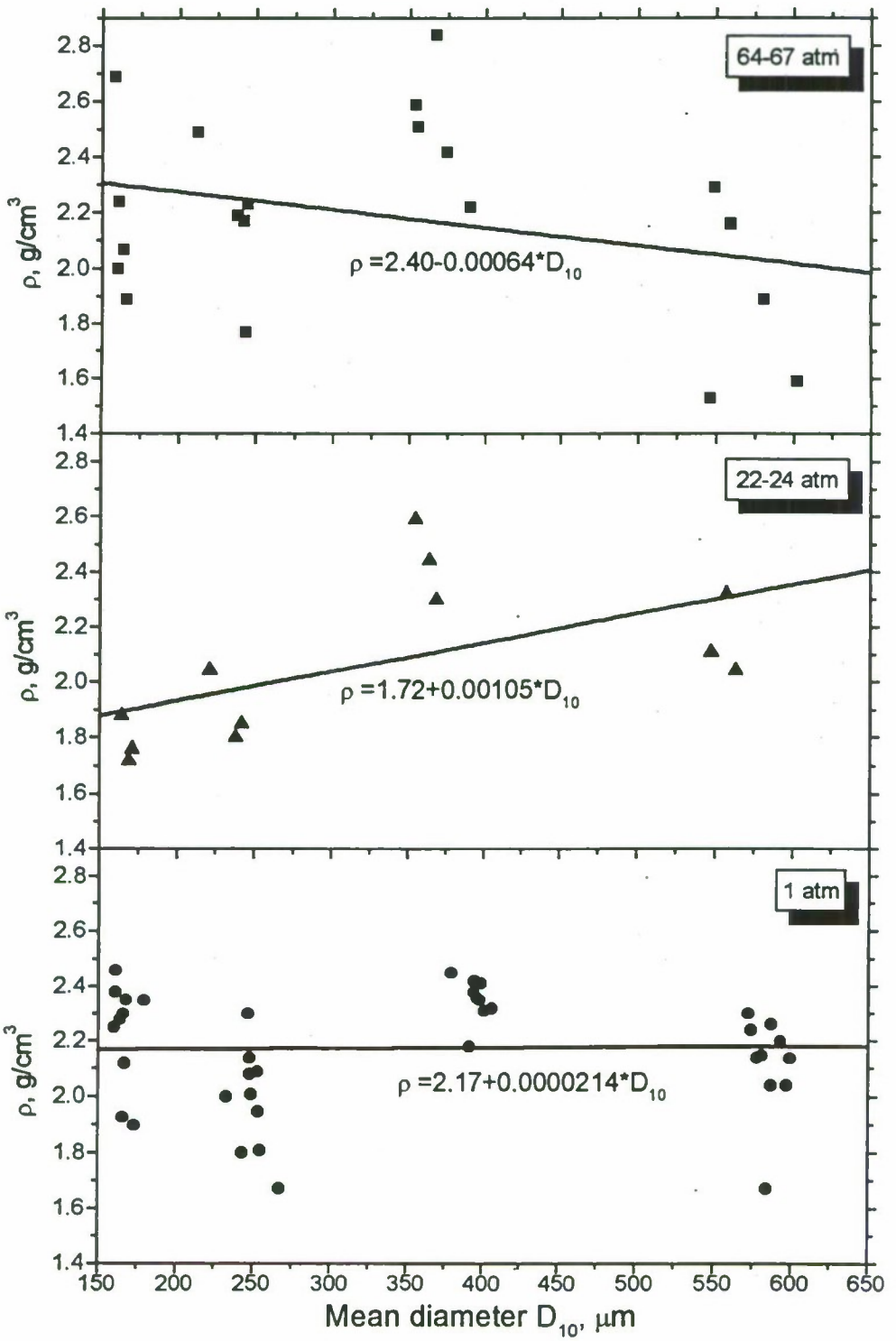

Fig. 4.9. Mean agglomerate density *vs* particle diameter. The selected data for agglomerates in size range D_L-D_R are presented for three pressure levels.

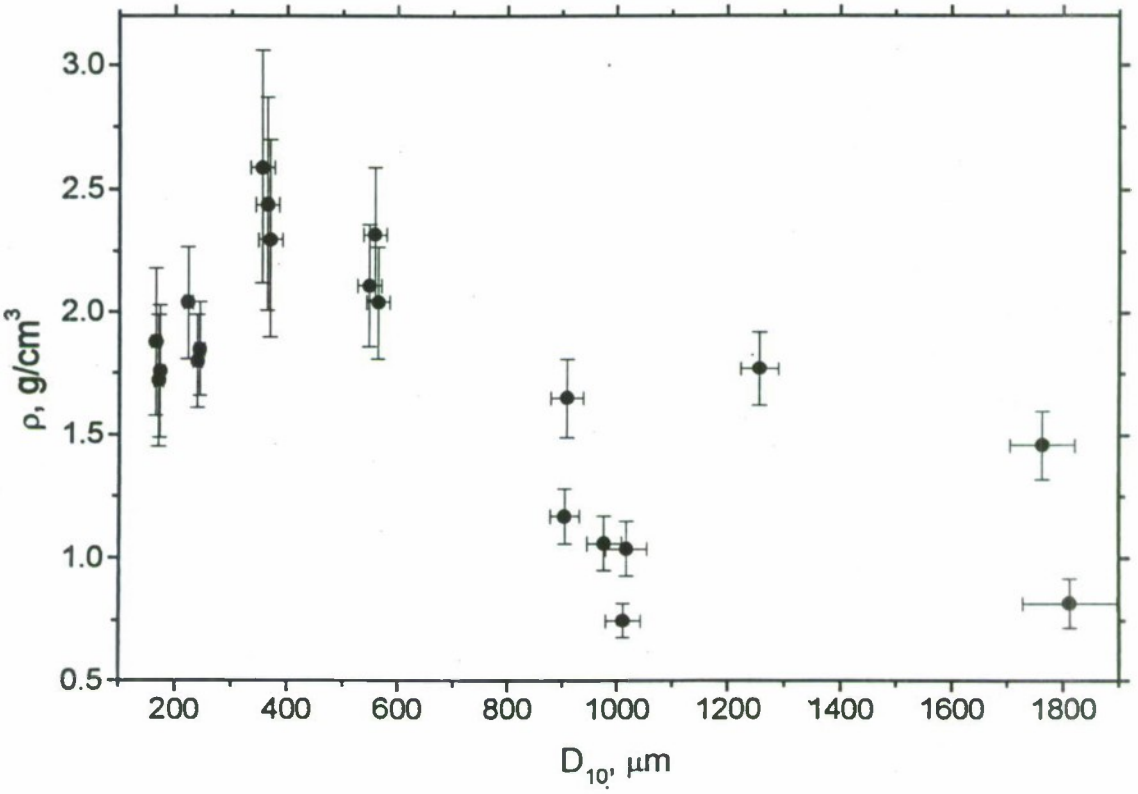

Fig. 4.10.

The illustration of the estimated experimental errors for agglomerate size and mean density. Presented data correspond to pressure 22-24 atm.

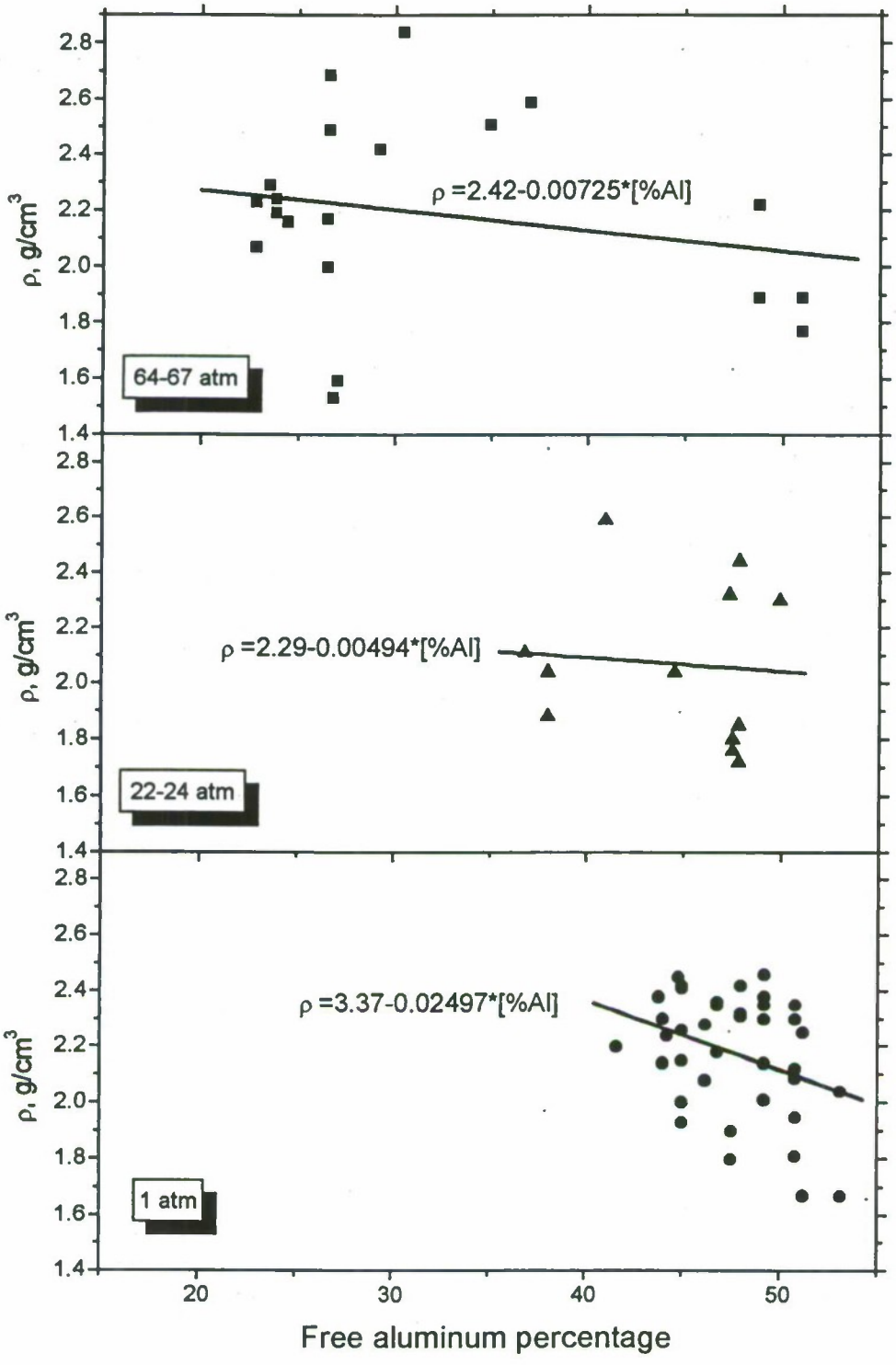

Fig. 4.11. Mean agglomerate density in dependence on free aluminum content. The data presented correspond to the "normal" agglomerates in size range D_L-D_R.

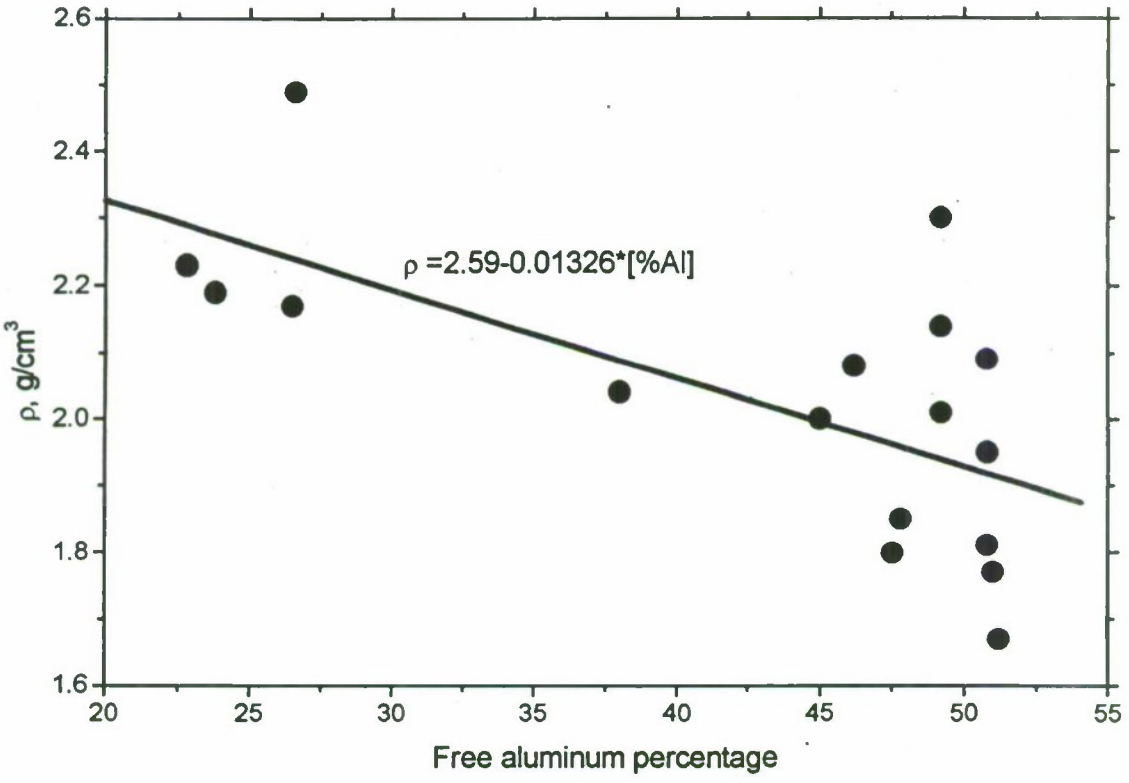

Fig. 4.12. Mean density of agglomerates in sieved fractions 160-280 μm in dependence on free aluminum content. The data presented corresponding to the pressures 1-67 atm and residence time 20-90 ms.

Fig. 4.13. Gaseous bubble inside the agglomerate.

4.5. Morphological analysis of coarse CCP particles

The CCP coarse particles (> 130 μm) were examined by optical stereoscopy microscope with magnification up to 56^X. The outward appearance of particles was different depending on the size and nature of material. Table 4.8 presents summary of the visualization data with subsequent description of typical view of collected particles.

Table 4.8. Observation of certain type particles in coarse CCP fractions.
The sequence of listing corresponds to frequency of observations.

Fraction, μm	Sampling conditions: Pressure and geometry type (*A*, *B*, *C*)		
	1 atm, *A*	1 atm, *B*	1 atm, *C*
130-150	Agg, AggIr, AggFu, Oxz	Agg,, AggFl	Agg
150-300	Agg, AggIr, AggFu	Agg, AggFl	Agg
300-450	Agg, AggIr, AggFu, DCap	Agg, AggIrr	Agg, DCap
450-600	Agg, AggIr, AggFu, AggMat	Agg, AggMat, AggIrr, Oxz	Agg
600-900	Agg, AggIr, AggFu	Agg, AggFus, AggIrr,AggMat	Agg, AggFu
900-965	Agg, AggIr, AggFu	AggFus, Agg	AggFu, Agg
> 965	Agg, AggIr, AggFu, DCap	-	AggFu
	22.3 atm, *A*	23.8 atm, *B*	24.3 atm, *C*
130-150	Agg	Agg	Agg
150-300	Agg	Agg	Agg
300-450	Agg	Agg	Agg, AggFu, AggMat
450-600	Agg	Agg	Agg, AggFu
600-900	Agg	Agg	Agg, AggFu
900-965	Agg	Agg, AggMat	Agg, AggFu, AggIr
> 965	AggFu, Agg	Agg, AggMat	Agg, AggFu
	63.5 atm, *A*	65.8 atm, *B*	67.3 atm, *C*
130-150	Agg, AggIr	Agg, OxC	Agg, OxC, OxH
150-300	Agg, Oxz, OxH	Agg, OxC	Agg, OxC
300-450	Agg, AggFu, AggFl, DCap	Agg, OxC, DCap	Agg, OxC
450-600	Agg, AggFu	Agg	Agg
600-900	Agg	Agg, AggMat	Agg, AggFu, DCap
900-965	Agg	Agg, AggFu, DCap	Agg, AggFu
> 965	AggFu	Agg, AggFu	AggFu, Agg,

Agg - agglomerate,
AggMat - matrix agglomerate,
AggIr - irregular agglomerate,
AggFl - flake of agglomerates,
AggFu - fused agglomerate,
Oxz - oxidizer (AP or HMX) grain,
OxC - compact oxide,
OxH - hollow oxide shell,
DCap - detached oxide cap.

Agg (agglomerate, Fig. 4.14) - major condensed product of combustion in the range 130-2000 μm. The particles have spherical or acorn-type shape and are covered with hard surface layer of dark gray or black color. The portion of particle surface covered with oxide "cap" does not depend directly on size of agglomerate. The particles of different appearance can be found at the same size fraction at pressure level 1 atm. In this case the portion of the particle surface covered with cap can be approximately 1/4-2/3. However, in the case of pressure ~64 atm and sometimes in the case of pressure ~24 atm, practically the whole agglomerate surface is covered with oxide shell. As a rule, there is only one hole in a surface layer with overflowing non-compact material that consists of individual small spheres. This material is certainly free aluminum containing because it readily reacts with NaOH solution that is easily detected by gas bubbles release. A hard layer probably consists of aluminum oxide and does not react with NaOH solution. When etching in NaOH, the agglomerate releases through the hole some unsolved condensed products (flakes) that may indicate the presence of some amount of aluminum oxide inside agglomerate. The final residue after long time etching in NaOH is hollow spherical shell. It can be seen through the hole a wrinkled interior surface of the shell.

The hard surface layer ("shell") of large agglomerates in sieved fractions with size exceeding 450 μm in most cases has numerous cracks, in which a non-compact material can be seen. It was possible sometimes to evaluate the shell thickness examining the crack's edge. The shell thickness was found to be about 10-25 μm for particles 300-450 μm in size, 10-40 μm for particles 450-900 μm, and up to 50 μm for particles exceeding 900 μm. Additionally, sometimes one can see the cavities through the hole in shell. It may be assumed that these cavities cause the low value of particle density.

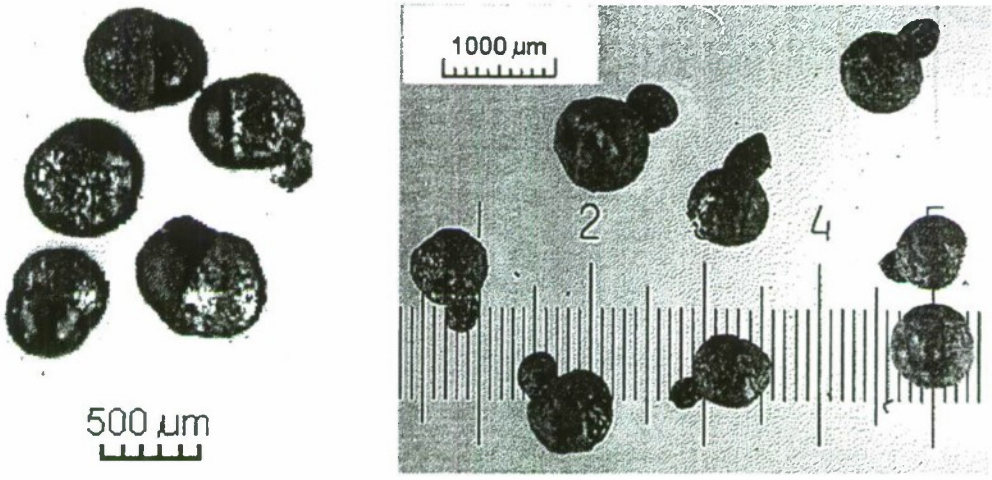

a) b)

Fig. 4.14. Agglomerate particles.

a) Acorn type with varied relative size of oxide cap (P=1 atm, geometry B, fraction 450-600 μm)
b) Closed type (P=24 atm, firing geometry type B, sieved fraction 600-900 μm).

AggMat (matrix agglomerate, Fig. 4.15). The peculiarities of their nature were described previously in [2, 8, 22]. The matrix agglomerates are characterized by numerous metal inclusions at the exterior surface. Long time etching with NaOH leaves the holes at the place of inclusions. The matrix agglomerates were rarely observed at all pressures.

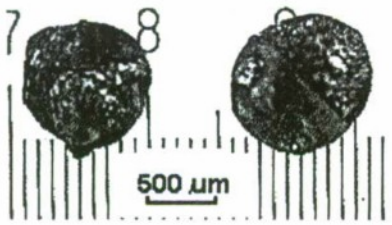

Fig. 4.15.
Matrix agglomerate.
(P=1 atm, firing geometry type A,
sieved fraction 900-965 µm).

AggIr (irregular agglomerate, Fig. 4.16) - grapes shape irregular aggregates consisting of spherical particles. They were revealed in various fractions of particles. When the fraction size decreases, they become more spherical (in shape) and similar to "normal" agglomerates.

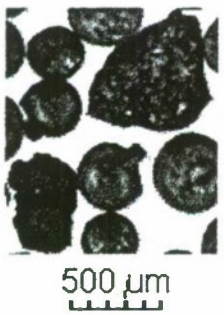

Fig. 4.16.

Two irregular shape agglomerates (aggregates) among normal agglomerates.
(P=64 atm, firing geometry type A,
sieved fraction 450-600 µm).

AggFl (flake of agglomerates) - non-spherical flat shape aggregates of sintered small particles were rarely observed mainly at atmospheric pressure. The possible way to form flake of agglomerates is to sinter CCP particles during their deposition on the metal sieves installed above the collecting filter. The flakes were not destroyed in course of wet and dry sieving of CCP.

AggFu (fused or melted agglomerate, Fig. 4.17). - non-spherical, non-compact aggregates consisting of 2-10 pseudo spherical large particles. Fused agglomerates were observed mainly in sieved fraction with size exceeding 600 µm. The reason for these particles formation is transient combustion process near the end of propellant sample (see Chapter 4.3.1).

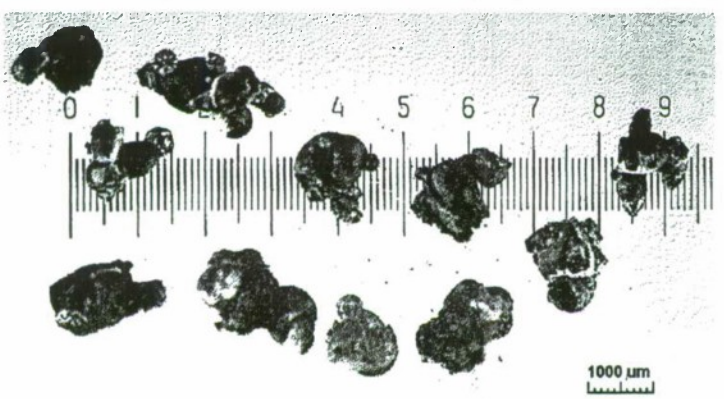

Fig. 4.17.
Fused (or semi melted) agglomerates.
(P=1 atm, firing geometry type B,
sieved fraction 900-965 µm).

Oxz - grains of oxidizer (AP or HMX, Fig. 4.18) were very rarely observed in different fractions from 130-150 μm up to 450-600 μm. Their contribution into total amount of CCP is negligibly small.

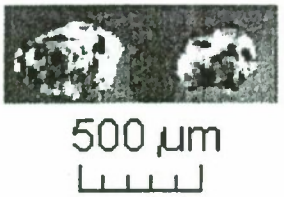

Fig. 4.18. Sampled oxidizer grains.

OxC (compact oxide) and **OxH** (hollow oxide) - white color oxide particles were observed in significant amount in fraction 130-150 μm at of pressure level ~64 atm in cases of sampling geometry type *B* and *C* that correspond to maximal aluminum depletion. In another cases they were observed very rarely.

DCap – oxide caps seems to be detached from agglomerates in course of sieving. In is interesting to note that their inner surface has numerous caverns, which look like gas bubbles existing between agglomerate and cap surfaces before destruction.

In conclusion of this section the agglomerate images are presented that can be treated as experimental evidence of opportunity for subsurface frame consisting of semi-sintered aluminum particles to hold the agglomerate on the burning surface, Fig. 4.19.

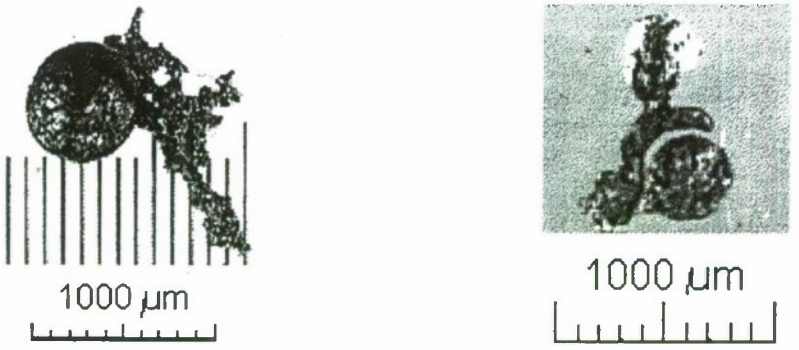

a) b)

Fig. 4.19. The bound of agglomerate with subsurface frame layer.

In Fig. b one may see the arc shape aggregate consisting of semi sintered aluminum particles. The radius of the aggregate corresponds to oxidizer grain size. Obviously, it represents the "frozen pocket" in propellant structure.

4.6. Fine CCP particles.

4.6.1. The technique of size analysis.

The size distribution of small particles (sieve fraction < 130 μm) was analyzed with commercial sizer Malvern 3600E using acetone as carrier liquid. The suspension was preliminary treated during 40 seconds by ultrasound and then was mechanically mixed in course of measurement. The total size range 0.5-118.4 μm was divided at 16 channels with exponential increment of sub-range width. We will use below the number (No.) of channel to characterize size of sampled particles. The correspondence between size range and its number is shown in Table 4.9. Left bound (0.5 μm) of the first interval has conventional meaning.

Table 4.9.
Histogram size of particle sizer Malvern 3600E for operational option with lens F=63 mm.

Channel No	Left bound, μm	Right bound, μm
1	0.5	1.2
2	1.2	1.5
3	1.5	1.9
4	1.9	2.4
5	2.4	3.0
6	3.0	3.9
7	3.9	5.0
8	5.0	6.4
9	6.4	8.2
10	8.2	10.5
11	10.5	13.6
12	13.6	17.7
13	17.7	23.7
14	23.7	33.7
15	33.7	54.9
16	54.9	118.4

4.6.2. Contamination of the condensed combustion products with products of sample holder combustion.

In previous works [2, 3] we found that use of epoxy compound for inhibition of the lateral surface of burning sample gave considerable contamination contribution into total mass of the condensed combustion products. In present work the cylinders made of plexiglas or teflon were used for lateral surface inhibiting. The masses of cylinder and bottom made of teflon, as well as protective tube made of plexiglas were measured before and after firing test to evaluate the contribution of contaminating products. Additionally, there could be some contamination contribution from igniting wire, but it was negligibly small in our experiments. It should be underlined that use of quartz tubes is not convenient because the burning agglomerates very readily adhere to quartz.

When analyzing the condensed combustion products of metalized propellants, one should also take into account contribution due to burning of non-metalized part of propellant. However, in the available literature there is no data on the magnitude of above listed contributions.

It is evident that products of combustion of materials contacting with hot combustion/decomposition products of propellant will contribute to the fine particles, because thermodynamic calculations show that the soot is most expected condensed product forming in course of plexiglas and teflon combustion. This is why we examine this problem in section devoted to the fine particles behavior.

The upper estimate of the maximum contribution of condensed products from plexiglas and teflon is presented in Table 4.10, where:

m_{ccp} is the mass of sampled CCP scaled by mass of propellant burnt M_{prop},

m_{wp} is the diminution of plexiglas mass scaled by mass of propellant burnt M_{prop},

m_{wt} is the diminution of teflon mass scaled by mass of propellant burnt M_{prop},

$m^c_{wp} = 0.60 \cdot m_{wp}$ – relative mass of carbon in plexiglas,

$m^c_{wt} = 0.24 \cdot m_{wt}$ – relative mass of carbon in teflon,

$m^c_w = m^c_{wp} + m^c_{wt}$ – total relative mass of soot,

m^c_w/m_{ccp} – mass ratio of maximal possible contamination by soot and experimental relative mass of sampled CCP.

It should be underlined that making this rough estimate we assume that all carbon containing in plexiglas or teflon converts into soot. Molecule of polymethylmetacrilate (plexiglas) is $[-CH_2-C(CH_3)(COOCH_3)-]_n$, molecule of teflon is $[-CF_2-CF_2]_n$. In reality only some portion of consumed carbon forms soot, another portion forms gaseous compounds like CO, CO_2, etc. The data in Table 4.10 give idea about maximal potential contamination of CCP due to holder material ablation. One can see that:

1) At identical conditions, the mass loss of cylinder made of teflon m_{wt} approximately twice as much than that of plexiglas one m_{wp} (compare shadowed cells of Table). Thus, plexiglas is more proper material for using in such experiments.

2) In most cases (excluding the geometry type *C* with elongated protective tube) the proportion of contamination mass and mass CCP m^c_w/m_{ccp} do not worse than 24:76. Practically it means that we must take into consideration the contaminating contribution only in the case of geometry type *C*.

Table 4.10. The upper estimate for potential contamination of CCP by plexiglas and teflon ablation products

P, atm	Geomety type, cylinder material	m_{ccp}	m_{wp}	m^c_{wp}	m_{wt}	m^c_{wt}	m^c_w	m^c_w/m_{ccp}
1	A, teflon	0.360	0	0	0.201	0.048	0.048	13:87
1	A, plexiglas	0.318	0.126	0.076	0.003	0.001	0.077	24:76
1	B, plexiglas	0.307	0.075	0.045	0.002	0.0005	0.0455	15:85
1	C, plexiglas	0.314	0.336	0.202	0.0003	0.0001	0.2021	64:36
22.3	A, plexiglas	0.366	0.096	0.058	0.002	0.0005	0.0585	16:84
23.8	B, plexiglas	0.344	0.055	0.033	0.002	0.0005	0.0335	10:90
24.3	C, plexiglas	0.470	0.415	0.249	0.001	0.0002	0.2492	53:47
63.5	A, plexiglas	0.385	0.073	0.044	0.001	0.0002	0.0442	12:88
65.8	B, plexiglas	0.363	0.071	0.043	0.005	0.001	0.0431	12:88
67.3	C, plexiglas	0.387	0.256	0.154	0.007	0.002	0.1542	40:60

For more correct consideration of contaminating products contribution into sampled CCP products it is necessary to perform more detailed chemical analysis with determining aluminum oxide, aluminum nitride, metallic aluminum, carbon (soot) and other compounds containing in sampled CCP.

4.6.3. Fine CCP particle characteristics.

The experimental data on evolution of fine CCP particles size distributions are presented in Figs. 4.20-4.22. The characteristic sizes D_{mn} calculated in size range (0.5 μm - D_L) are presented in Table 4.11, while the mass parameters are presented in Table 4.12.

Below we analyze the evolution behavior of fine particles at different pressures when varying sampling geometry type (*A*, *B*, *C*).

At pressure 1 atm the firing geometry practically does not affect mass size distribution (Fig. 4.20). The presence of local maxima in 5-6th histogram size intervals, i. e. within the range 2.4-3-3.9 μm, and in 9th histogram size interval (6.4-8.2 μm) is typical feature of all distributions. Additionally, one may see the increment of amplitude in first size interval (0.5-1.2 μm) that results in weak decrease of mean sizes (Table 4.11). Actually, the mass parameters (Table 4.12) are approximately constant: relative mass of fine particles m_f = 0.15-0.16, mass fraction of fine particles in CCP m_f/m_{ccp} = 0.47-0.52. Content of free aluminum in fine particles $[Al]_f$ amounts 0.5-2.3% that contributes 1-5% of total unburnt aluminum in CCP.

At pressure ~22 atm one can see again the main peak localized in 5th size interval (2.4-3 μm) at geometry *A*, *B* or in 6th size interval (3-3.9 μm) at geometry *C*. Besides, the peak with some less amplitude can be observed in 9th histogram size interval (6.4-8.2 μm) upon testing in all geometry types (Fig. 4.21). Taking into account the scatter of experimental results, we conclude that the size distributions, corresponding to the geometry *A* and *B*, are practically the same. The mass parameters (Table 4.12) are following: relative mass of fine particles m_f = 0.24-0.26, mass fraction of fine particles in CCP m_f/m_{ccp} = 0.70, free aluminum content $[Al]_f$ = 0.3-1.2% that contributes 1-6% of total unburnt aluminum in CCP. The distribution corresponding to firing geometry *C* with protective tube having the typical modes in 5-6th and 8th size intervals, demonstrates the some specific distinctive features: negligible mass of particles in 1st and 2nd size intervals and in the last intervals starting from No 10. In other words, the main mass of fine particles in this case concentrates in 3-10 channels or in size interval 1.5-10.5 μm. It gives following change in mean sizes: D_{10} decreases (as compared with *A* and *B* geometry), the variation in particle mean sizes diminishes ($D_{43} \rightarrow D_{10}$). Relative mass m_f is greater than in the cases of *A* and *B* geometry and amounts 0.37 instead of 0.24-0.26. Possible reason for such behavior is formation of alternative condensed combustion products (aluminum nitride, soot) due to protective tube influence (for example, through the decrease of the flame temperature). This assumption does not contradict to thermodynamic calculations, see Table 4.6.

At pressure ~64 atm there is the main peak which is localized in 5-6th size intervals (2.4-3-3.9 μm) through all firing geometry types (Fig. 4.22). The amplitude of the peak slightly increases with residence time. Besides, the peak with lower amplitude can be recognized in 9th histogram size interval (6.4-8.2 μm) in the case of firing geometry *C*. Additionally, one may see considerable increment in the amplitude of mode in 1-2 channels of histogram that leads to some decrease of mean sizes (Table 4.11). This peak is localized in first size interval (0.5-1.2 μm) in the case of geometry *A* and *B* and shifts to 2nd interval (1.2-1.5 μm) in the case of geometry *C*. Size distributions for geometry types *A* and *B* are very similar. The values of the mass parameters at

pressure ~64 atm are close to those at ~24 atm (Table 4.12): relative mass of fine particles m_f = 0.24-0.26, mass fraction of fine particles in CCP m_f/m_{ccp} = 0.67-0.68, free aluminum content $[Al]_f$ = 0.5-0.9% that contributes 4-6% of total unburnt aluminum in CCP. Thus, the evolution of size distribution caused by elongation of protective tube (increase of residence time) results only in perturbations in 1-2 histogram channels. Taking into account the cessation of agglomerate combustion in experiments at pressure ~64 atm, one may assume that the observed fact is the result of soot formation. In experiments with geometry type *C* the great amount of very light soot-like black material was actually observed. However, this fact can not be treated as the exclusive effect of protective tube ablation. The fine particle size distribution obtained in "pure" experiment with propellant sample burning without any contaminating inhibitors of lateral surface is presented in Fig. 4.23. One can see the same modes in 1, 5 and 8th size intervals. The two types of fine particles are observed in this test – soot-like residue trapped by wire mesh screens and white colored residue sampled on the filter. Thus, the propellant itself (or its non-metalized part) produces the soot-like particles.

In general, comparing the data corresponding to different pressure levels and geometry types, one may conclude that:

- In most cases the fine CCP particles size distribution has three modes in the size ranges 0.5-1.5 μm, 2.4-3.9 μm and 6.4-8.5 μm, with the main peak being in interval 2.4-3.9 μm. Agglomerate combustion increases the total mass of fine particles but does not make effect on their size distribution.
- For the first time the distinctive feature in size distribution (narrowing to the interval 1.5-10.5 μm) was observed in the case of pressure 24 atm and the longest protective tube. The formation of alternative condensed products (aluminum nitride, for example) may be assumed to cause this peculiarity. Special experiments and analyses should be performed to elucidate this finding.
- The 0.5-1.5 μm peak may increase with residence time. This mode presumably consists of soot-like substance forming in combustion of non-metalized part of propellant and partially by ablation of protective tube material.

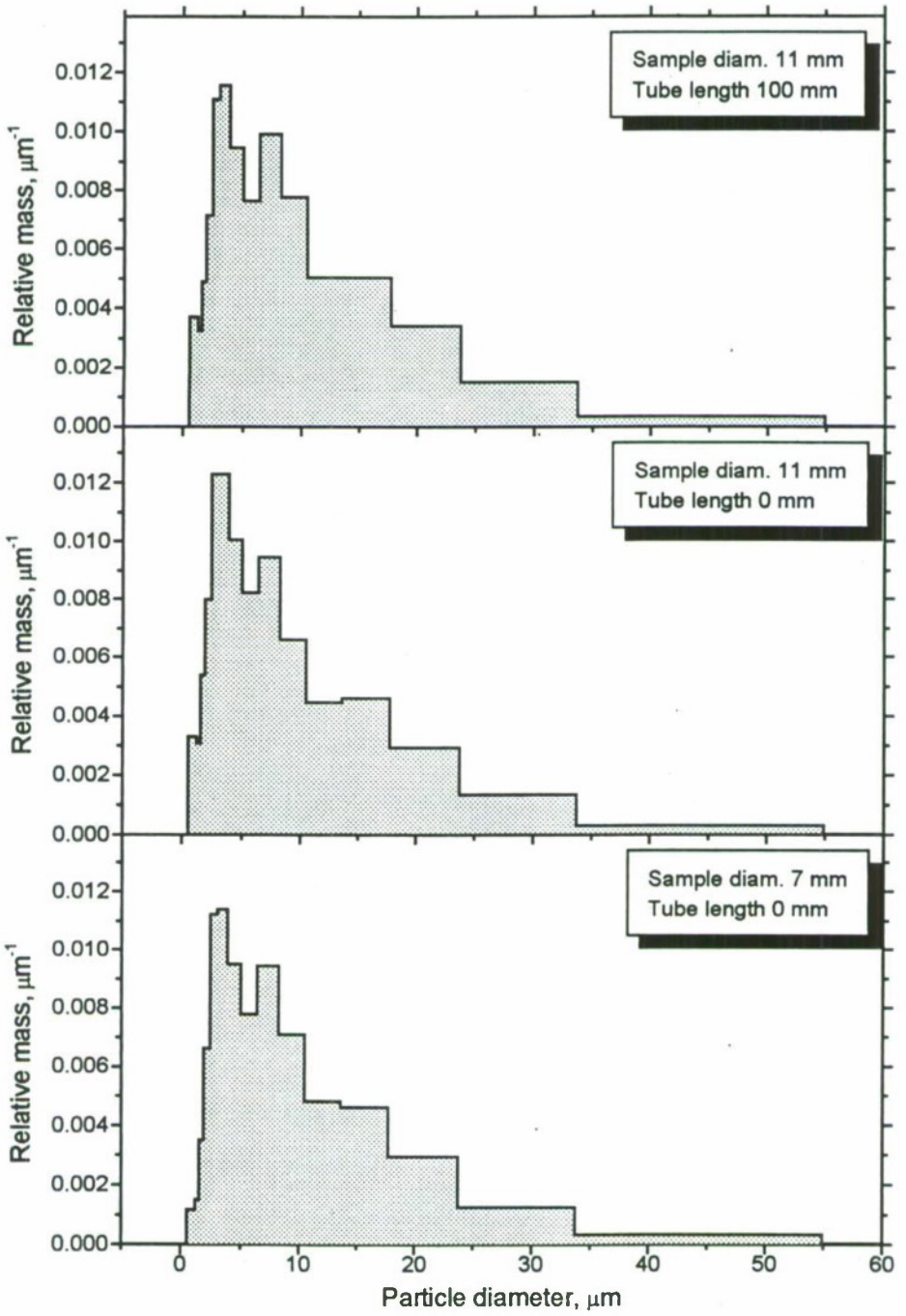

Fig. 4.20. Mass size distribution of fine CCP particles at varied firing geometry type (bottom – *A*, middle – *B*, top – *C*. The residence time increases from the bottom to top). Pressure 1 atm.

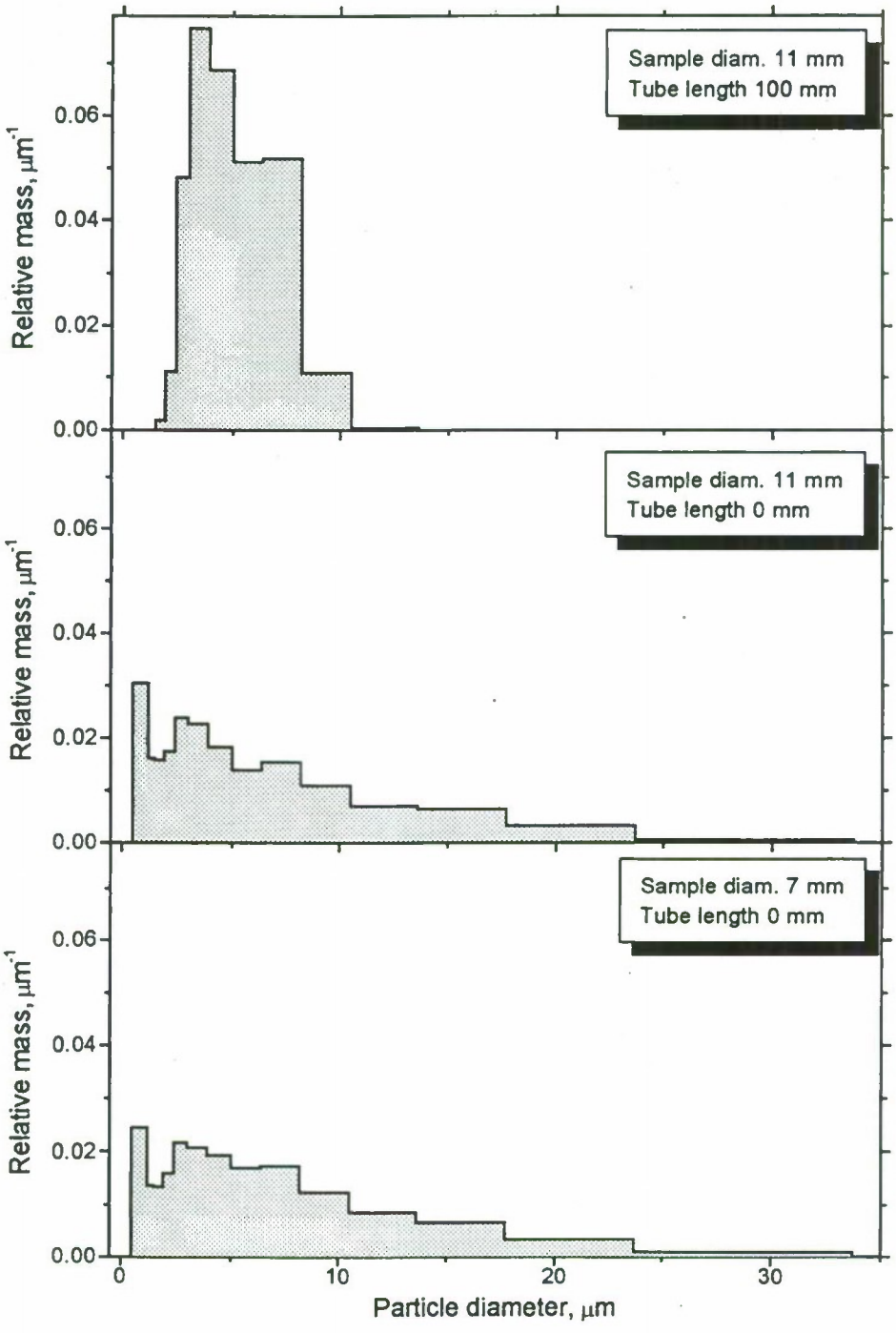

Fig. 4.21. Mass size distribution of fine CCP particles at varied firing geometry type (bottom – *A*, middle – *B*, top – *C*. The residence time increases from the bottom to top). Pressure level 20 atm, more precisely 22.3, 23.8 and 24.3 atm in the cases of *A*, *B* and *C* geometry type, correspondingly.

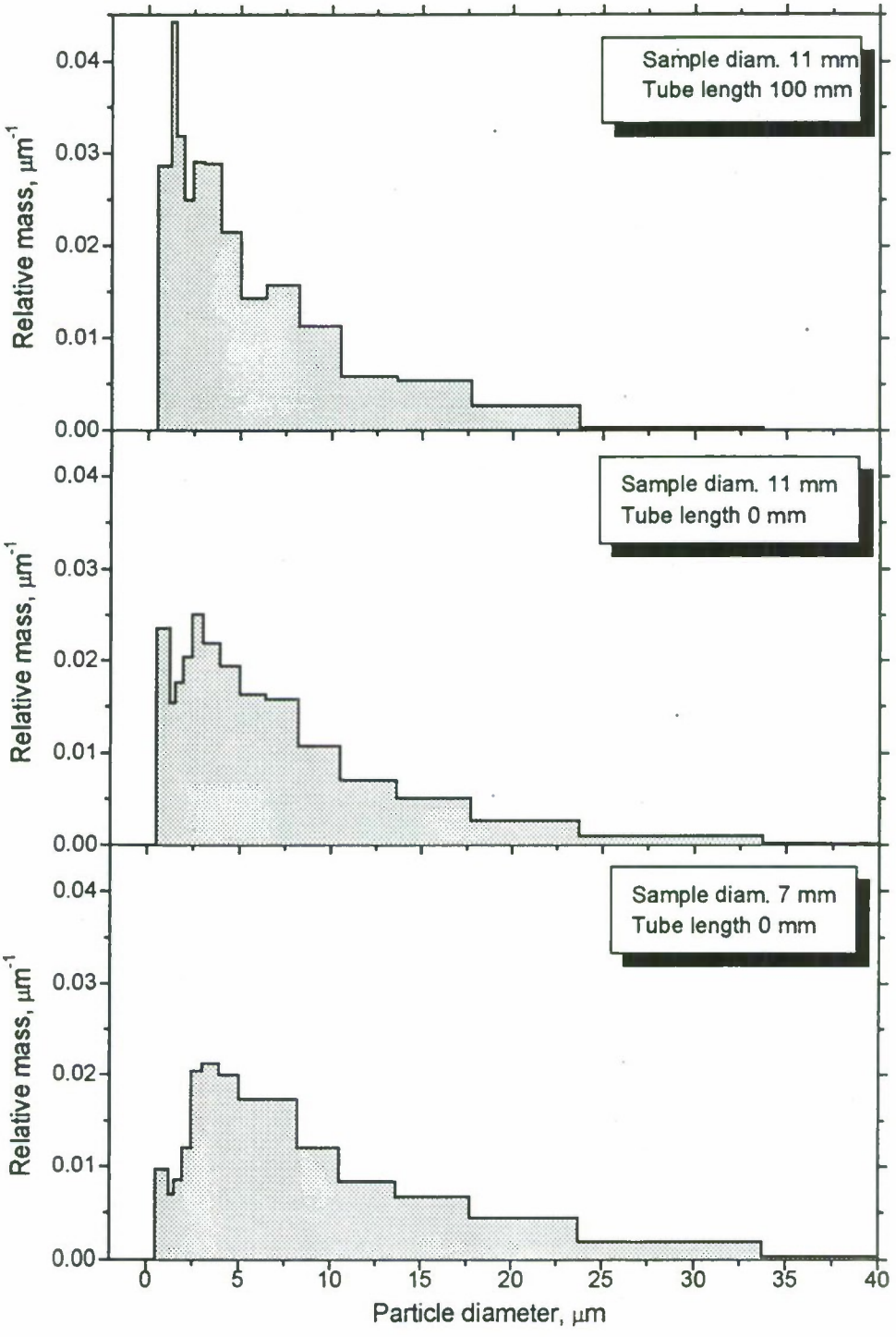

Fig. 4.22. Mass size distribution of fine CCP particles at varied firing geometry type (bottom – *A*, middle – *B*, top – *C*. The residence time increases from the bottom to top). Pressure level 60 atm, more precisely 63.5, 65.8 and 67.3 atm in the cases of *A*, *B* and *C* geometry type, correspondingly

Table 4.11. Mean diameter D_{mn} (μm) of fine CCP particles, calculated in the size range (0.5 μm-D_L), in dependence on sampling conditions.

P, atm	Geometry type	D_L, μm	D_{10}	D_{20}	D_{30}	D_{21}	D_{32}	D_{43}	D_{53}
1	A, teflon	87	1.5	2.1	2.8	2.8	5.4	9.3	11.5
1	A	119	2.0	2.7	3.7	3.6	7.0	14.2	19.6
1	B	119	1.5	2.1	3.0	2.8	6.2	13.1	17.3
1	C	127	1.4	2.0	3.0	2.8	6.5	13.6	17.6
22.3	A	87	1.1	1.4	2.0	1.7	4.1	9.2	11.8
23.8	B	95	1.1	1.3	1.8	1.6	3.6	8.5	10.8
24.3	C	87	3.6	3.8	4.1	4.1	4.7	5.4	5.7
63.5	A	127	1.3	1.8	2.6	2.4	5.6	11.6	15.1
65.8	B	119	1.1	1.4	1.9	1.7	3.9	9.2	12.7
67.3	C	44	1.1	1.4	1.8	1.6	3.3	7.3	9.4

Table 4.12. Mass characteristics of fine CCP particles, calculated in the size range (0.5 μm-D_L), in dependence on sampling conditions.

P, atm	Geom. type	m_f	m_f/m_{ccp}	m_{ag}/m_f	$m^{Al}{}_f$	$m^{Al}{}_{ag}/m^{Al}{}_f$	$[Al]_f$, %	$m^{Al}{}_f/m^{Al}{}_{prop}$
1	A, teflon	0.2046	0.568	43:57	0.0030	96:4	1.5%	0.015
1	A	0.1501	0.472	53:47	0.0026	97:3	1.7%	0.013
1	B	0.1536	0.500	50:50	0.0008	99:1	0.5%	0.004
1	C	0.1624	0.517	48:52	0.0037	95:5	2.3%	0.019
22.3	A	0.2554	0.698	30:70	0.0008	99:1	0.3%	0.004
23.8	B	0.2422	0.703	30:70	0.0029	94:6	1.2%	0.015
24.3	C	0.3711	0.790	21:79	0.0035	91:9	0.9%	0.018
63.5	A	0.2617	0.680	32:68	0.0012	96:4	0.5%	0.006
65.8	B	0.2422	0.667	33:67	0.0021	94:6	0.9%	0.011
67.3	C	0.2601	0.671	33: 67	0.0012	96:4	0.5%	0.006

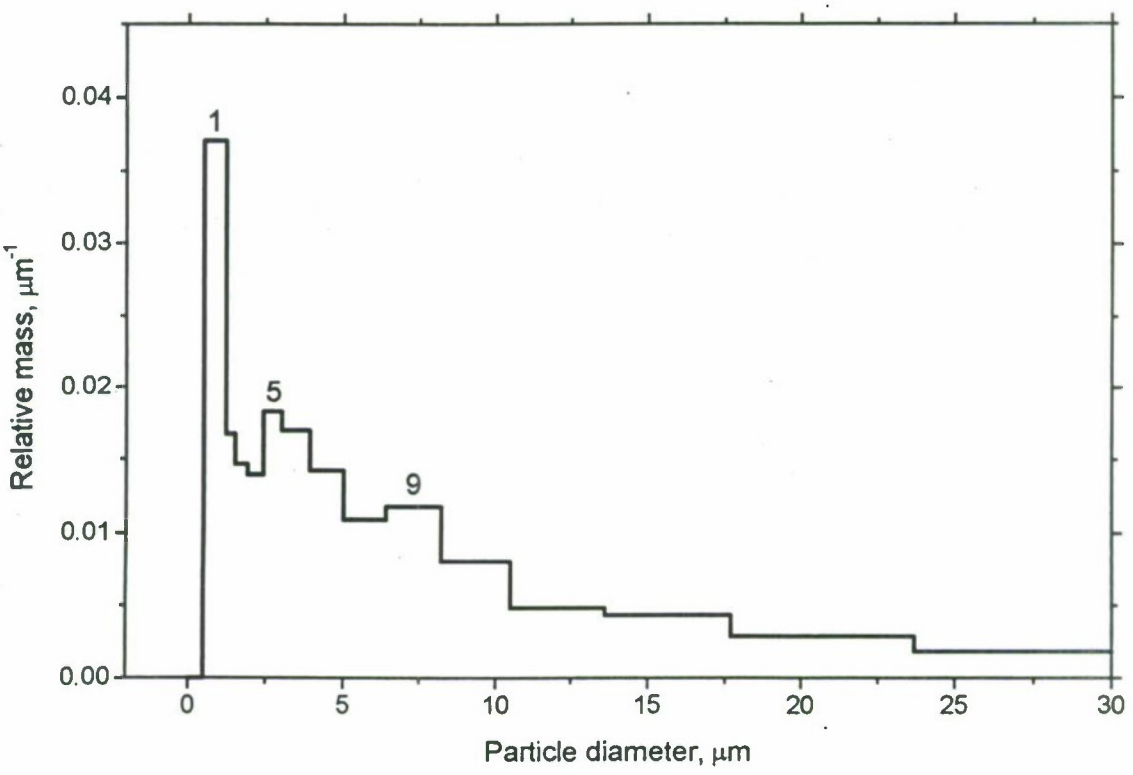

Fig. 4.23. Mass size distribution of fine CCP particles sampled in "pure" experiment with non-inhibited propellant sample fixed on glass plate. Typical modes (peaks) corresponding to the 1st (0.5-1.2 μm), 5th (2.4-3 μm), and 9th (6.4-8.5 μm) channels of Malvern histogram are presented. Pressure 11.8 atm.

4.7. Total mass characteristics and sampling method representativity

The experimental data on sampled fine and coarse CCP particles has been discussed above. In reality, some portion of particles can be lost unavoidably even if the sampling method is perfect. The main possible reasons for those losses are depositing the particles onto the bomb interior (walls, etc.) and losing the particles in course of bomb discharging and particle preparation for analyses. The estimate of the value of mass loss is very important but difficult. In present Chapter we try to evaluate the sampling method representativity on the basis of the experimental determined total mass characteristics for whole population of sampled CCP.

The **representativity** R is defined as the ratio of sampled mass to theoretical mass of condensed combustion products. The last one can be defined by different ways. Therefore, we used designations R_1, R_2, R_3 for these values, correspondingly. The results are presented in Table 4.13.

Three ways for calculation of R step by step are described below. In all cases the values M_{prop} (mass of propellant burnt in grams), m_{ccp} (relative mass of CCP), [Al] (free aluminum percentage in CCP) are taken from experimental data.

Option 1. ***The assumption: all burnt aluminum is converted into aluminum oxide.***

- Initial mass of aluminum in propellant = M_{prop}·(aluminum content).
- Mass of CCP = M_{prop}·m_{ccp}.
- Mass of free aluminum in CCP = Mass of CCP ·[Al]·100.
- Mass of burnt out aluminum = (Initial mass of aluminum in propellant) – (Mass of free aluminum in CCP).
- Mass of formed oxide = (Mass of burnt out aluminum)·1.88946.
- Theoretical mass of CCP = (Mass of free aluminum in CCP)+(Mass of formed oxide).
- R_1 = (Mass of CCP)/(Theoretical mass of CCP).

Option 2. ***The assumptions: all burnt aluminum is converted into aluminum oxide, burnt in experiments plexiglas and teflon from sample holder contribute into total mass of CCP the mass of soot, which is proportional to carbon content in these plastic materials.***

- Initial mass of aluminum in propellant = M_{prop}·(aluminum content).
- Mass of CCP = M_{prop}·m_{ccp}.
- Mass of free aluminum in CCP = Mass of CCP ·[Al]·100.
- Mass of burnt out aluminum = (Initial mass of aluminum in propellant) – (Mass of free aluminum in CCP).
- Mass of formed oxide = (Mass of burnt out aluminum)·1.88946.
- Mass of soot formed due to plexiglas combustion = (Mass loss of plexiglas cylinders)·60.055/100.117.
- Mass of soot formed due to teflon combustion = (Mass loss of teflon bottoms)·24.022/100.016.
- Theoretical mass of CCP = (Mass of free aluminum in CCP)+(Mass of formed oxide)+(Mass of soot formed due to plexiglas combustion)+(Mass of soot formed due to teflon combustion).
- R_2 = (Mass of CCP)/(Theoretical mass of CCP).

In this case the mass loss of propellant sample holder consisting of plexiglas cylinder and teflon bottom is determined experimentally by weighting the subjects before and after firing test (see Chapter 4.6.2 and Table 4.10).

Option 3. ***The assumptions: all burnt aluminum is converted into aluminum oxide, burnt in experiments plexiglas and teflon from sample holder contribute into total mass of CCP the soot mass which is estimated via thermodynamic calculation.***

- Initial mass of aluminum in propellant = M_{prop}·(aluminum content).
- Mass of CCP = $M_{prop} \cdot m_{ccp}$.
- Mass of free aluminum in CCP = Mass of CCP ·[Al]·100.
- Mass of burnt out aluminum = (Initial mass of aluminum in propellant) – (Mass of free aluminum in CCP).
- Mass of formed oxide = (Mass of burnt out aluminum)·1.88946.
- Mass of soot formed due to plexiglas and teflon combustion is determined in thermodynamic calculation made by ASTRA-2 code for conventional three-component propellant sample that consists of mass of propellant, mass of burnt plexiglas and mass of burnt teflon. All these values are taken from experiment.
- Theoretical mass of CCP = (Mass of free aluminum in CCP)+(Mass of formed oxide)+(Mass of soot formed due to combustion of conventional propellant containing plexiglas and teflon.
- R_3 = (Mass of CCP)/(Theoretical mass of CCP).

Table 4.13. Mass characteristics of CCP and representativity R_i of the sampling technique

P, atm	Geom. type	D_{max}, μm	D_L, μm	m_{ccp}	[Al], %	$(m^{Al}_{ccp})/(m^{Al}_{prop})$	R_1	R_2	R_3
1	A, teflon	2210	87	0.3604	20.5	0.370	1.15	1.00	0.87
1	A	2540	119	0.3184	26.5	0.422	1.05	0.84	0.95
1	B	1630	119	0.3070	23.1	0.354	0.97	0.86	1.03
1	C	2450	127	0.3141	22.2	0.349	0.99	0.61	1.01
22.3	A	3540	87	0.3660	14.3	0.261	1.10	0.94	0.91
23.8	B	1820	95	0.3444	14.7	0.254	1.03	0.94	0.97
24.3	C	2210	87	0.4695	8.6	0.201	1.37	0.79	0.91
63.5	A	1910	127	0.3850	8.8	0.169	1.10	0.98	0.90
65.8	B	2190	119	0.3630	9.6	0.175	1.04	0.93	0.96
67.3	C	1900	44	0.3874	8.8	0.170	1.11	0.77	0.91

Analyzing the data presented in the Table 4.13 one can conclude that representativity of used sampling and preparation technique is high enough. For more reliable evaluation of the representativity it is necessary to perform more detailed chemical analysis with determining the content of aluminum oxide, aluminum nitride, metallic aluminum, carbon (soot) and other compounds in sampled CCP.

4.8. Reproducibility of experimental procedure

The reliability of obtained experimental data is constrained by both the reproducibility of particles sampling and analyzing procedure and the reproducibility of relatively small propellant samples combustion characteristics. The last one depends on the uniformity of propellant formulation and boundary effects. For estimation of these factors, special experiments were performed with testing six small size propellant samples (weight about 0.7 g each) followed by their independent treatment like as separate experimental series. The tests were made in firing geometry *A* at pressure 1 atm. The results of tests are presented below in Figs. 4.24-4.25 and Tables 4.14-4.16. Table 4.14 presents the data on mean diameters calculated in size range 100 μm-$D_{max.}$, i. e. without excluding the extra large agglomerates, formed during transient combustion near the end of propellant sample (see Chapter 4.3.1). Table 4.15 presents the data on mean diameters calculated in size range (D_L-D_R) (for "true" agglomerates). The method to establish this size interval was given in Chapter 4.3.1. The last line in both Tables presents the instrumental error of particle size measurement. It was estimated as a half histogram size interval for corresponding particle size.

The overall view of mass size distributions for coarse CCP particles is presented in Fig. 4.24.

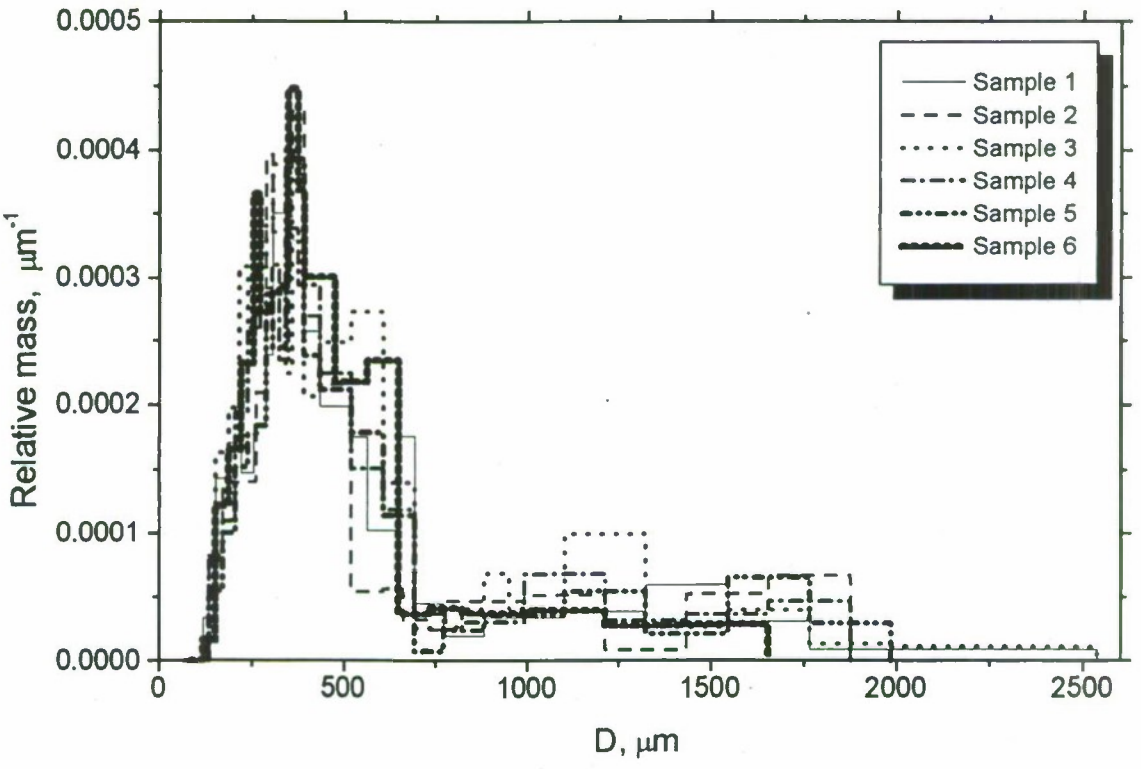

Fig. 4.24. Mass size distribution of coarse CCP particles sampled in firing tests of six individual samples. Pressure 1 atm.

Table 4.14. Mean diameters D_{mn} (μm) of coarse CCP particles calculated in the size range 100 μm-D_{max}. The results of individual tests of propellant samples with diameter 7 mm at pressure 1 atm in geometry type *A*.

Sample No.	D_{10}	D_{20}	D_{30}	D_{21}	D_{32}	D_{43}	D_{53}
1	261	291	337	325	451	722	919
2	267	295	339	326	447	707	879
3	267	297	342	330	456	713	892
4	271	300	343	332	448	675	821
5	284	314	360	348	475	722	885
6	275	301	335	329	414	554	651
Instrumental accuracy ΔD, μm	9	9	22	22	22	55	55

Table 4.15. Mean diameters D_{mn} (μm) of coarse CCP particles calculated in the size range from D_L to D_R (μm). The results of individual tests of propellant samples with diameter 7 mm at pressure 1 atm in geometry type *A*. Shadowed lines correspond to joining data for three samples.

Sample No	D_L-D_R	D_{10}	D_{20}	D_{30}	D_{21}	D_{32}	D_{43}	D_{53}
1	119 - 831	256	278	303	302	357	416	443
2	119 - 754	261	279	297	298	338	378	397
3	119 - 714	261	280	303	302	352	407	432
4	119 - 853	267	287	309	308	358	411	436
5	127 - 714	277	297	318	319	366	412	432
6	119 - 853	272	293	315	315	366	419	443
Σ1-3	119 - 800	260	280	302	302	351	405	430
Σ4-6	127 - 825	272	292	314	314	364	416	440
Instrumental accuracy ΔD, μm		9	9	22	22	22	~22	~22

Analyzing data presented one may see that the difference in mean diameters D_{10}, D_{20}, D_{30}, D_{21}, and D_{32} is slight in both Tables and does not exceed the instrumental error. However, in the cases of diameters D_{43} and D_{53}, calculated on the basis of non-corrected size distribution function (Table 4.14), the difference can reach sizable value: D_{43} = 554-722 μm, D_{53} = 651-919 μm. At the same time, the difference in this diameters calculated in size range D_L-D_R is small enough: D_{43} = 378-419 μm, D_{53} = 397-443 μm. This fact can be treated as follows. The non reproducibility in high-order mean diameters is caused by extra large particles, forming at the end of sample combustion. The mean characteristics for "true" agglomerates are close in individual tests and practically coincide when superposition treatment by three samples was performed (shadowed lines in Table 4.15).

Through examination of Table 4.15 reveals some difference in mean diameters corresponding to the sample 2. This difference may be caused by the non-uniformity of the propellant, but the value of the difference is close to experimental error. When three histograms are overlapped, the difference is suppressed statistically. Thus, one may determine the agglomerate mean diameters

$D_{10}...D_{53}$ with the error not exceeding the experimental accuracy using even three sample statistics.

The data on mean diameters of fine particles are presented in Table 4.16. The difference does not exceed 30% for individual tests and not exceeds 15% for joint (Σ1-3) and (Σ4-6) data.

Table 4.16. Mean diameters D_{mn} (μm) of fine CCP particles calculated in the size range from 0.5 μm to D_L. The results of individual tests of propellant samples with diameter 7 mm at pressure 1 atm in geometry type *A*. Shadowed lines correspond to joining data by three samples.

Sample No	D_L	D_{10}	D_{20}	D_{30}	D_{21}	D_{32}	D_{43}	D_{53}
1	119	2.2	3.0	4.2	4.0	8.0	15.8	20.7
2	119	2.1	2.8	3.7	3.6	6.6	11.4	14.2
3	119	1.9	2.5	3.5	3.4	7.0	15.6	22.4
4	119	2.3	3.0	4.1	4.0	7.8	15.7	21.3
5	127	2.3	3.0	4.1	3.9	7.4	14.5	19.1
6	119	2.5	3.2	4.4	4.2	7.9	14.6	18.5
Σ1-3	119	2.0	2.7	3.7	3.6	7.0	14.2	19.6
Σ4-6	127	2.3	3.1	4.2	4.0	7.7	15.0	19.9

The main mass characteristics are presented in Table 4.17. The series of three samples with teflon cylinders was performed also at pressure equals 1 atm in firing geometry *A*.

The mass CCP characteristics have larger scatter as compared with that for mean diameters. The relative mass of fine particles has the greatest variation: $m_f = 0.10\text{-}0.20$. Probably, it is caused by contamination of CCP with non-propellant combustion products. Consequently, the scatter of relative mass of CCP m_{ccp} from 0.24 to 0.40 is induced by deviation of m_f. Using three samples statistics one may determine the value of m_{ccp} with 23% relative error, and the value of m_f with 50% relative error. It should be noted here that usually 5-samples series was made in the case of firing geometry *A*.

Table 4.17. Mass characteristics CCP particles calculated for individual tests performed with diameter 7 mm at pressure 1 atm in geometry type *A*. Shadowed lines correspond to joining data by three samples.

Sample No	D_L	m_{ccp}	m_f	m_{ag}/m_f
1	119	0.2537	0.0961	62:38
2	119	0.3121	0.1604	49:51
3	119	0.3963	0.1991	50:50
4	119	0.2797	0.1178	58:42
5	127	0.2393	0.0842	65:35
6	119	0.2656	0.1027	61:39
Σ1-3	119	0.3184	0.1501	53:47
Σ4-6	127	0.2616	0.1017	61:39
Teflon *)	87	0.3604	0.2046	43:57

*) – experiments with teflon cylinders instead of plexiglas ones.

The mass characteristics concerning aluminum content in CCP particles are presented in Table 4.18. Only joint data can be used for calculation of these characteristics because the mass of particles sampled after combustion of individual sample is not enough for chemical analysis. For comparison, the data obtained in series with sample holders made of teflon are presented in last line of the Table 4.18.

Analyzing the data one may see that the mass parameters, which characterize aluminum content in sampled CCP, have better reproducibility than CCP mass parameters given in Table 4.17. The main parameter $m^{Al}_{ag} / m^{Al}_{prop}$ used for description of incompleteness of aluminum combustion varies in the range 0.41-0.39 (shadowed cells). Treating these values as two random realizations one may calculate the mean value, standard error and confidence interval. Using Student coefficient equal 2 that corresponds to reliability level 70%, the following estimate was obtained: $(m^{Al}_{ag} / m^{Al}_{prop}) = 0.40 \pm 0.02$. Thus, the relative error for the determined value is about 5%.

Table 4.18. Mass characteristics CCP particles calculated in the size range D_L-D_{max} (μm). All tests performed at pressure 1 atm in geometry type *A* with samples 7 mm in diameter. Joint data for groups by three burnt sample.

Series	D_L-D_{max}	m_{ag}/m_f	m^{Al}_{ag}/m^{Al}_f	$[Al]_{ag}$, %	$[Al]_f$, %	$m^{Al}_{ag}/m^{Al}_{prop}$	m^{Al}_f/m^{Al}_{prop}	$m^{Al}_{ccp}/m^{Al}_{prop}$
Σ1-3	119 - 2537	53:47	97:3	49.6%	1.7%	0.409	0.013	0.422
Σ4-6	127 - 1986	61:39	98:2	48.1%	1.6%	0.385	0.008	0.393
Teflon*)	87-2207	43:57	96:4	45.5%	1.5%	0.355	0.015	0.370

*) – experiments with teflon cylinders instead plexiglas ones.

4.9. Agglomeration characteristics and propellant formulation. Generalization of experimental data.

In this section we summarize the data on agglomeration characteristics obtained in present work, in works under Contracts with BYU [3] and EOARD [2], and in Project INTAS-93-2560.

All referred data were obtained via sampling method in firing geometry *B* for propellants with similar geometric structure and burning rate but varied composition. The propellants under study contained AP and HMX as oxidizer and different types of binder: inert (based on butadiene and isoprene rubber) and energetic (nitryl rubber plasticized with DEGDN).

The propellant formulations are presented in Table 4.19. The more detailed data on granulometric composition of used powder components are available in corresponding sources. In the Table the coarse fractions of oxidizers are titled using their D_{43} mean size. Burning rate dependencies on pressure are given in Table 4.20.

Table 4.19. Propellant formulations (% mass.)

Prop	No. and type of binder	Bin-der, %	Al 13 μm	AP 6000 cm^2/g	AP 2700 cm^2/g	AP 200-315 μm	RDX "400"	HMX "630"	HMX "600"
E1	E#1 nitryl/DEGDN	20	20	7	-	18	-	35	-
E12	E#1 nitryl/DEGDN	20	20	7	-	18	-	-	35
R	E#1 nitryl/DEGDN	20	20	7	-	18	35	-	-
I2	I#2 isoprene+3%Cat	15+3	18	27	-	37	-	-	-
I1	I#1 butadiene	15	16.8	31.8	-	13.1	-	23.3	-
E2	E#1 nitryl/DEGDN	30	18	15	-	37	-	-	-

I#1 - inert binder: butadiene rubber (20%), transformer oil (76%), additives (4%).

I#2 - inert binder: isoprene rubber (26.4%), transformer oil (69.6%), additives (4%)

E#1 - energetic binder: nitryl rubber plasticized with DEGDN (98%), additives (2%).

Catalyst (in propellant I2 only): 1'1-bis (dimethyloctoxylil) ferrocene.

Table 4.20. Burning rate r (mm/s) at varied pressures P

Propellant	r at 1 atm	r at elevated P	Pressure range
E1	0.8	$r = 1.88 \cdot P^{0.52}$	6-64 atm
E12	1.0	$r = 1.88 \cdot P^{0.45}$	23-65 atm
R	1.1	$r = 0.88 \cdot P^{0.62}$	22-66 atm
I2	NA	$r = 5.21 \cdot P^{0.21}$	22-85 atm
I1	NA	$r = 1.13 \cdot P^{0.65}$	6-64 atm
E2	NA	$r = 6.12 \cdot P^{0.24}$	22-85 atm

Selected experimental results are presented in Table 4.21. The relative error for reported mass characteristics $\delta m/m$ estimated via reproducibility tests amounts 6-15%. The experimental error of microscopic determination of the particle diameter equals ±9 μm for particles with size 100-300 μm and ±22 μm for particles with size 300-600 μm. These absolute errors estimated as a half of the histogram size interval.

Table 4.21. Characteristics of condensed combustion products - **agglomerates**

Prop	Agglomeration group	P, atm	r, mm/s	D_L-D_R, μm	$[Al]_{ag}$, %	$m^{Al}_{ag}/m^{Al}_{prop}$	D_{10}, μm	D_{30}, μm	D_{43}, μm
	Column #1	#2	#3	#4	#5	#6	#7	#8	#9
E1	1	1	0.8	135-1954	32.8%	0.245	263	311	460
	1	6	2.8	135-1831	33.0%	0.248	270	317	477
	1	22	11.8	102-1698	44.3%	0.300	267	314	500
	1	62	15.4	119-2039	34.0%	0.286	260	309	529
E12	1	1	1.0	123-767*	45.1%	0.340	270	310	402
	1	24	7.9	95-1818*	46.8%	0.239	234	253	301
	1	66	12.7	119-671*	27.1%	0.164	207	224	272
R	1	1	1.1	55-2348*	40.0%	0.361	317	433	814
	1	24	6.0	24-1772*	40.8%	0.322	303	357	495
	1	65	10.5	24-2239*	29.2%	0.275	270	309	428
I2	1	22	8.9	61-1245	21.3%	0.220	91	126	383
	1	43	10.8	61-1187	24.1%	0.251	235	344	669
	1	85	12.7	51-1568	22.3%	0.234	197	276	486
I1	2	6	1.3	119-1000*	36.3%	0.063	242	266	333
	2	22	10.6	61-1000*	17.4%	0.002	106	144	293
	2	64	16.1	61-1000*	9.6%	0.003	119	148	215
E2	3	22	12.4	51-380*	24.3%	0.096	124	133	156
	3	44	15.6	61-520*	4.4%	0.009	123	137	173
	3	84	17.8	61-600*	6.6%	0.007	97	109	157

Comment to column #4:
The above-described procedure for determining of D_R was used in the cases signed with (*). In another case $D_R=D_{max}$.

Continued at next page...

Table 4.21. Characteristics of condensed combustion products
(continued from previous page)

				Fine particles		Total condensed combustion products			
Prop	Agglomeration group	P, atm	r, mm/s	$[Al]_f$, %	m^{Al}_f/m^{Al}_{prop}	m_{ccp}	$m^{Al}_{ccp}/m^{Al}_{prop}$	$m_f:m_{ag}$	$m^{Al}_f:m^{Al}_{ag}$
	Column #1	#2	#3	#10	#11	#12	#13	#14	#15
E1	1	1	0.8	0.8%	0.008	0.35	0.253	57:43	3:97
	1	6	2.8	1.7%	0.013	0.31	0.261	51:49	5:95
	1	22	11.8	0.4%	0.005	0.37	0.305	63:37	2:98
	1	62	15.4	0.4%	0.005	0.39	0.291	57:43	2:98
E12	1	1	1.0	1.4%	0.010	0.29	0.350	49:51	3:97
	1	24	7.9	1.2%	0.015	0.34	0.254	70:30	6:94
	1	66	12.7	0.9%	0.011	0.36	0.175	67:33	6:94
R	1	1	1.1	1.4%	0.009	0.31	0.370	42:58	2:98
	1	24	6.0	0.3%	0.003	0.32	0.325	50:50	1:99
	1	65	10.5	1.0%	0.006	0.35	0.281	54:46	3:97
I2	1	22	8.9	0.4%	0.004	0.38	0.224	51:49	2:98
	1	43	10.8	0.6%	0.005	0.35	0.256	46:54	2:98
	1	85	12.7	0.7%	0.011	0.47	0.244	60:40	4:96
I1	2	6	1.3	19.7%	0.413	0.38	0.476	92:8	87:13
	2	22	10.6	2.6%	0.058	0.38	0.060	99:1	97:3
	2	64	16.1	0.8%	0.014	0.32	0.017	98:2	83:17
E2	3	22	12.4	0.4%	0.007	0.37	0.103	81:19	7:93
	3	44	15.6	0.2%	0.006	0.60	0.015	94:6	40:60
	3	84	17.8	0.4%	0.012	0.53	0.019	97:3	63:37

4.9.1. Agglomeration scenarios

Examination of Table 4.21 shows that experimental data can be divided into three groups according to different scenarios of agglomeration process.

The **first** group includes propellants **E1**, **E12** (nitryl/DEGDN binder, HMX), **R** (nitryl/DEGDN binder, RDX) and **I2** (isoprene binder, no HMX) and corresponds to the classical well pronounced agglomeration. In this case 30%-58% mass of CCP (column #14 in Table 4.21) belongs to agglomerates that contribute approximately 95%-99% (column #15) of total mass of unburnt aluminum. The size of agglomerates is in the large scale (D_{43} in the range 270-814 μm, column #9). The fine particles consist practically of pure oxide (column #10). The distinctive feature of this scenario is relatively high completeness of metal combustion in agglomerates before leaving the burning surface.

The long residence time and growing the agglomerates size are provided by keeping them in sub-surface layer or on the burning surface with hypothetical frame that consists of carbon residue of binder and semi sintered, partially oxidized aluminum particles. Chemical reacting with active participation of aluminum particles presumably is necessary condition for this scenario realization. Then (in gas phase) the combustion of agglomerates may cease due to capsulation of metal with a thick oxide shell.

The **second** group consists of propellant **I1** (butadiene binder, HMX) and is characterized by weak intensity of agglomeration and very specific scenario. In this case rather small mass (1%-8%, column #14) of CCP is formed by agglomerates which contribute only 3%-17% (column #15) of total mass of unburnt aluminum. The content of free aluminum in agglomerates (column #5) is the function of pressure: it decreases from 36.3% to 9.6% when the pressure increases from 6 atm to 64 atm. There is a sizable amount of free aluminum in fine particles (column #10), and its value decreases with pressure: 19.7% at 6 atm and only 0.8% at 64 atm. It should be noted that burning rate has the same order of magnitude as for propellants in previous group.

In this scenario the burning surface does not hold metal particles which leave surface in the form of irregular grape/coral shape aggregates or in the form of individual particles. As the pressure increases, the ignition distance decreases and the relative number of aggregates ignited at the burning surface increases. The formation of coarse particles with size D_{43} = 215-333 μm is relatively rare event. It can be caused by anomalies in propellant packing/structure. One may expect that burning law for agglomerates in this case is close to that for individual aluminum particles because the aggregates have relatively small residence time at the burning surface. The processes providing high efficiency of aluminum conversion into oxide particles proceed in gas phase. This scenario can be called as "coarse aggregates dispersion".

The **third** group consists of propellant **E2** (nitryl/DEGDN binder, no HMX). When compare with propellant I2, one may observe that in spite of very similar geometrical structure and small difference in burning rates, the combustion behavior of these two is very different. The size D_{43} of agglomerates is smaller (156-173 μm as compared with 383-669 μm, column #9) and incompleteness of aluminum combustion is lower (0.10-0.02 as compared with 0.22-0.26, column #13) in case of propellant E2. We suppose that the higher efficiency of aluminum combustion for propellant with energetic binder is caused by more complete conversion of aluminum in subsurface layer. At pressure 22 atm the agglomeration process follows qualitatively to "classical scenario": the agglomerates contain relatively large quantity of free aluminum (24.3%, column #10), their contribution in total mass CCP is high (19%, column #14) and they contribute about 93% of unburnt aluminum (column #15). The difference between propellant E2 at 22 atm and propellants

of the first group E1 and I2 is the default of surface layer of E2 to keep aluminum particles for a long time. At pressures 44 and 84 atm the agglomeration process seems to be close to second scenario (irregular shape aggregates leaving the burning surface): the portion of agglomerates in CCP becomes small (3-6%, column #14) but the size of agglomerates is the same. Agglomerates and virgin aluminum particles just leaving propellant surface burn out very fast and incompleteness of aluminum combustion in case of propellant E2 is rather low (~0.02, column #13) at pressures 44 and 84 atm. As the result, the fraction of fine particles is high (94-97%, column #14) and small particles consist of almost pure oxide (free aluminum content is 0.2-0.4%, column #10).

The diagram in Fig. 4.25 gives an idea on trends in agglomeration process characteristics in terms of parameters (m_{ag}/m_{ccp}) and D_{30} . The ratio (m_{ag}/m_{ccp}) characterizes the efficiency of conversion of virgin aluminum particles in propellant mainly into small smoke oxide. Indirectly, it corresponds to intensity of two-phase flow losses. The size D_{30} characterizes probability of precipitation of large particles at the walls of rocket motor chambers (slagging). Qualitatively, the less parameters (m_{ag}/m_{ccp}) and D_{30} , the better propellant performance in solid rocket motor.

4.9.2. Concluding remarks

- The results of the study show significant difference in metal combustion behavior for different formulation propellants. In fact, there are several scenarios of the agglomeration process. Four studied propellants (E1, E12, R and I2) follow classical agglomeration scenario characterized by sizable growing of agglomerates when they hold for a long time on the burning surface. It seems that chemical reacting of aluminum within the condensed phase is necessary condition for growing the agglomerates.
- The presence of RDX affects the agglomeration intensity qualitatively similar to HMX, but may be stronger.
- The size and free aluminum content in agglomerates is governed by not only geometrical structure of propellant but also the nature of binder and presence of alternative oxidizer (HMX) through modification of the properties of subsurface layer which can affect the intensity of chemical reaction in condensed phase and ability to hold the particles on the surface.
- In case of energetic (nitryl rubber /DEGDN) binder based formulations the presence of HMX leads to significant increase in agglomeration intensity. However, in case of inert binder formulations the presence of HMX does not obligatory increase the agglomeration intensity (propellants I1 and I2). It means that the difference in properties of butadiene and isoprene binders plays more significant role than replacement of part of AP by HMX.
- The results of this study stress the necessity of further detailed investigation of the effects of propellant formulation on agglomeration in terms of studying the microstructure of propellant, physical properties of ingredients at elevated temperatures and chemical reactions between metal particles and products of binder and oxidizer decomposition.

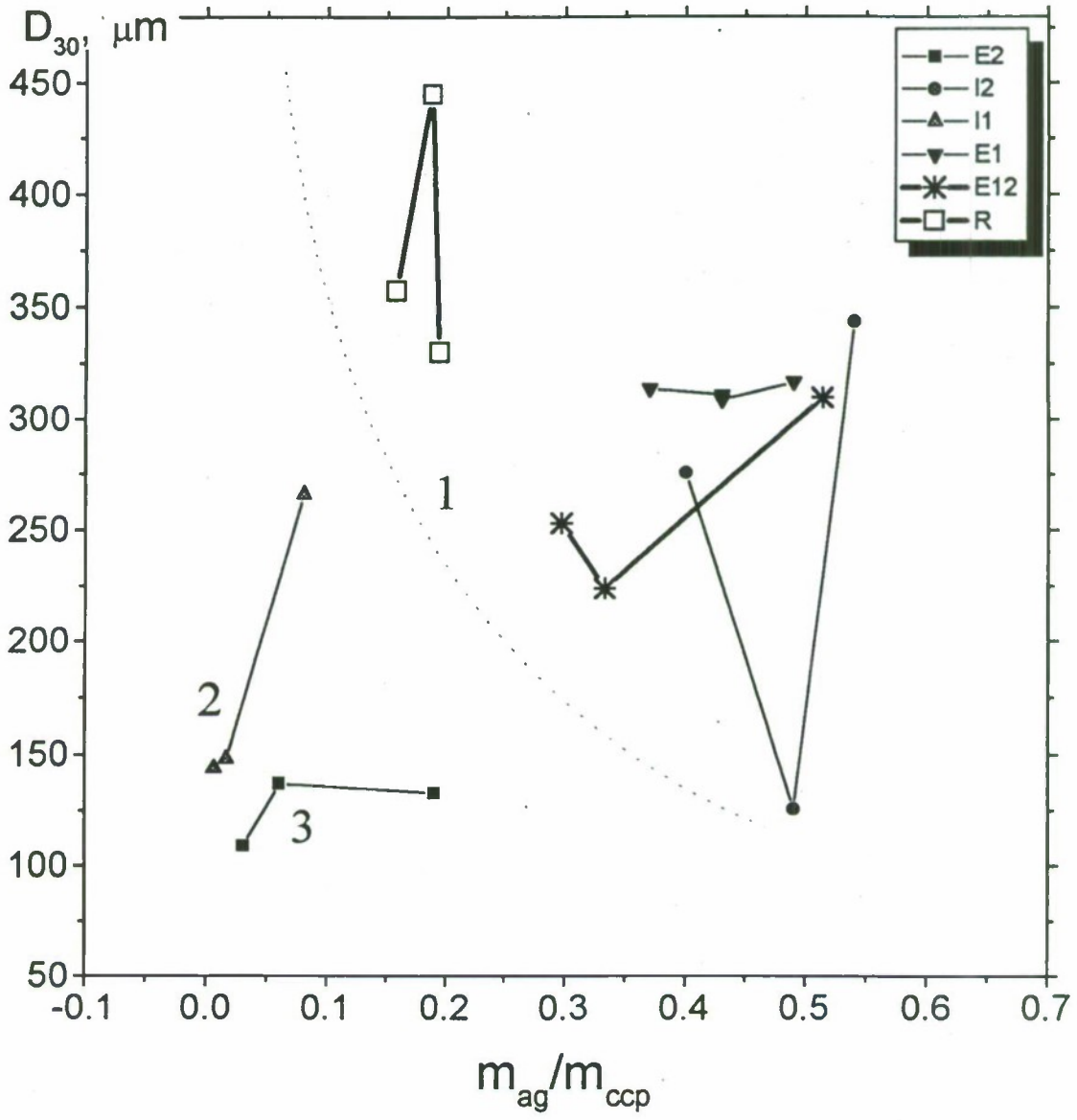

Fig.4.25. Diagram of the agglomeration intensity for different propellant formulations. Numbers 1-3 are the group of agglomeration.

5. STUDYING THE RECOIL FORCE SIGNAL BEHAVIOR

5.1. Experimental approach

In this Chapter the results concerning behavior of burning rate under the radiant flux are presented. Experimental setup consist of Nd:YAG laser, recoil force transducer and acquisition system. The detailed description of experimental equipment is in [2]. We used the sinusoidal and step-wise changes in the radiant flux recording simultaneously the reactive force of flowing combustion products and the signal of photodiode that measures the integral flame radiation.

In experiments we used cylindrical samples with length 1.0 cm and diameter (d) 0.7 and 1.0 cm. To provide one-dimensional flow of gaseous combustion products the specimens were tightly inserted into protecting tube that also served as inhibition of lateral surface. Another kind of lateral surface inhibition was the polymer solution of Solprein (trade mark). It was used as a combustible coating. In the all experiments as extra inhibition was a nitrogen flow along a sample with speed of moving 1 cm/s. A stationary burning rate of samples of d = 1.0 cm with Solprein was about 13% grater then in the case of 0.7 cm diameter samples in the PMMA tube.

A non-metallized propellant was used to provide a comparison with the base system. This propellant contents 20% of binder, 45% of HMX (size > 250 μm), 10% of AP (11 μm) and 23% of AP (200-315 μm).

The digitized signal of recoil force was analyzed by means of Discret Fast Fourier Transformation (DFFT). To obtain auto-spectrums of recorded signals in self-sustaining regime of combustion the records were divided into arrays of 2^N elements and then DFFT was applied. It was used "tapering window of Hanning" and other recommendations of [23] to avoid effects of spectral leakage suppression.

5.2. Experimental results

The recoil force signal of propellant under study is characterized by pronounced unsteady behavior. A record of recoil force signal in self-sustaining combustion regime is presented in Fig. 5.1 while Fig. 5.2 represents a Fourier spectrum of the signal. According to experimental data the correlation between recoil force F and burning rate r has the form

$$F = const \cdot r^{1.1} .$$

Therefore, results of the analysis of recoil force behavior can be applied for analysis of burning rate behavior as well.

The relative amplitude of the recoil force oscillations

$$\frac{\Delta F}{F_{mean}} = \frac{F_{max} - F_{min}}{F_{max} + F_{min}}$$

amounts 20% of mean value of the signal. At the same the estimated amplitude of recoil response to the sinusoidal low-frequency perturbations of radiant flux with mean value 11.7 cal/(cm^2·s) and

depth of modulation 35% is equal 7.5%. It follows from stationary dependence of burning rate on radiant flux (Fig. 5.3). The pair of Fourier spectrums of recoil signal in combustion under sine-modulated radiant flux with constant frequency 4 Hz is shown in Fig. 5.4. It is seen that the spectrums shows relative values of spectral components $(F_F(\omega)/F_{mean})/(q_F(\omega)/q_{mean})$ derived in experiments with sine-modulated radiant flux. Note that at frequencies below 10 Hz there is a big scatter of experimental data. All this findings reflect the fact that the recoil force signal contains noisy components exceeding in amplitude the response on modulation of external radiant flux. To diminish the contribution of noise it would be desirable to extend experimental statistics up to 20-25 runs. But is too time and labor consuming.

As for the source of noise, it is, probably, caused by peculiarities of combustion of metal, which is accompanied with agglomeration, and ejection of melted particles from the burning surface. The indirect confirmation of this statement one may find analyzing recoil force records and their Fourier spectrums (Figs. 5.6, 5.7) for the same propellant formulation but without metal. The non-metallized propellant exhibit pronounced resonance-type behavior of the recoil force (Fig. 5.8).

The results obtained show practical impossibility of getting data on dependence of parameters of disperse phase on the variation of radiant flux amplitude.

With the purpose of better understanding of noise phenomena in propellant combustion the recoil force characteristics of self-sustained combustion were studied. The experimental records (time series data) of recoil force were considered like implementations of some random process. The methods of random processes theory [23, 24] were used for data treatment. Tests show in according to inversion method [23] that in the frequency range greater then 0.5 Hz experimental time series data can be considered as stationary random process (it were used 6 experiments). In this case there is a possibility to estimate intensity of stochastic fluctuations by means of relative standard deviation $\Delta\sigma_F$:

$$\Delta\sigma_F = \frac{\sigma_F}{<F>}$$

$$\sigma_F = \sqrt{\frac{1}{N-1}\sum_{i=1}^{N}(F_i - <F>)^2} \qquad (5.1)$$

$$<F> = \frac{1}{N}\sum_{i=1}^{N}F_i$$

Here $<F>$ and σ_F - sampling mean and sampling standard deviation of amplitude of the recoil force $F_i = F(t_i)$ correspondingly, N – number of sample points.

In according to (5.1) the mean value of $<\Delta\sigma_F>$ for 6 records divided into 1 second intervals was estimated. $<\Delta\sigma_F>$ = 0.3±0.02 for samples (d = 0.7 cm) in PMMA tube and $<\Delta\sigma_F>$ = 0.19±0.03 for samples (d = 1.0 cm) with Solprein inhibition.

Another important characteristic of a stationary random process is auto-spectral density function $<G_{FF}(f)>$, which represents distribution of power of random oscillations on frequency [23, 24]:

$$<G_{FF}(f)> = \frac{2}{NT}\sum_{i=1}^{N}\left|S_{Fi}(f,T)\right|^2$$

Here N and T - number and duration of time series data and $S_{Fi}(f,T)$ – DFT representation of recoil force $\{F_i\}$. It should to note that value $1/T = \Delta f$ – is a frequency resolution.

The Fig 5.9 shows estimation of the auto-spectral density function $<G_{FF}(f)>$ for the base metalized propellant (samples were d = 0.7 cm in PMMA tube) with N = 6 and Δf = 0.27 Hz. It should to note some peculiarities of obtained estimation of $<G_{FF}(f)>$:

1. Spectral density has the maximum at frequency 2 Hz and quickly decreases when frequency tend to zero. To demonstrate this phenomena the low frequency filtration of original record (Fig. 5.10) was made. There are results of using 7.5 and 0.75 Hz filters in the Fig. 5.11. You can see that only fluctuations with the small amplitudes are present after application of 0.75 Hz filter.
2. The magnitude of spectral density is appreciably in the narrow bandwidth from 0.5 to 10 Hz.
3. In the frequency range 2 – 50 Hz the spectral density decreases as the function $1/f^2$, and for higher frequencies it looks like "white noise".

This is the narrow-band random process. The similar auto-spectrums were obtained in experimental investigations of isotropic turbulence [25, 26]. The turbulence flow was generated by blowing gas through the net with the sell size about 250 μm. There are experimental evidence [27] and theoretical model [28, 29] of turbulence character of composite propellant combustion. This is one of the possible explanations. Another reason of the stochastic oscillations of recoil force is connected with time evolution of metal agglomerates on the burning surface.

There is no doubt that recoil force spectrums characterize the non-uniformity of combustion process of composite propellant including agglomeration processes. The detailed investigations are able to give correlation between recoil force behavior and processes on the burning surface by the help of synchronous shooting and recoil force recording.

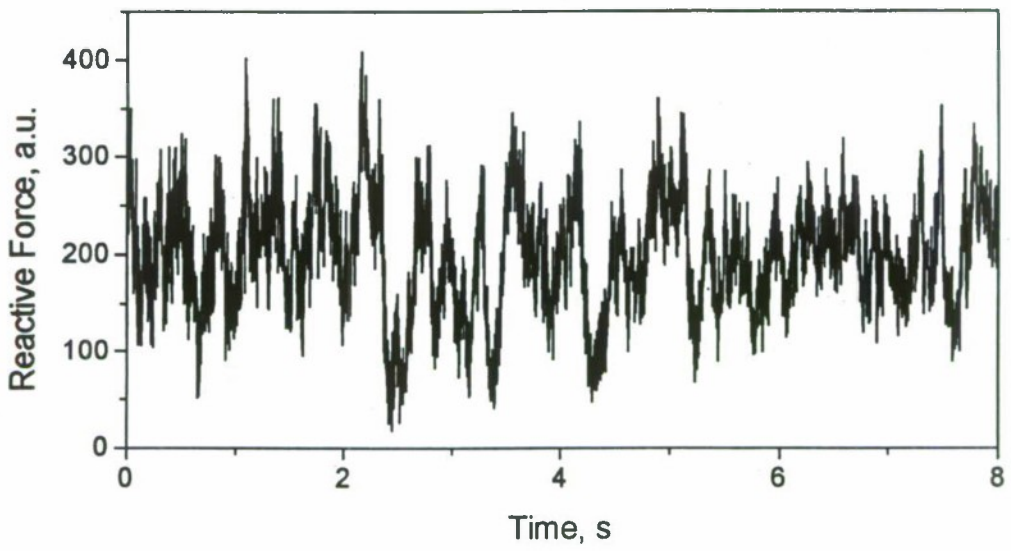

Fig. 5.1. Reactive force behavior of self-sustained combustion of metalized propellant.

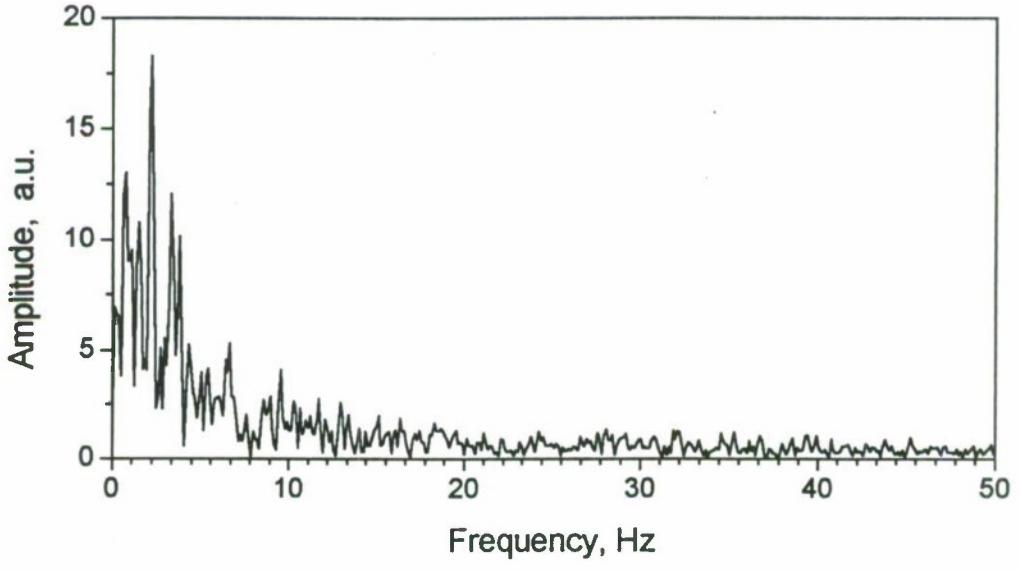

Fig. 5.2.
Fourier spectrum of reactive force of self-sustained combustion of metalized propellant.

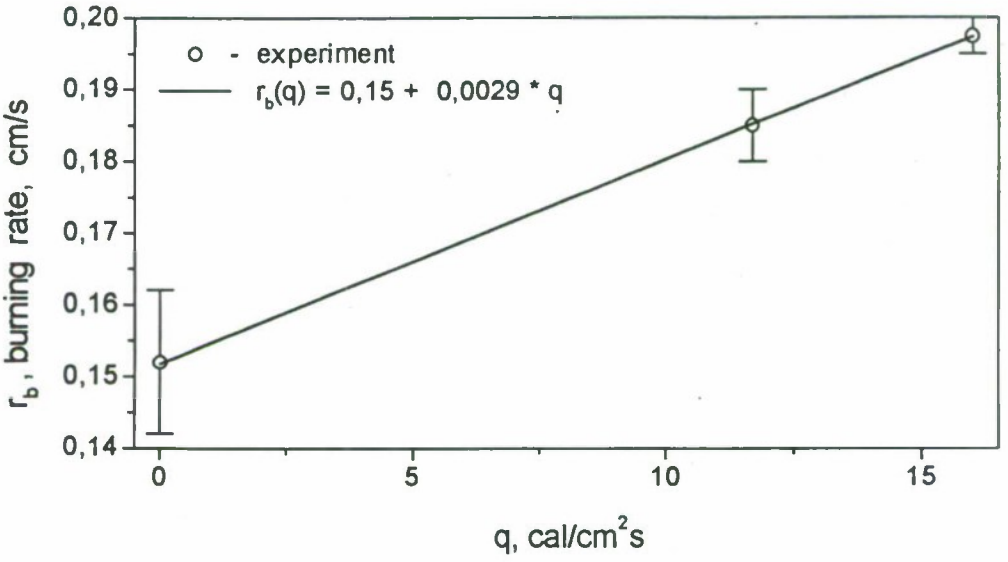

Fig. 5.3. Stationary burning rate of metalized propellant *vs* laser radiant flux.

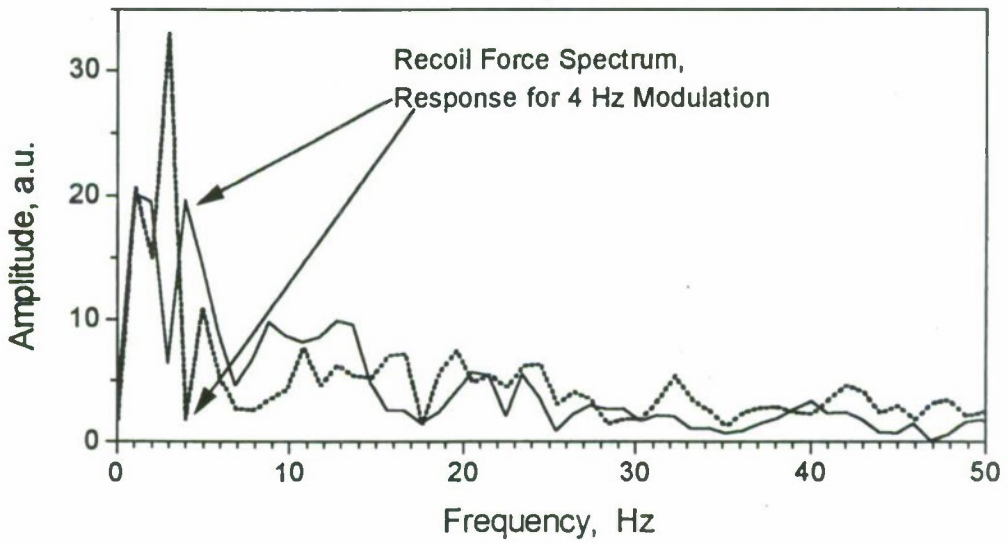

Fig. 5.4.
Two reactive force response spectrums for combustion under the modulated radiant flux.

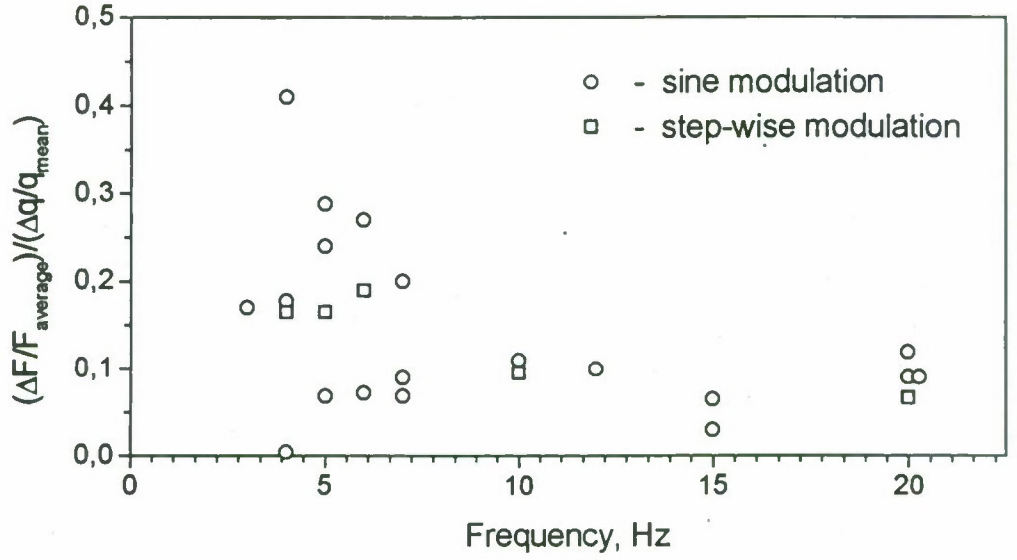

Fig. 5.5. Relative reactive force response of metalized propellant.

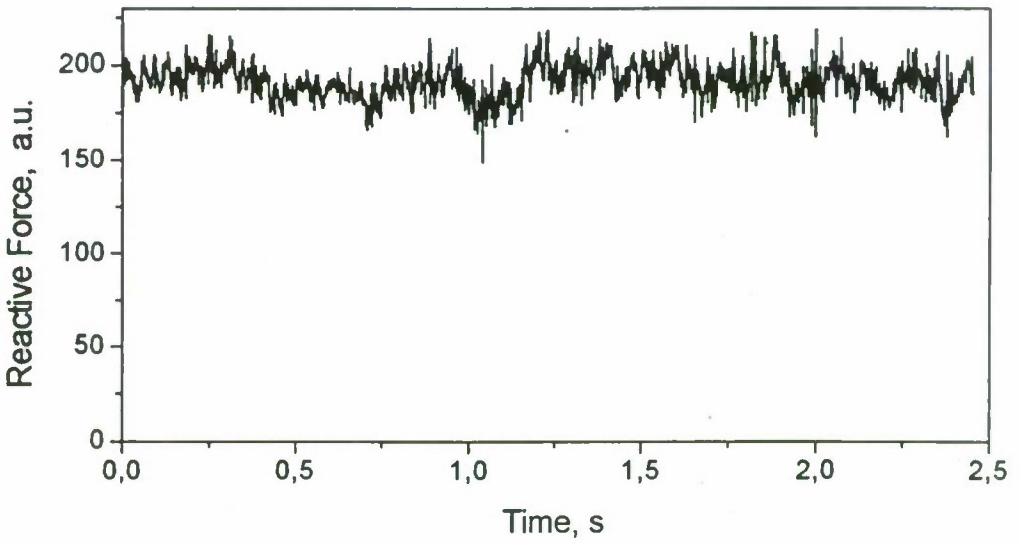

Fig. 5.6. Reactive force behavior of self-sustained combustion of non-metalized propellant.

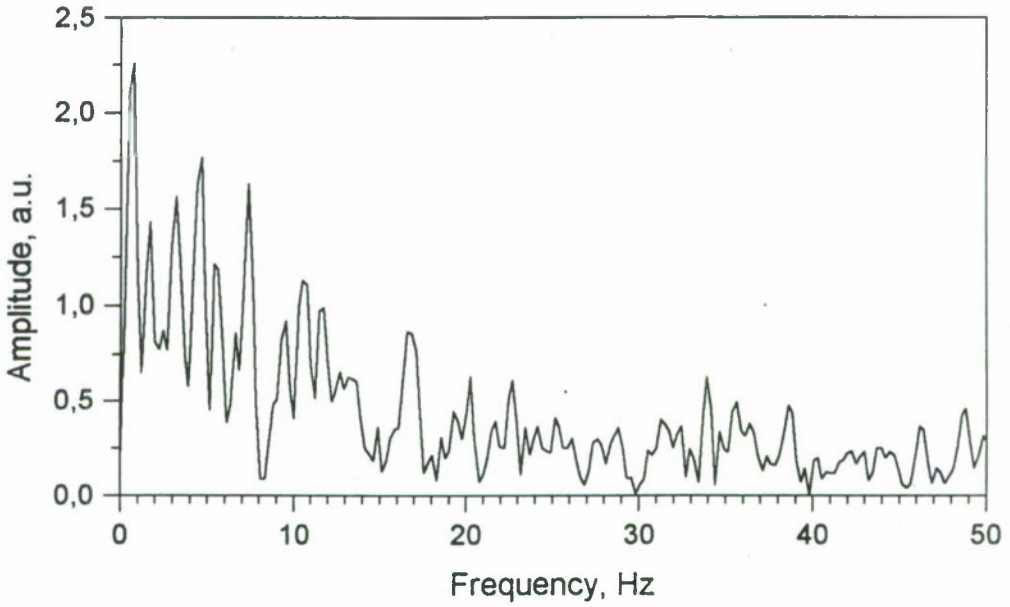

Fig. 5.7.
Fourier spectrum of reactive force of self-sustained combustion of non-metalized propellant.

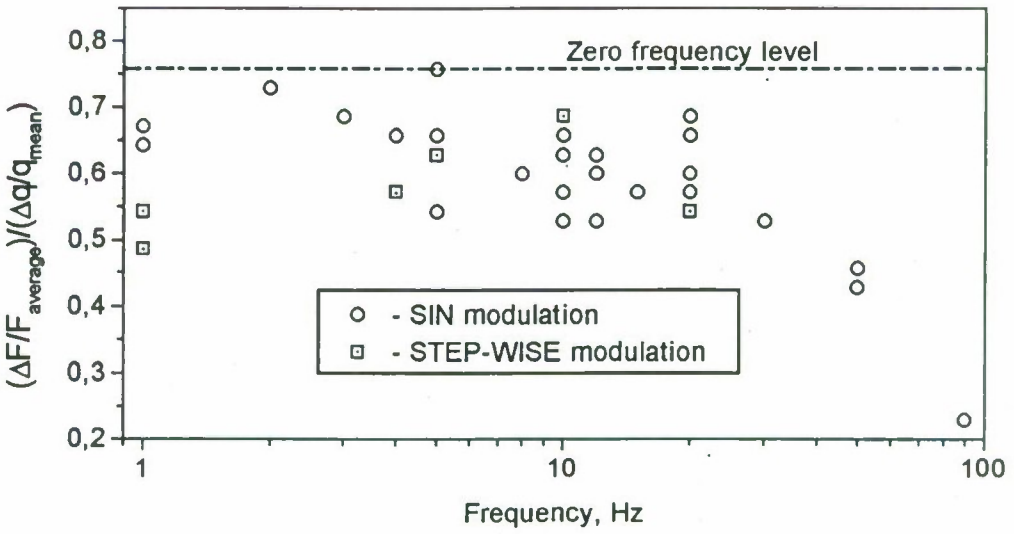

Fig. 5.8. Relative reactive force response of non-metalized propellant.

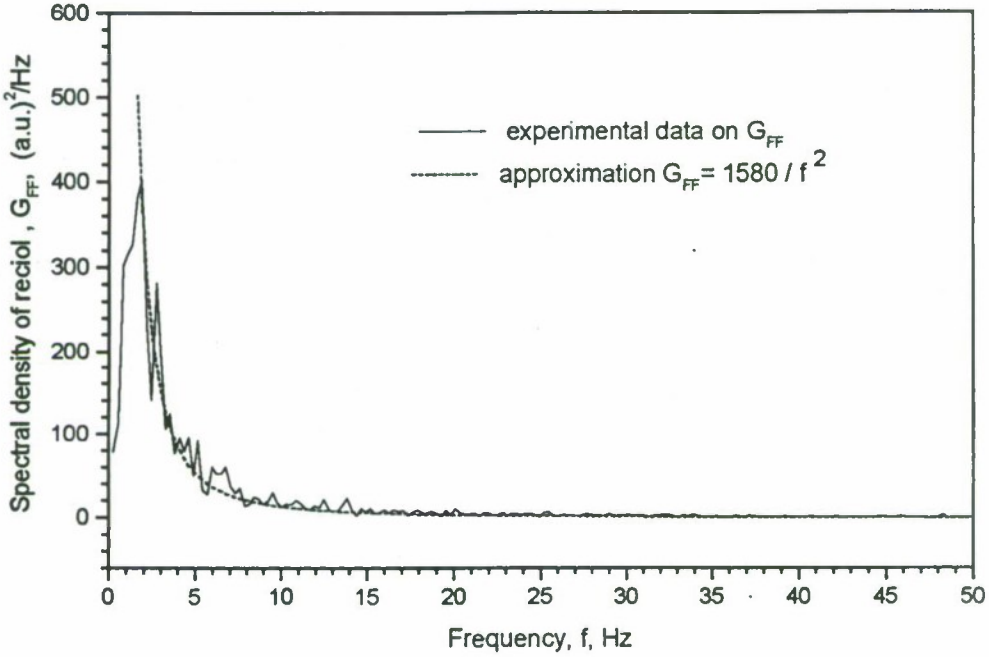

Fig. 5.9. Auto-spectral density function for the base metalized propellant. It was averaged over 6 samples.

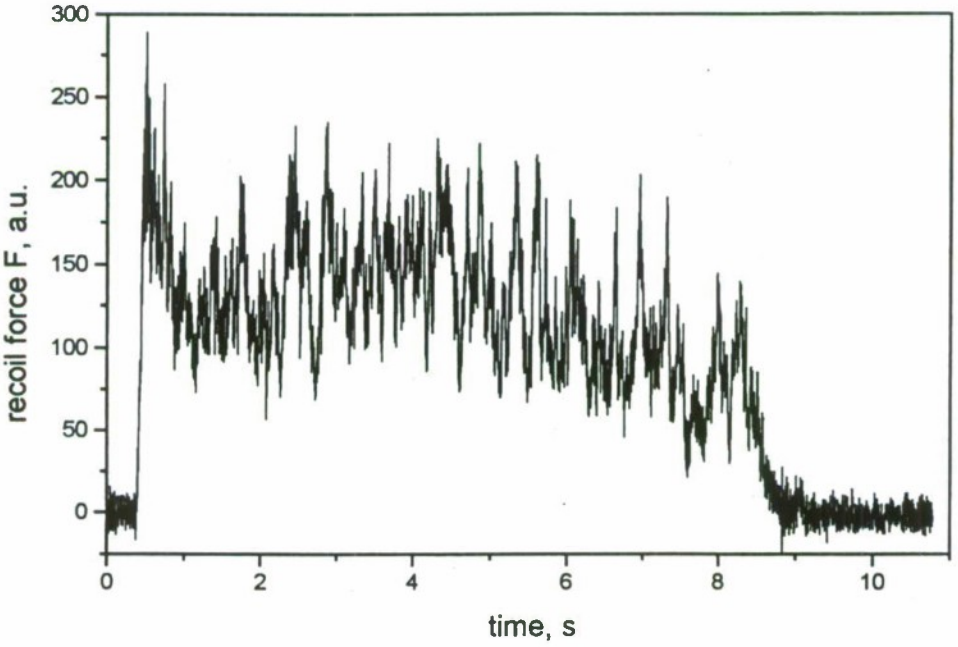

Fig. 5.10. Example of recoil force record.

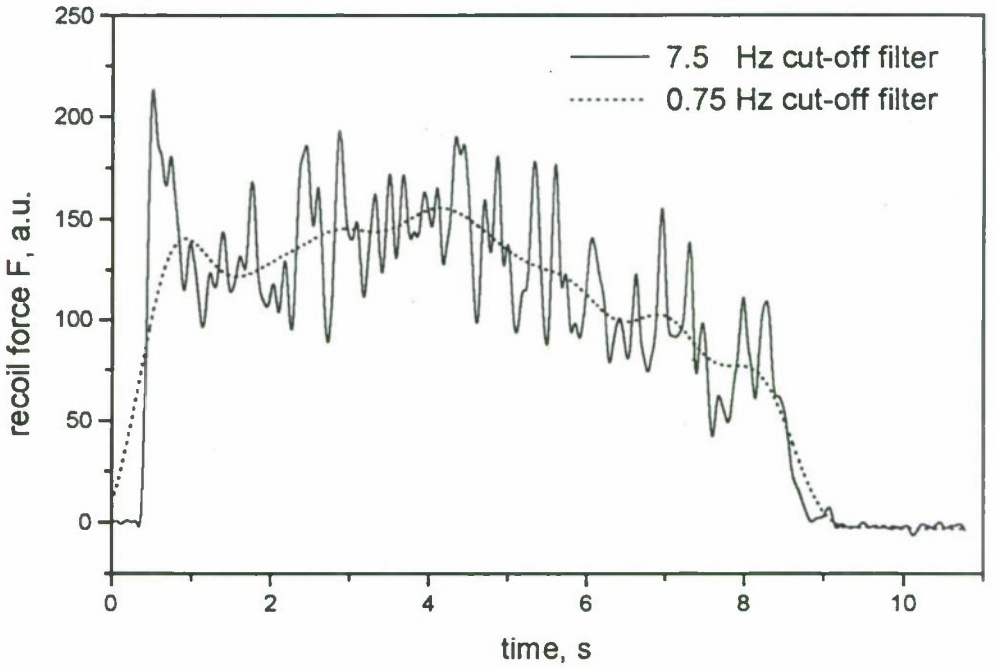

Fig. 5.11. Example of recoil force record after filtration.

CONCLUSIONS

The present work deals with the investigation of the formulation effect on the combustion behavior of metalized propellants, namely on evolution of condensed combustion products (CCP) and non-steady combustion characteristics. The study has been performed on model propellants with well characterized powder components using two original methods – collection of CCP particles quenched at varied distance from burning surface and use of micro-force transducer for the recoil measurements of propellant sample burning in self sustaining regime or under perturbing conditions. The propellant formulation based on HMX/AP/Al and energetic binder was studied in present work.

To summarize findings of this and previous studies, three agglomeration scenarios were briefly described in present work. The currently studied propellant follows to the classical scenario which is characterized by: 1) sizable growing of agglomerates holding for a long time on the burning surface, and 2) content of practically entire amount (91%-99%) of unburnt aluminum in agglomerates. Meanwhile, the studied propellant exhibits some specific peculiarities in the agglomeration behavior:

1. The main mass and size characteristics more strongly depend on pressure than on residence time for agglomerates in flame. The following parameters decrease with pressure: percentage of free aluminum in agglomerates $[Al]_{ag}$, relative mass of agglomerates m_{ag}, mass of free aluminum in agglomerates m^{Al}_{ag}, mass fraction of agglomerates in CCP m_{ag}/m_{ccp}, the proportion between masses of agglomerate and oxide particles m_{ag}/m_f, incompleteness of aluminum combustion $m^{Al}_{ag}/m^{Al}_{prop}$, mean sizes of agglomerates. To illustrate the comparative dependencies on pressure and on residence time (provided by protective tube length variation), one can cite the data on D_{43} as an example. The values of D_{43} corresponding to different tube length are in interval 380-405 μm at P=1 atm, 290-311 μm at P=24 atm, and 272-303 μm at P=74 atm.
2. The classical agglomerate structure can be described as sack-like object, sometimes containing cavities, consisting of individual (close to original size) particles covered as whole with relatively thin oxide layer. The density of agglomerate matter is always lower than pure aluminum and aluminum oxide one. For given propellant, additionally, the content of unburnt aluminum in sieved fractions in the range 130-600 μm is approximately constant for each pressure levels in the range 1-64 atm. The density of agglomerates does not depend on size in the range 130-600 μm, but slightly increases with oxide content while pressure increases. Typical value for sampled agglomerate density is 2.16 g/cm^3.
3. There is specific behavior of aluminum consumption at different pressures for given propellant. At pressure ~65 atm no change in aluminum content is observed in time interval 30-95 ms, and amount of free aluminum in agglomerates has lowest value as compared with that for another pressures. Obviously, in this case a significant portion of aluminum was consumed at the first stage of formation and detachment from the burning surface. Additionally, one can suppose that the remaining aluminum is capsulated under thick layer of oxide and not available for oxidation. At atmospheric pressure there is a noticeable change in aluminum content during time interval 20-25 ms, and then it is approximately constant while residence time is 25-70 ms. If the slow oxidation of aluminum is caused by its encapsulation, it is necessary to note that the level of limiting consumption value depends on pressure. At pressure ~22 atm the intermediate behavior is observed. No significant evolution of size distribution of agglomerates was observed even in the cases of 1 atm and 22 atm when burning out of aluminum took place. A possible explanation

is that some consumed portion of agglomerate aluminum is replaced by aluminum oxide (another part of oxide mass go out in with gas flow in the form of smoke particles). The total agglomerate mass is modified very slightly during this process.

Regarding the fine (oxide) particles, we may conclude that:

4. In most cases the fine CCP particles size distribution has three modes in the size ranges 0.5-1.5 μm, 2.4-3.9 μm and 6.4-8.5 μm, with the main peak being in interval 2.4-3.9 μm. Agglomerate combustion increases the total mass of fine particles but does not make effect on their size distribution.
5. For the first time some unusual form of size distribution function (narrowing to the interval 1.5-10.5 μm) was observed in the case of pressure 24 atm and the longest protective tube. The formation of alternative condensed products (aluminum nitride, for example) can be assumed as a cause of this peculiarity. Special experiments and analyses should be performed to elucidate this finding.
6. The 0.5-1.5 μm peak may increase with residence time. This mode presumably consists of soot-like substance forming in combustion of non-metalized part of propellant and partially by ablation of protective tube material.

The results of studying transient combustion characteristics can be described as follows:

7. Self-sustaining combustion of propellant under investigation under atmospheric pressure is characterized by noticeable pulsations of the recoil force. These force oscillations, when analyzed by stationary stochastic process theory, exhibit auto-spectrum similar to isotropic turbulence where 80% of oscillations energy is released in the frequency range 0.5-10 Hz.
8. The presence of intense noise in the recoil signal due to chaotic pulsations of the burning rate makes impossible (unreliable) correct determining radiation-driven recoil response function.
9. Excluding of aluminum from propellant formulation leads to significant (by order of magnitude) decrease in amplitude of chaotic recoil signal oscillations.

The results of this study stress the necessity of further systematic investigation of the effects of propellant formulation (that includes variation of the nature of components and properties of metallic component) on agglomeration and its correlation with recoil force characteristics in terms of studying physical properties and microstructure of propellant and chemical reactions between metal particles and products of binder and oxidizer decomposition. It will be important to establish in the future research the correlation between observed combustion behavior of metalized propellants, propellant formulation, and characteristics of the combustion wave such as temperature profile and degree of metal consumption.

LITERATURE CITED

1. Price, E. W. (1984). "Combustion of Metalized Propellants", In: *Fundamentals of Solid Propellant Combustion,* Progress in Astronautics and Aeronautics, Vol. 90, pp. 479-514.

2. Zarko, V. E., Glotov, O. G., Karasev, V. V., Simonenko, V. N., Kiskin, A. B., Svit, A. G. (1997). "Studying the formulation effects on steady-state and transient combustion behavior of aluminized propellants". Final tecnical report under EOARD Contract F61708-96-W0270. Novosibirsk,. 64 pages.

3. Zarko, V. E., Glotov, O. G, Karasev, V. V. (1996). "The effect of solid propellant binder on the formation and evolution of condensed combustion product particles". Final technical report under Brigham Young University Contract. Novosibirsk,. 81 pages.

4. Glotov, O. G., Zarko, V. E., Karasev, V. V., Beckstead, M. W. (1997). "Effect of Binder on the Formation and Evolution of Condensed Combustion Products of Metalized Solid Propellants", In: *Combustion and Detonation. 28th Int. Annual Conf. of ICT*, Karlsruhe, Germany, Report 75, 14 pages.

5. Glotov, O. G., Zarko, V. E., Karasev, V. V. (1997). "Study of disperse phase of HMX-based aluminized propellants. 1. Steady-state combustion characteristics". In: *Intra-Chamber Processes, Combustion and Gas Dynamics of Dispersed System,* S-Petersburg, 3 pages.

6. Karasev, V. V., Glotov, O. G., Kiskin, A. B., Simonenko, V. N., Svit, A. G. (1997). "Study of disperse phase of HMX-based aluminized propellants. 2. Transient combustion characteristics". In: *Intra-Chamber Processes, Combustion and Gas Dynamics of Dispersed System,* S-Petersburg, 3 pages.

7. Glotov, O. G., Zarko, V. E., Karasev, V. V., Beckstead, M. W. (1998). "Condensed combustion products of metalized propellants of variable formulation". AIAA-98-0449, 6 pages.

8. Glotov, O. G., Zyryanov, V. Ya. (1991). "The Effect of Pressure on Characteristics of Condensed Combustion Products of Aluminized Solid Propellant". Archivum Combustionis, Vol. 11, No. 3-4, pp. 251-262.

9. Glotov, O. G., and Zyryanov, V. Ya. (1995). "The Condensed Combustion Products of Aluminized Solid Propellants. I. The Method of Quenching at Various Distances from Burning Surface for Studying the Evolution of Particles". *Combustion, Explosion and Shock Waves*, Vol. 31, No. 1.

10. Fedotova, T. D., Malachov, V. V., Glotov, O. G., Kir'yanova, A. G. (1992). "Permanganatometric Determination of Metallic Aluminum in Condensed Combustion Products". *Siberian Chemical Journal*, No. 2, pp. 37-38 (in Russian).

11. Duterque J. (1996). "Experimental Studies of Aluminum Agglomeration in Solid Rocket Motors". In: *4th Int. Symp. on Special Topics in Chemical Propulsion*, Stockholm, Sweden. (ONERA TR 1996-48, available on the Internet at address: http://www.onera.fr/RECH/BASIS/public/web_fr/document/DDD/243366.pdf.

12. Grigor'ev, V. G., Zarko, V. E., Kutsenogii, K. P., Bobryshev, V. P., and Sakovich, G. V. (1981). "Model for the Agglomeration of Metal Powder in the Combustion of Composite Mixtures", *Doklady Akademii Nauk SSSR*, Vol. 259, No. 4, pp. 881-885. (in Russian).

13. Grigor'ev, V. G., Zarko, V. E., and Kutsenogii, K. P. (1981). "Experimental Investigation of the Agglomeration of Aluminum Particles in Burning Condensed Systems". *Combustion, Explosion and Shock Waves*, Vol. 17, No. 3

14. Cohen, N. S. (1983). "A Pocket Model for Aluminum Agglomeration in Composite Propellants". *AIAA Journal*, Vol. 21, No. 5, pp. 720-725.

15. Zyryanov, V. Ya. (1986). "Model for Prediction of Agglomeration in Combustion of Metalized Systems", In: *Condensed Systems Combustion*, Chernogolovka. (in Russian). pp. 59-62.

16. Kovalev, O. B. (1989). "Physicomathematical Model of the Agglomeration of Aluminum in the Combustion of Mixed Condensed Systems". *Combustion, Explosion and Shock Waves*, Vol. 25, No. 1.

17. Kovalev, O. B., Petrov, A. P., and Fol'ts, A. V. (1987). "Simulating Aluminum Powder Aggregation in Mixed Condensed-System Combustion". *Combustion, Explosion and Shock Waves*, Vol. 23, No. 2.

18. "Theory of Turbulent Jets" (1984). Moscow, Nauka publ., 716 p.

19. Timnat, Y. M. (1987). "Advanced Chemical Rocket Propulsion". Academic Press. Harcourt Brace Jovanovich, Publishers.

20. Afifi, A. A., Azen, S. P. (1979). "Statistical Analysis. A Computer Oriented Approach". Academic Press, New York-San Francisco-London.

21. Taylor, J. R. (1982). "An Introduction to Error Analysis". University Science Books Mill Valley, California.

22. Babuk, V. A., Belov, V. P., Khodosov, V. V., and Shelukhin, G. G. (1988). "Study of the Structure of Agglomerates With Combustion of Aluminized Mixed Condensed Systems". *Combustion, Explosion and Shock Waves*, Vol. 24, No. 5.

23. Bendet, J.S., Piersol, A.G., (1986). "Random Data", Jon Wiley&Sons, Inc., New York.

24. Bendet, J.S., Piersol, A.G. (1980). "Engineering Applications of Correlation and Spectral Analysis", Jon Wiley & Sons, Inc., New York.

25. Taylor, G. I., (1938). "The Spectrum of Turbulence", *Proc. Roy. Soc.*, ser. A, Vol. 164, No. 919, pp. 476-490.

26. Favre, A., Gaviglio, J., Dumas, R., (1954). "Quelques fonctions d'auto-correlation et derepartitions derepartitions spectrales d'energie, pour la turbulence en aval des diverses grilles". *C. r. Acad. Sci.*, Vol. 238, No. 15, pp.1561-1563.

27. Murphy, J. L., Netzer, D. W., (1974). "Ammonium Perchlorate and Ammonium Perchlorate – Binder Sandwich Combustion". *AIAA Journal*, Vol. 12, No. 1, pp. 13-14.

28. Hermance, C. E., (1967), ACRPG/AIAA 2-nd Solid Propulsion Conf., Anaheim, Calif.

29. Zyryanov, V. Ya., Bolvanenko, V. M., Glotov, O. G., and Gurenko Yu. M. (1988). "Turbulent Model of Mixed Solid Fuels Combustion", *Combustion, Explosion, and Shock Waves*, Vol. 24, No. 6.